Bulletin of the Geological Survey of Japan, vol. 76 (1/2), p. 51–100, 2025

Article

Accretionary age of the Jurassic accretionary complex of the North Kitakami Belt: new data from zircon geochronology in the Kado District

MUTO Shun[1,*]

MUTO Shun (2025) Accretionary age of the Jurassic accretionary complex of the North Kitakami Belt: new data from zircon geochronology in the Kado District. *Bulletin of the Geological Survey of Japan*, vol. 76 (1/2), p. 51–100, 21 figs and 13 appendices.

Abstract: The study on the accretionary history of the Jurassic accretionary complex of the North Kitakami Belt in Northeast Japan has been hampered by the scarcity of reports on radiolarians due to metamorphism of Cretaceous plutons. Recently, zircon geochronology is being employed to elucidate the age of accretion from strata that yield rare or no microfossils. This study reports zircon U–Pb ages from igneous zircons in tuff and detrital zircons in sandstone from the 1: 50,000 Kado District in northeast Iwate Prefecture. Based on compilation of available data, the accretionary complex distributed in the main part of the northern Kitakami Mountains is classified mainly into the following seven tectonostratigraphic units: The Kadoma Unit of Rhaetian to Middle or early Late Jurassic age, the Misugo Unit of undetermined age, the Aalenian to Bathonian Otori Unit, the Bathonian to Kimmeridgian Seki Unit the Oxfordian to Kimmeridgian Takayashiki Unit, the Kayamori Unit of undetermined age and the Kimmeridgian Ekari Unit. The former six units are structurally stacked up in this order. The exact structural position of the Ekari Unit is not clear, but it is correlated to the Takayashiki Unit or a lower and younger unit, in terms of age. The new data in this study provided constraints on the accretionary age of the Ekari, Takayashiki, Seki, Otori and Kadoma units, although detrital zircons from sandstone were not always useful. The Ekari Unit lies in fault contact between older units, meaning that the faults have vertical displacements. Such faults and kilometre-scale folds interrupt the general oceanward younging trend of the accretionary complex of the North Kitakami Belt. Zircons in tuffs have not widely been used to estimate accretionary ages, but this study shows that they can be powerful tools, especially when microfossils are difficult to obtain.

Keywords: accretionary age, detrital zircon, Quadrangle Series, sandstone, tuff, U–Pb age

1. Introduction

The North Kitakami–Oshima Belt in Northeast Japan is defined by the distribution of mainly Jurassic accretionary complexes (Ehiro *et al.*, 2005; Kojima *et al.*, 2016; Fig. 1A). In characterization of accretionary complexes, the time of accretion at the subduction zone plays a key role (e.g., Matsuoka *et al.* 1998; Nakae, 2000) and is estimated based on the age of trench-fill clastic rocks at the top of the oceanic plate stratigraphy. Herein, I refer to this age as the trench-arrival age (TAA), since the trench-fill clastic rocks are deposited when the oceanic plate arrives at the trench area. This terminology aims to distinguish the depositional age of the clastic rocks from the timing of actual accretion, which takes place when the subducting plate submerges beneath the overriding plate. Based on radiolarian fossils and zircon dating, the TAA of the North Kitakami Belt–Oshima Belt is mostly within the Jurassic, but the oldest part is late Triassic or even late Permian, and the youngest part is Early Cretaceous (Fig. 1B). Compilation of available data (Suzuki *et al.*, 2007a; Ehiro *et al.*, 2008; Uchino and Suzuki, 2020) indicate a general younging of TAA from the southwest to northeast (landward to oceanward) (Fig. 1B). On the other hand, age data on TAA is limited in the North Kitakami–Oshima Belt compared to coeval accretionary complexes in Southwest Japan, due to the poor occurrence of radiolarians as a result of contact metamorphism of Cretaceous plutons. Recent development of zircon U–Pb chronology provided the potential to obtain age data from clastic rocks from which extraction of identifiable radiolarians is almost hopeless (e.g., Ueda *et al.*, 2018; Uchino, 2019; Muto *et al.*, 2023; Osaka *et al.*, 2023). However, U–Pb dating of zircons are mostly conducted on detrital zircons in

[1] AIST, Geological Survey of Japan, Research Institute of Geology and Geoinformation
[*] Corresponding author: MUTO, S., AIST Tsukuba Central 7, 1-1-1 Higashi, Tsukuba, Ibaraki 305-8567, Japan. Email: s-muto@aist.go.jp

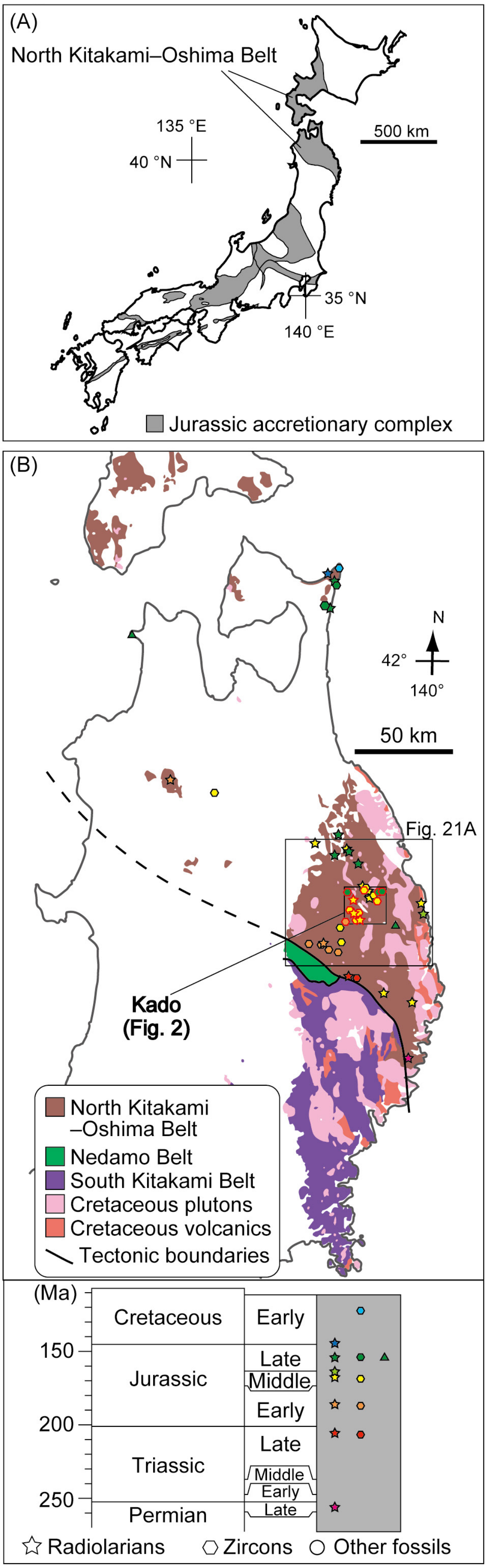

Fig. 1 (A) Distribution of the Jurassic accretionary complex in Japan (after Isozaki *et al.*, 2010). (B) Geology of the basement rocks of the northern Tohoku Region (modified from Geological Survey of Japan, AIST, 2020). Age constraints for time of accretion are based on the compilation by Uchino and Suzuki (2020), this study and additional references in Muto *et al.* (2023). Data plots closed in red were obtained in this study and Muto *et al.* (2025).

sandstones. It is known that young detrital zircons are usually only a small portion of the entire population, and the age of the youngest population may appear older than the depositional age by tens of millions of years, at least in the North Kitakami–Oshima Belt (Uchino, 2021; Muto *et al.*, 2023). Thus, it is important to obtain data from tuffs that will point to the depositional age of the strata.

The present author has worked on the production the 1: 50,000 geological map of the Kado District for the Quadrangle Series of the Geological Survey of Japan, AIST, which is located within the area of the North Kitakami Belt (the segment of the North Kitakami–Oshima Belt distributed in Honshu). As part of this project, tuffs and sandstones were investigated for U–Pb zircon geochronology. The age data from the tuffs provide depositional ages of clastic rocks that were previously poorly dated or not dated at all. Sandstones were investigated to compare the age of the youngest cluster in detrital zircons to that of tuffs from a nearby horizon. New data are compiled with previous studies to present the present understanding of the accretionary history and geological structure of the North Kitakami Belt.

2. Geological outline

The Kado District of the 1: 50,000 Quadrangle Series is situated in the central area of the North Kitakami Belt. The Jurassic accretionary complex in this district can generally be divided into two areas with respect to the quality and quantity of available geological data. The northeast part, including the area around the Akka River, was the target of detailed geological studies by Sugimoto (1974, 1980). Although researchers at that time were not aware that the studied strata were formed through accretionary processes, more recent studies adopting the concept of accretionary complexes (Takahashi *et al.*, 2016; Nakae *et al.*, 2021) proved the distribution of lithofacies and geological structures illustrated by Sugimoto (1974, 1980) to be mostly correct. The tectonostratigraphic division of Jurassic accretionary complexes in this area has been slightly different between researchers (see Muto *et al.*, 2023). In this study, we distinguish the Takayashiki, Seki and Otori units in tectonically ascending order, based on data obtained during the production of the 1: 50,000 geological map of the Kado District by the present author (Fig. 2). The division basically follows Nakae *et al.* (2021), while the Kassenba and Seki complexes are

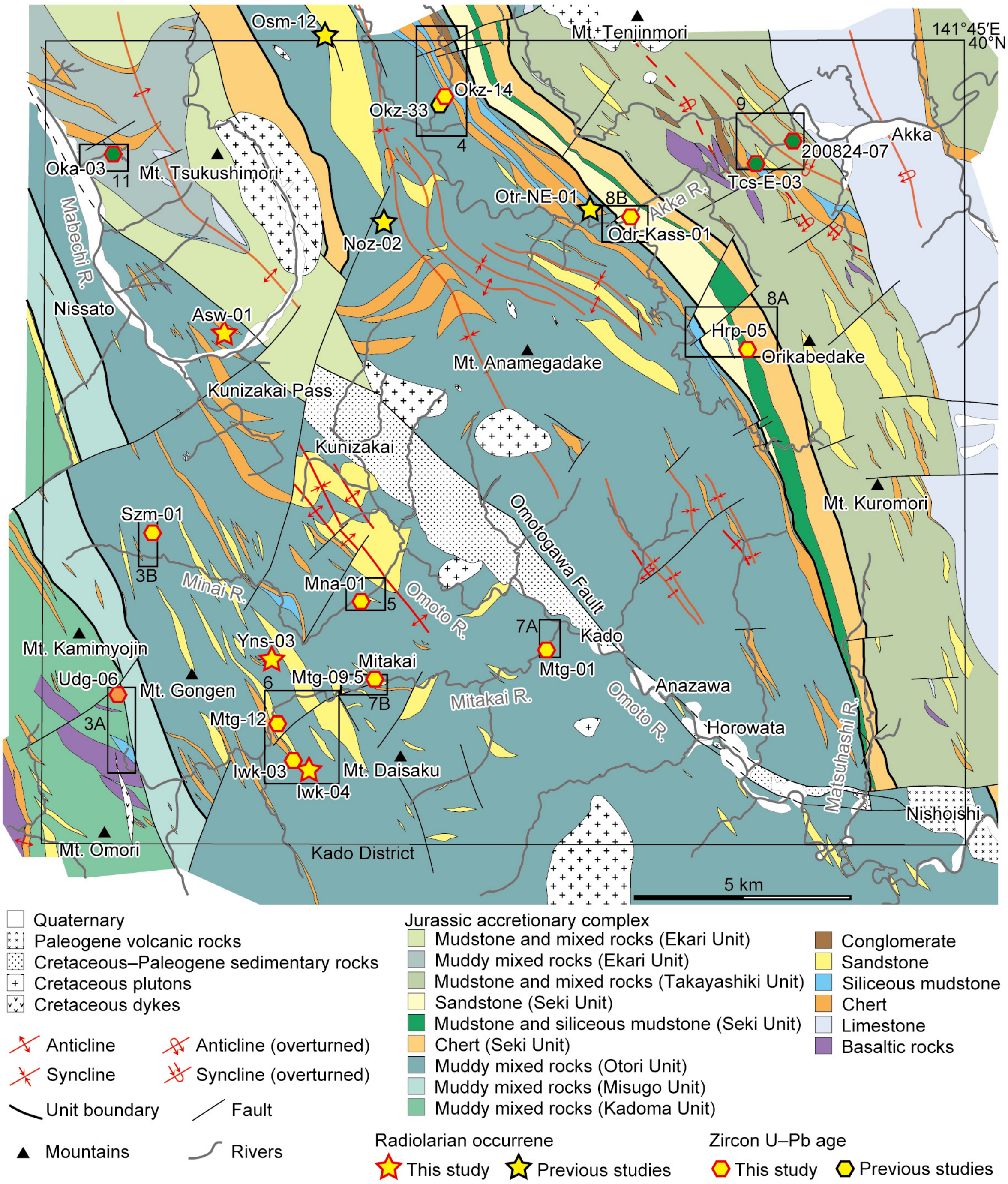

Fig. 2 Geological outline of the Kado District based on geological surveys conducted for the 1: 50,000 geological map of the Kado District for the Quadrangle Series of the Geological Survey of Japan, AIST by Muto, S. Areas of traverse maps (Figs. 3–9, 11) are shown with black boxes. The prefix "Fig." for these boxes are omitted. For legends to colours of the age data plots, see Fig. 1B.

united into the Seki Unit as in Takahashi *et al.* (2016) ("complex" in Nakae *et al.* (2021) is equivalent to "unit" in this paper). This area is one of the best studied areas in the North Kitakami Belt.

The southwest part of the Kado District, consisting of a large part of the catchment area of the Omoto River and the catchment area of the Mabechi River, is less well studied. In this area, partly overlapping geological maps were published by Onuki (1969), Yamaguchi (1981) and Murai *et al.* (1985, 1986). These studies date before the acceptance of subduction–accretion processes by scientists working on the North Kitakami Belt. Due to the lack of detailed traverse maps of type localities or any age data from clastic rocks, it is difficult to reinterpret the published maps as accretionary complexes or to establish precise correlation between different units recognized therein. Based on geological surveys for the Kado District obtained by the present author, most of the Jurassic accretionary complex in the southwest part of the district not classified by the detailed maps of Sugimoto (1974, 1980) is included in the Otori Unit (Fig. 2). The exception is the Ekari Unit in the northwest corner of the district, and the Misugo and Kadoma units in the southwest corner (Fig. 2). The Ekari and Misugo units are newly recognized units and will be detailed in the outcoming 1:50,000 map of the Kado District. The Ekari Unit is mainly composed of broken facies of mudstone with sandstone layers, alternating mudstone and sandstone and muddy mixed rocks. It is bounded by faults between the Seki Unit to the east and the Otori Unit to the west (Fig. 2). The Misugo Unit is composed of muddy mixed rocks and characterized by intercalations of light green claystone within mudstone. The Kadoma Unit was defined by Kawamura *et al.* (2013) and corresponds to the Nakatsugawa Unit of Uchino (2019). The distribution of this unit continues from the southwest edge of the Kado District to the southwest boundary of the North Kitakami Belt, where it is in contact with the Nedamo Belt.

In the revised tectonostratigraphic division, the Jurassic accretionary complex in the Kado District is divided into the Takayashiki, Seki, Otori, Misugo, Kadoma and Ekari units. The first five units are stacked in this tectonically ascending order, while the strict position of the Ekari Unit is not determined. Based mainly on radiolarian occurrences, the Seki Unit accreted during the Bathonian of the Middle Jurassic to the Kimmeridgean of the Late Jurassic (Nakae and Kamada, 2003; Nakae, 2016), and the northeastern part of the Otori Unit accreted around the Bathonian (Suzuki *et al.*, 2007b; Ehiro *et al.*, 2008; Muto *et al.*, 2023). The Takayashiki Unit was considered to be accreted during the Oxfordian based on an ammonoid-bearing float (Suzuki *et al.* 2007a), but this sample needs to be viewed with great caution (see Chapter 5).

The samples investigated in this study cover all the tectonostratigraphic units in the Kado District except the Misugo Unit, from which suitable samples were not obtained. Tuff samples were obtained from tuff layers with a sedimentary contact in clastic or hemipelagic rocks, or from bedded tuffs, rather than tuff blocks in mixed rocks. Sandstone samples were mostly taken from medium grained bedded sandstones. Details on the sampling horizons are explained in the following text and figures (Figs. 3–11).

3. Methods

The author investigated eight tuff samples and five sandstone samples. Samples were observed in thin section to check for the presence of zircons. Zircon separation and U–Pb dating were conducted by Kyoto Fission-Track Co. Ltd. Zircon U–Pb dating was conducted at the Hirata-Lab. of the University of Tokyo by laser ablation inductively coupled plasma mass spectrometry (LA-ICP-MS). The LA part was CARBIDE (LIGHT CONVERSION) and the ICP-MS part was New Plasma II (Nu instruments). Ablation pit size was 10 µm, energy density was 3.2 J/cm^2, and pulse repetition rate was 10 Hz. Laser ablation was conducted on polished sections of zircons embedded in PFA Teflon sheets. Analyses were performed after one-shot cleaning. The details of the analysis are described in Iizuka and Hirata (2004) and Hirata *et al.* (2005). Primary standard was the Plešovice zircon with a ^{238}U–^{206}Pb age of 337.13 ± 0.37 Ma (Sláma *et al.*, 2008). Secondary standard was the standard zircon 91500 with a ^{238}U–^{206}Pb age of 1062.4 ± 0.4 Ma (Wiedenbeck *et al.*, 1995) and zircon OD-3 with a ^{238}U–^{206}Pb age of 33.04 ± 0.10 Ma (Iwano *et al.*, 2013). U–Pb age data with ^{238}U–^{206}Pb age/^{235}U–^{207}Pb age ratio between 90 % and 110 % were regarded as concordant age data (Tokiwa *et al.*, 2019). For tuffs, the zircon population with a maximum number of grains where all the grains fall within the 95 % confidence interval of the weighted average of the population within 2σ errors were considered to indicate the age of eruption. For sandstones the weighted mean age of the youngest two or more grains (YC1σ; Dickinson and Gehrels, 2009) was considered for estimation of accretionary age.

4. Zircon U–Pb geochronology

4. 1. Kadoma Unit

One tuff sample from the Kadoma Unit was investigated in this study. No sandstone samples were investigated.

The analyzed sample (Udg-06) was obtained in a small tributary of Udouge Stream in the uppermost reaches of the Mitakai River in northwest Iwaizumi Town (Fig. 3A). The lithofacies of the Kadoma Unit around the locality is composed of muddy mixed rocks with blocks of basaltic rocks, siliceous and tuffaceous mudstone and chert, in this order of abundance. These rocks of the Jurassic accretionary complex are intruded by dyke rocks, notably porphyric tonalite up to 30 m thick. Sample Udg-06 is a grey tuff bed in black mudstone. The tuff bed has a sharp contact at the base and grades upwards into mudstone (Fig. 12A). The tuff part of the sampled horizon is composed of fine sand- to silt-sized grains supported in a matrix of microcrystalline to cryptocrystalline quartz and white mica (Fig. 14A–C). The grains are mostly quartz including shards with low roundness and sphericity with smaller amounts of plagioclase, opaque minerals and zircons (Fig. 14B, C). Part of the quartzose and micaceous matrix appear to be pseudomorphs of felsic grains. The sedimentary contact between tuff and mudstone is confirmed in thin section as well (Fig. 14A). Only the tuff part of the sample was processed for zircon extraction. Thirty zircon grains were analyzed for U–Pb dating, all of which yielded concordant U–Pb ages (Fig. 18A; Table A1). The age of the grains cluster around 200 Ma, and twenty-eight of the cluster are accepted as grains indicating the age of

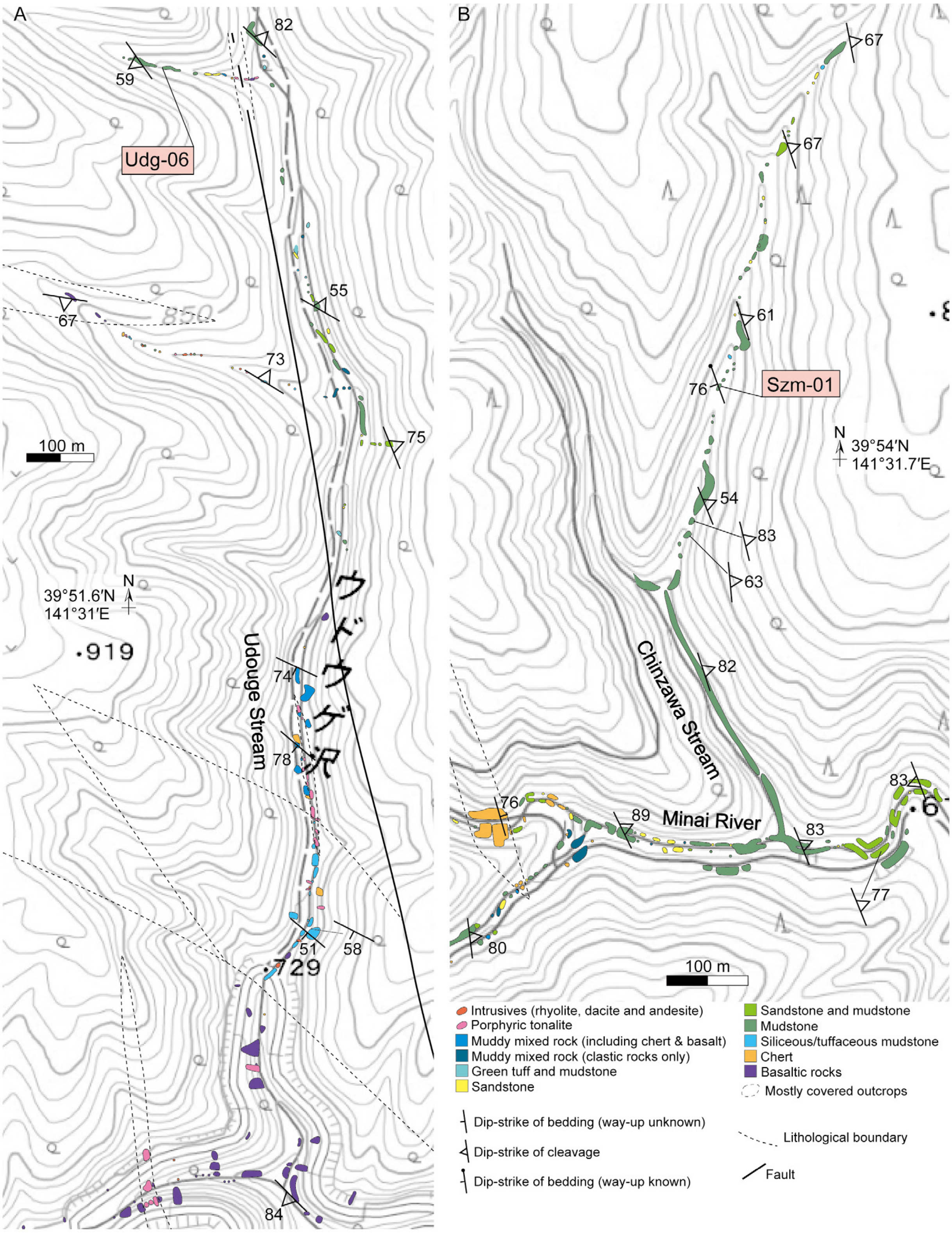

Fig. 3 Geological traverse maps of (A) Chinzawa Stream (sampling locality of Szm-01) and (B) Udouge Stream (sampling locality of Udg-06), both in Kamatsuta-Gongen, Iwaizumi Town. Base map produced from XYZ tiles provided by the Geospatial Information Authority of Japan.

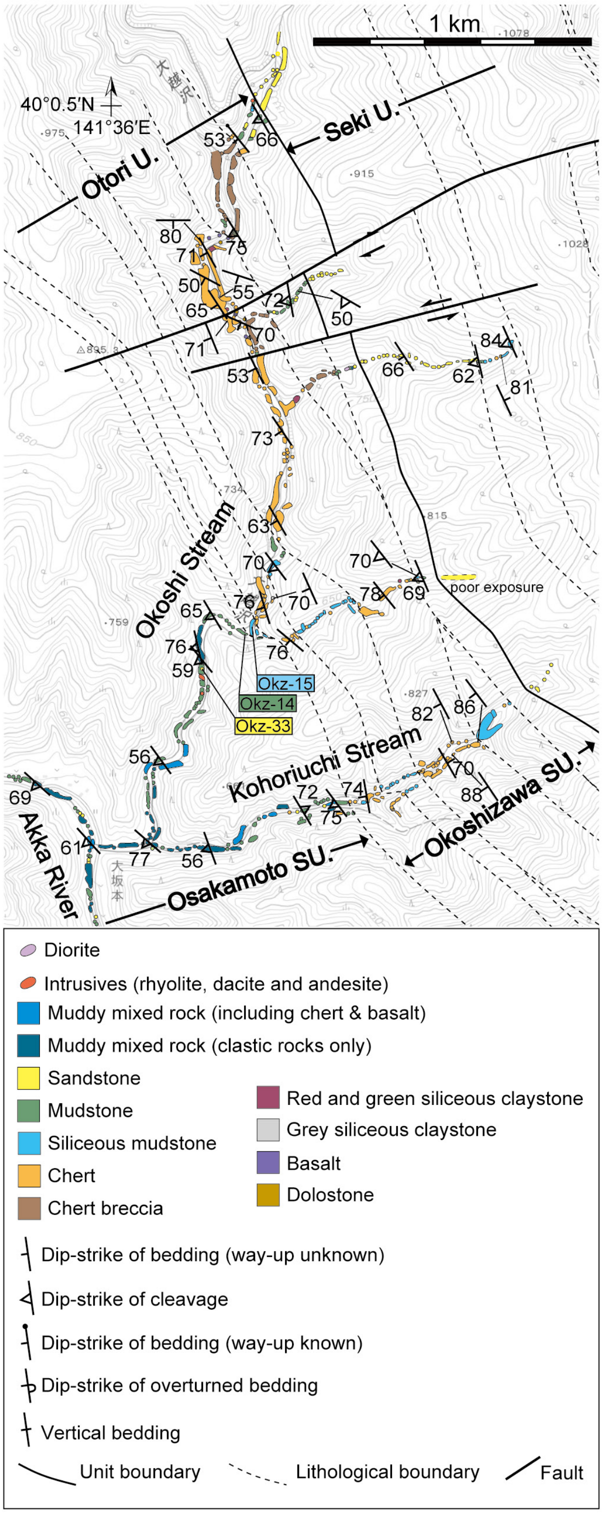

Fig. 4 Geological traverse map of Okoshi Stream, Akka, Iwaizumi Town (sampling locality of Okz-14). Modified from Muto *et al.* (2023). Localities of samples Okz-14 and -33 in Muto *et al.* (2023) are also shown. Base map produced from XYZ tiles provided by the Geospatial Information Authority of Japan.

eruption, resulting in a weighted average of 203.1 ± 1.2 Ma (Fig. 20).

4. 2. Otori Unit

Four tuff samples and three sandstone samples were analyzed in this study. From the northeast part of the Otori Unit, which is relatively well-studied and has been included in the Otori Unit by previous studies, one tuff sample (Okz-14) was analyzed. In this area, detrital zircons from sandstone blocks have been analyzed by Muto *et al.* (2023). The southwest part of the Otori Unit is much less studied and is combined into this unit for the first time. From this part of the unit, three tuff samples (Mna-01, Iwk-03, Szm-01) and three sandstone samples (Mtg-01, Mtg-09.5, Mtg-12) were analyzed.

4. 2. 1 Tuff (Okz-14, Mna-01, Iwk-03, Szm-01)

Sample Okz-14 was obtained from the northeast part of the Otori Unit in Okoshi Stream, a tributary of the Akka River in north Iwaizumi Town (Fig. 4). The rocks distributed around the locality are coherent chert–siliceous mudstone sequences and mixed facies of mudstone, chert and sandstone. Muto *et al.* (2023) named the former as the Okoshizawa Subunit and the latter as the Osakamoto Subunit. Muto *et al.* (2023) also reported radiolarians from siliceous mudstone and detrital zircons from sandstone along the same route. Sample Okz-14 was obtained from a white tuff bed in black mudstone that overlies a coherent chert–siliceous mudstone sequence (Figs. 4, 12B). In thin section, this sample is composed of quartz grains with low sphericity supported in a matrix composed of microcrystalline to cryptocystalline quartz and white micas (Fig. 15A, B). Part of the matrix appears to be pseudomorphs of felsic grains. Zircons and opaque minerals are present as accessory minerals. The tuff bed is in contact with radiolarian-bearing mudstone with a sedimentary boundary (Fig. 15A, B). Thirty zircon grains from sample Okz-14 were analyzed for U–Pb dating, all of which yielded concordant U–Pb ages (Fig. 18B; Table A2). All grains are accepted as grains indicating the age of eruption, resulting in a weighted average of 166.69 ± 0.95 Ma (Fig. 20).

Sample Mna-01 was obtained from the southwest part of the Otori Unit along the Minai River, a tributary of the Omoto River in northwest Iwaizumi Town (Fig. 5). The lithofacies around the locality is composed mainly of muddy mixed rocks, sandstone and bedded coherent mudstone. The latter two are considered to be blocks within muddy mixed rocks on scales of kilometres. Sample Mna-01 was collected from bedded tuffaceous mudstone within an outcrop composed mostly of mudstone (Figs. 5, 12C). In thin section, this sample is composed of mostly silt-sized grains and a matrix composed of microcrystalline to cryptocystalline quartz and clay minerals (Fig. 14D, E). The grains are largely quartz, but also include lithic fragments and plagioclase. Some of the quartz grains are shards that are angular and have low-sphericity.

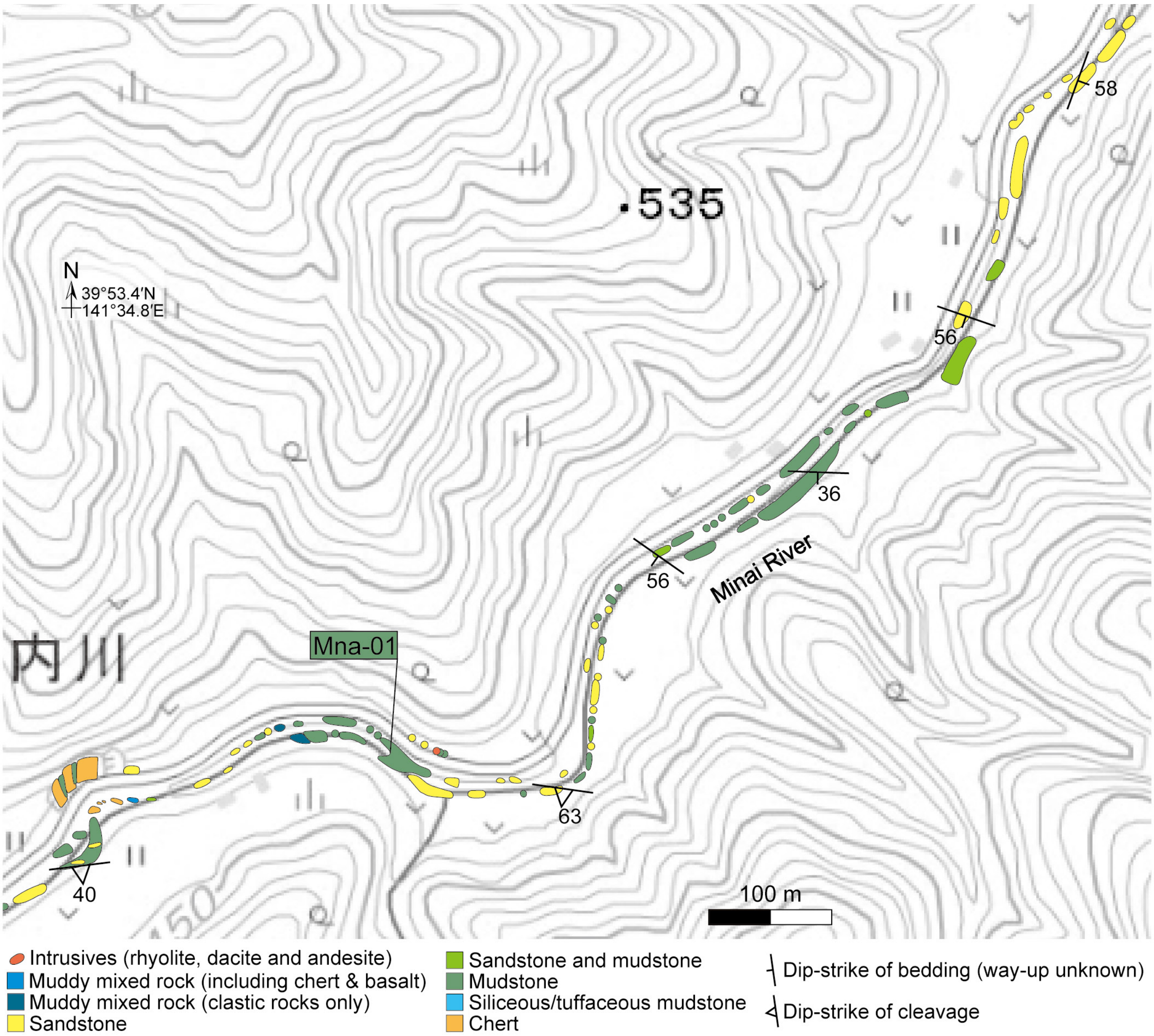

Fig. 5 Geological traverse map around Minaikawa, Kado, Iwaizumi Town (sampling locality of Mna-01). Base map produced from XYZ tiles provided by the Geospatial Information Authority of Japan.

Radiolarian tests and zircons are present as accessory components. The association of components imply that this sample was deposited as a mixture of volcanic tuff, detrital grains and radiolarian skeletons in the hemipelagic to trench area. Thirty zircon grains from sample Mna-01 were analyzed for U–Pb dating, all of which yielded concordant U–Pb ages (Fig. 18C; Table A3). Two has an age of ~1800 Ma and the age of all other grains are around 175 Ma (Fig. 18C). Twenty-five of the young zircons are accepted as grains indicating the age of eruption, resulting in a weighted average of 174.46 ± 0.93 Ma (Fig. 20).

Sample Iwk-03 was obtained from the southwest part of the Otori Unit in a locality south of Mt. Iwakura along Orikabe Stream, a tributary of the Mitakai River in northwest Iwaizumi Town (Fig. 6). The lithofacies around the locality is composed mainly of muddy mixed rocks, sandstone, chert and bedded coherent mudstone. The latter three are blocks within muddy mixed rocks on scales of kilometres. Sample Iwk-03 was collected from pale yellow bedded tuff, which is a minor lithological component in the area (Figs. 6, 12D). A radiolarian-yielding Mn-nodule sample was obtained close to sample Iwk-03 (Fig. 6) (Iwk-04; Muto *et al.*, 2025). The position of the sampled pale yellow tuff in the oceanic plate stratigraphy is not immediately obvious. However, this pale yellow tuff is closely associated with siliceous mudstone and mudstone in this route, implying that it can be roughly correlated to a position near the boundary between hemipelagic siliceous mudstone and trench-fill mudstone. In thin section, this sample is composed of two parts. The first part is composed mainly of quartz and lithic grains with clayey and siliceous matrix, and the second

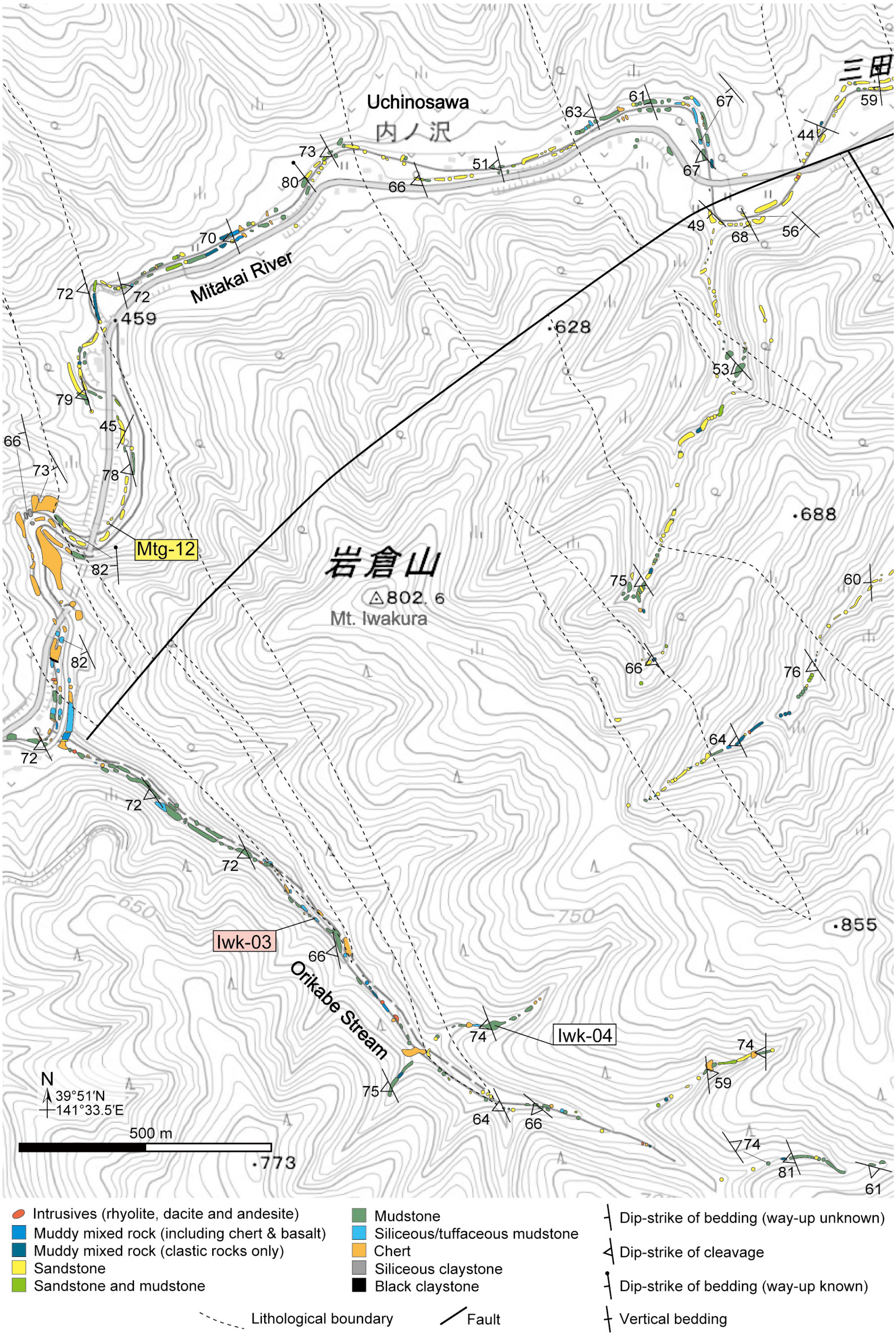

Uchinosawa
内ノ沢
三田
Mitakai River
Mt. Iwakura
岩倉山
△802.6
Orikabe Stream
Mtg-12
Iwk-03
Iwk-04
·459
·628
·688
·855
·773
N
39°51′N
141°33.5′E
500 m
Intrusives (rhyolite, dacite and andesite)
Muddy mixed rock (including chert & basalt)
Muddy mixed rock (clastic rocks only)
Sandstone
Sandstone and mudstone
Mudstone
Siliceous/tuffaceous mudstone
Chert
Siliceous claystone
Black claystone
Dip-strike of bedding (way-up unknown)
Dip-strike of cleavage
Dip-strike of bedding (way-up known)
Vertical bedding
Lithological boundary
Fault

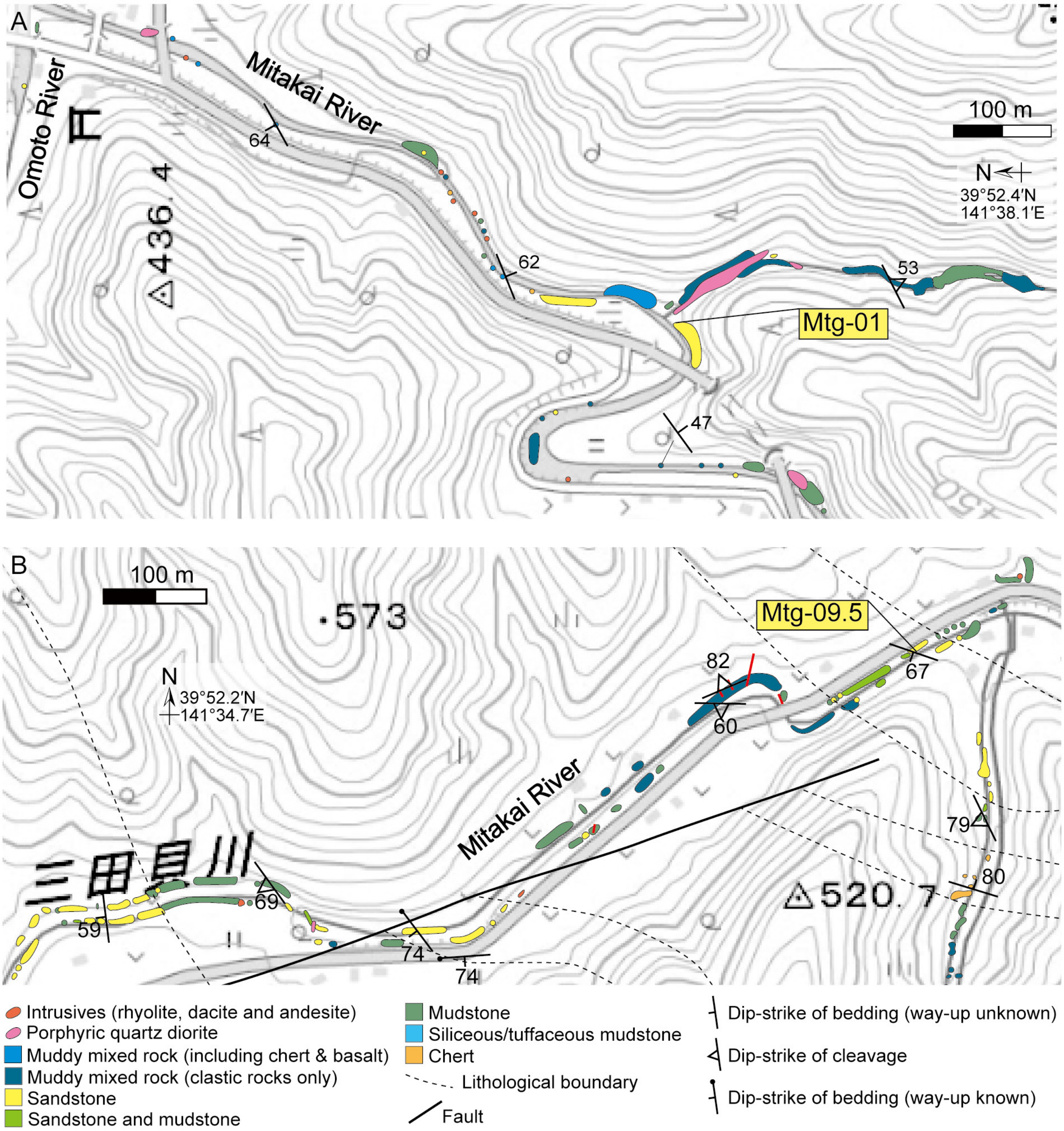

Fig. 7 Geological traverse maps of the Mitakai River around (A) the junction with the Omoto River (sampling locality of Mtg-01) and (B) Mitakai (sampling locality of Mtg-09.5), both in Kado, Iwaizumi Town. Base map produced from XYZ tiles provided by the Geospatial Information Authority of Japan.

(← p. 58)
Fig. 6 Geological traverse map around Mt. Iwakura, Kamatsuta-Gongen, Iwaizumi Town (sampling locality of Iwk-03 and Mtg-12). Sample locality of Muto *et al.* (2025) is also shown. Base map produced from XYZ tiles provided by the Geospatial Information Authority of Japan.

part is composed mainly of quartz grains supported in a matrix of microcrystalline and cryptocrystalline quartz and white mica (Fig. 14F, G). Comparing this with other samples of known stratigraphic position, it is supported that this lithofacies belongs to the hemipelagic interval of the oceanic plate stratigraphy, probably in its upper part. Thirty zircon grains from sample Iwk-03 were analyzed for U–Pb dating, all of which yielded concordant U–Pb ages (Fig. 18D; Table A4). The age of two of them is ~220

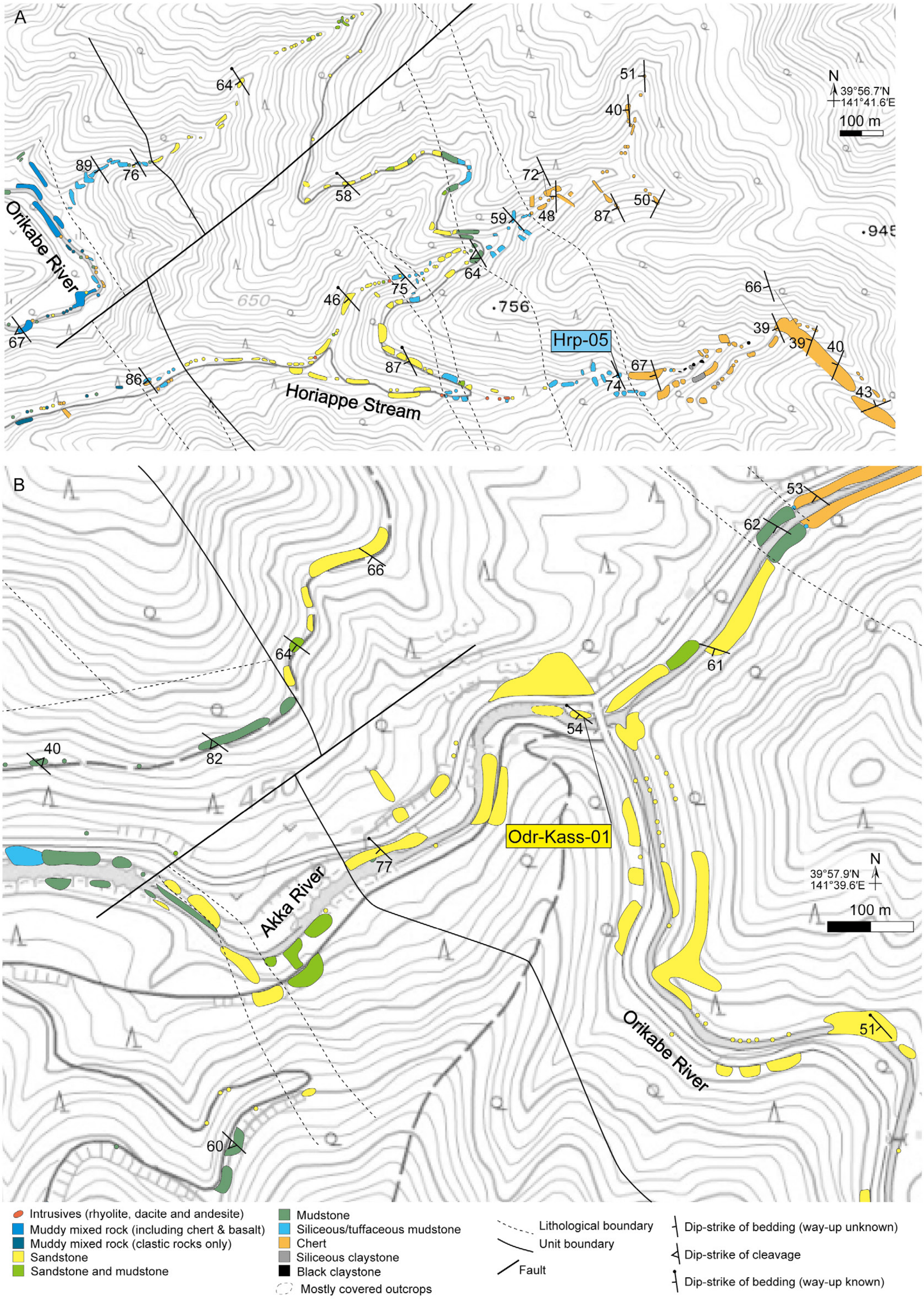
A
N
39°56.7'N
141°41.6'E
100 m
Orikabe River
Horiappe Stream
Hrp-05
650
.756
.945
B
Akka River
Orikabe River
Odr-Kass-01
450
N
39°57.9'N
141°39.6'E
100 m
Intrusives (rhyolite, dacite and andesite)
Muddy mixed rock (including chert & basalt)
Muddy mixed rock (clastic rocks only)
Sandstone
Sandstone and mudstone
Mudstone
Siliceous/tuffaceous mudstone
Chert
Siliceous claystone
Black claystone
Mostly covered outcrops
Lithological boundary
Unit boundary
Fault
Dip-strike of bedding (way-up unknown)
Dip-strike of cleavage
Dip-strike of bedding (way-up known)

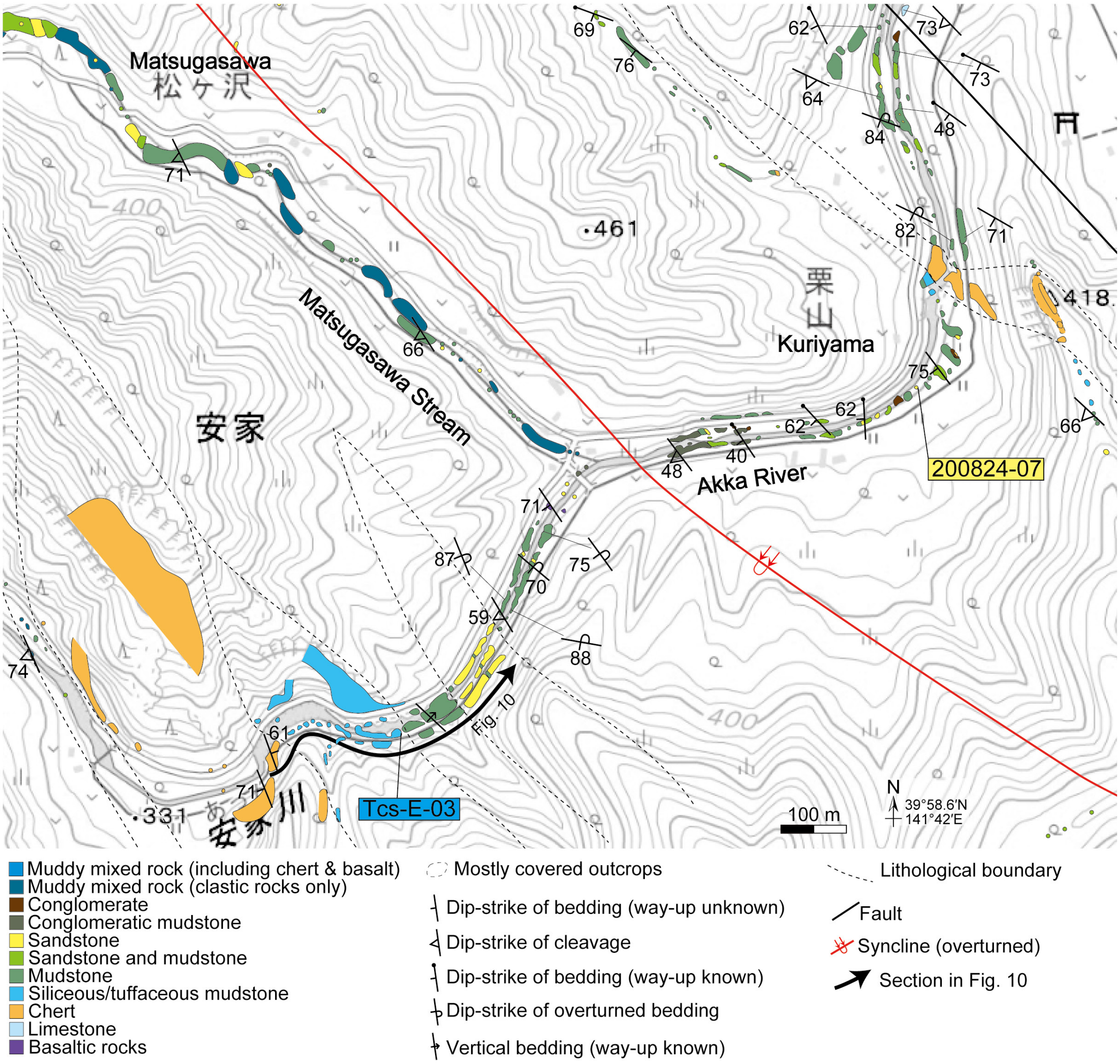

Fig. 9 Geological traverse map around Kuriyama, Akka, Iwaizumi Town (sampling locality of Tcs-E-03 and 200824-07). The route along which Fig. 10 was measured is shown. Base map produced from XYZ tiles provided by the Geospatial Information Authority of Japan.

(← p. 60)

Fig. 8 Geological traverse maps of (A) Horiappe Stream (sampling locality of Hrp-05) and (B) the junction of the Akka and Orikabe Rivers (sampling locality of Odr-Kass-01), both in Akka, Iwaizumi Town. Base map produced from XYZ tiles provided by the Geospatial Information Authority of Japan. Note that the exposures in the northeast edge of (B) have been altered due to construction.

Ma and the age of all other grains cluster around 175 Ma (Fig. 18D). All grains in this cluster is accepted as grains indicating the age of eruption, resulting in a weighted average of 174.87 ± 0.78 Ma (Fig. 20).

Sample Szm-01 was obtained from the southwest part of the Otori Unit along Chinzawa Stream, a tributary of the Minai River in northwest Iwaizumi Town (Fig. 3B). The lithofacies around the locality is composed mainly of mudstone with smaller amounts of sandstone and chert as blocks in matrix. Sample Szm-01 was collected from a horizon of mudstone with abundant tuff layers within an outcrop composed mostly of mudstone (Fig. 3B). In thin section, this sample is composed of mostly silt-sized

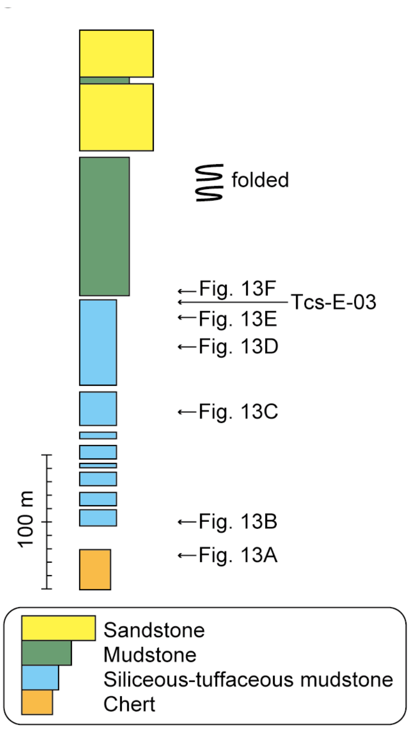

Fig. 10 Apparent stratigraphic column of the chert–clastic sequence at the sampling locality of Tcs-E-03.

grains of quartz, opaque minerals, apatite, plagioclase and zircon, in this general order of abundance (Fig. 14H–K). These grains are supported in a matrix composed of microcrystalline to cryptocrystalline quartz and white mica. Part of the quartzose and micaceous matrix appear to be pseudomorphs of felsic grains. The tuff layers have a sharp sedimentary base and grades upwards into mudstone (Fig. 14H). The tuff-poor parts in the sample were too thin to be trimmed and were thus included in zircon extraction. Thirty zircon grains from sample Szm-01 were analyzed for U–Pb dating, of which twenty-nine yielded concordant U–Pb ages (Fig. 18E; Table A5). Despite tuff-poor parts being included in the sample processing, all grains are accepted as grains indicating the age of eruption, resulting in a weighted average of 171.9 ± 1.6 Ma (Fig. 20).

4. 2. 2 Sandstone (Mtg-01, Mtg-09. 5, Mtg-12)

Sample Mtg-01 was obtained along the Mitakai River near its junction with the Omoto River in northwest Iwaizumi Town (Fig. 7A). The lithofacies around this locality is composed mainly of mixed mudstone and sandstone with irregular boundaries and poorly developed cleavage. These rocks of the Jurassic accretionary complex are intruded by many dyke rocks, most of which are andesites or porphyric quartz diorites. Sample Mtg-01 was obtained from a massive sandstone outcrop surrounded

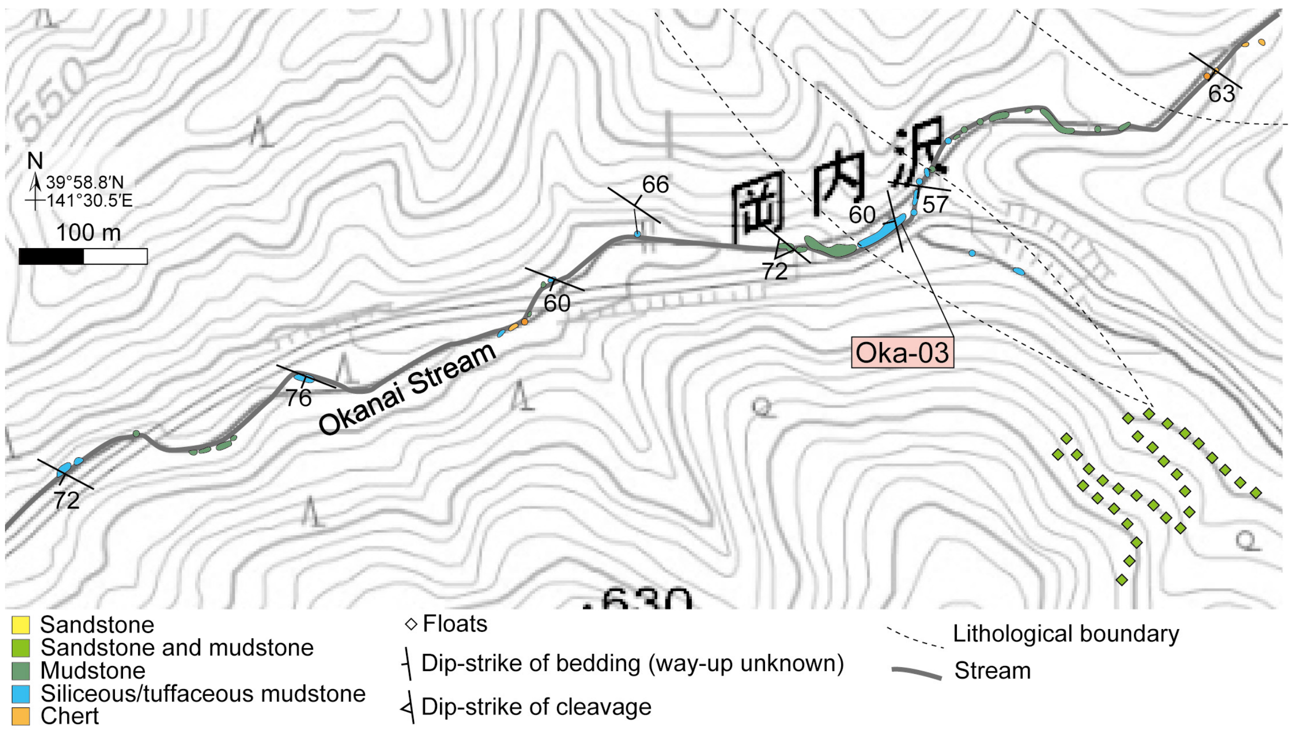

Fig. 11 Geological traverse map of Okanai Stream, Ekari, Kuzumaki Town (sampling locality of Oka-03). Base map produced from XYZ tiles provided by the Geospatial Information Authority of Japan. The actual flow of the stream is different from that on the base map and is indicated in dark grey.

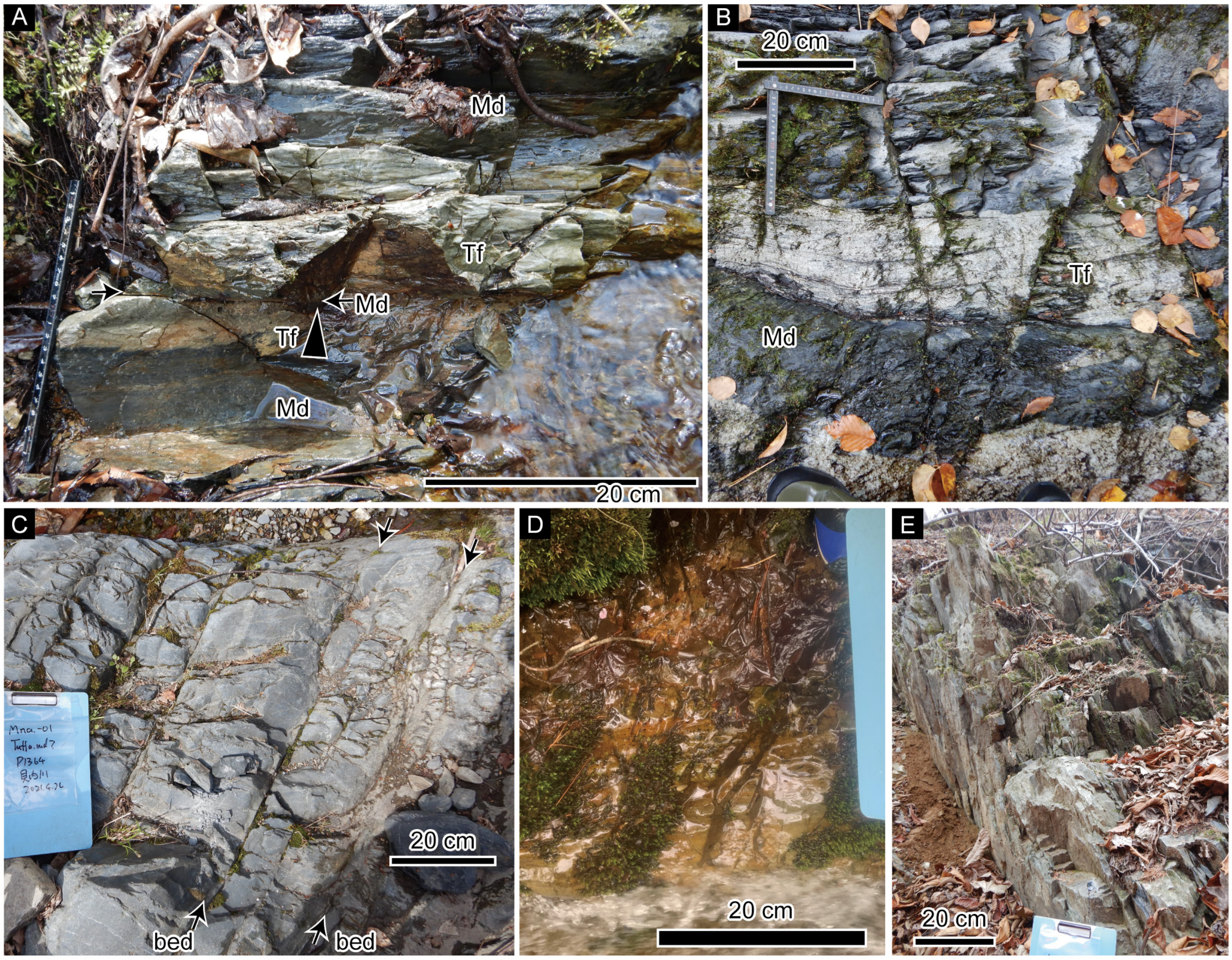

Fig. 12 Outcrop photographs of analyzed tuffs and associated lithologies. (A) Tuff bed in mudstone (sample Udg-06). Black triangle indicates grading of tuff into mudstone. (B) Tuff bed in mudstone (sample Okz-14). (C) Tuffaceous mudstone (sample Mna-01). Bedding planes are indicated by arrows labeled as "bed". (D) Bedded pale yellow tuff (sample Iwk-03). (E) Tuff in siliceous mudstone (sample Hrp-05).

by mixed rocks of mudstone and sandstone (Fig. 7A). This sample consists mainly of medium grains of quartz, plagioclase and lithic fragments and also contains accessory components such as zircons (Fig. 17A). Sixty zircon grains were analyzed for U–Pb dating, all of which yielded concordant U–Pb ages (Fig. 19F; Table A6). The majority of grains fall within the Permian, accompanied by grains of Carboniferous through Cambrian and pre-Cambrian age (Fig. 19D, E). The YC1σ age is calculated from eleven grains and has a weighted average of 254.1 ± 1.5 Ma (Fig. 19E).

Sample Mtg-09.5 was obtained along the Mitakai River, west of Mitakai Settlement in northwest Iwaizumi Town (Fig. 7B). The lithofacies around this locality is composed mainly of sandstone partly interbedded with mudstone, mudstone, mixed facies of mudstone and sandstone, and chert. Sandstone and chert are tectonic blocks in mixed facies at the scale of kilometres. Sample Mtg-09.5 was obtained from an outcrop of bedded sandstone with mudstone interbeds (Figs. 16A). This sample consists mainly of medium grains of quartz, plagioclase and lithic fragments. Sixty-two zircon grains were analyzed for U–Pb dating, all of which yielded concordant U–Pb ages (Fig. 19I; Table A10). The majority of grains fall within the late Permian to Jurassic, accompanied by grains of Cambrian and pre-Cambrian age (Fig. 19G, H). The late Cenozoic grains seem to consist of several clusters with populations around 170 Ma, 190 Ma, 220 Ma and 260 Ma (Fig. 19H). The YC1σ age is calculated from fifteen grains, the largest number of grains in a youngest cluster of detrital zircons in this study, and has a weighted average of 168.1 ± 1.0 Ma (Fig. 20).

Sample Mtg-12 was obtained along the Mitakai River west of Mt. Iwakura in northwest Iwaizumi Town (Fig. 6). This locality is close to the locality of the tuff sample Iwk-03, and the lithofacies around this locality is explained in the previous text. Sample Mtg-12 was obtained from an outcrop of bedded sandstone with black mudstone

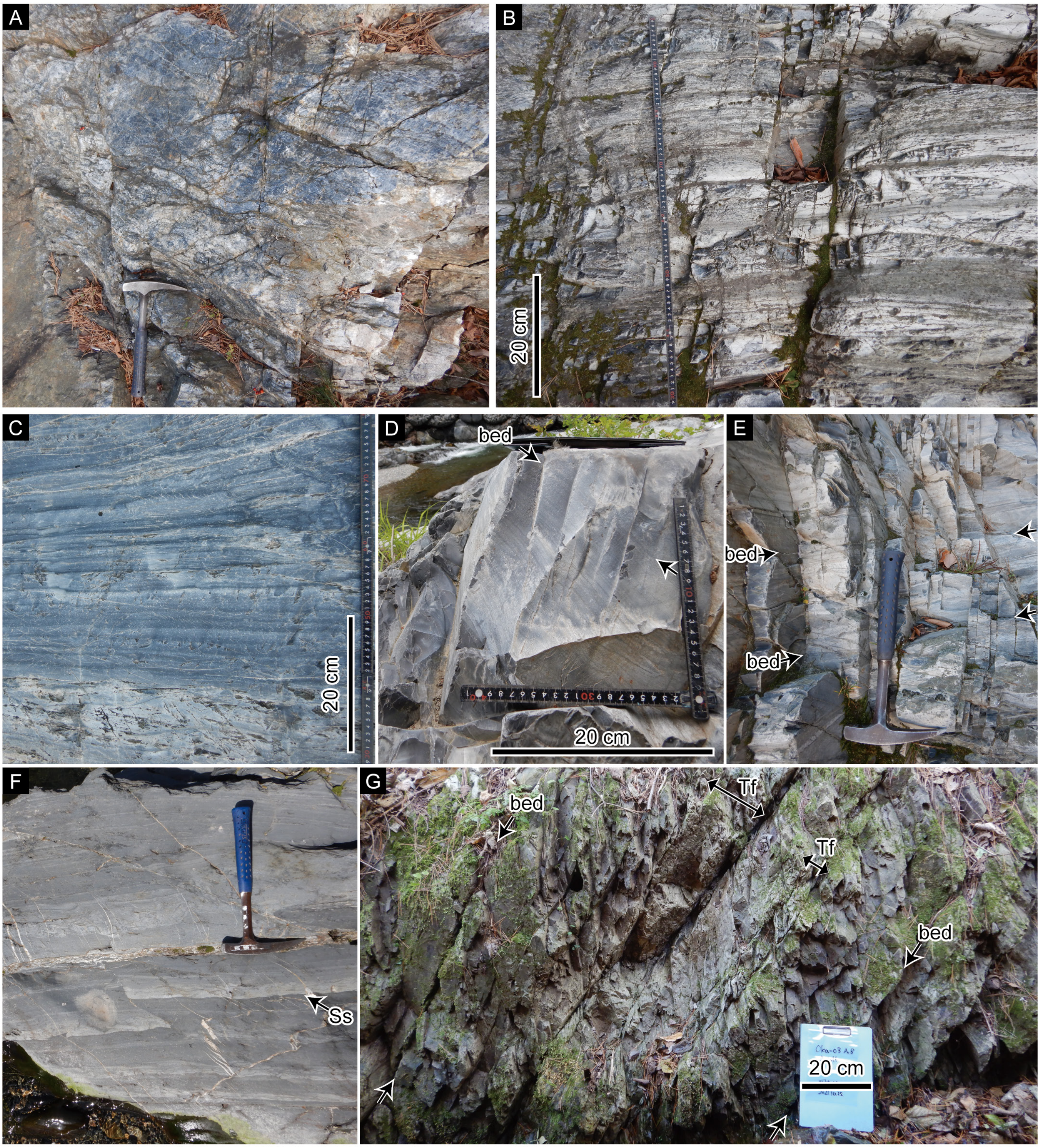

Fig. 13 Outcrop photographs of analyzed tuffs and associated lithologies. (A) Chert below sample Tcs-E-03. (B) Siliceous mudstone below sample Tcs-E-03. (C) Tuffaceous mudstone below sample Tcs-E-03. Intermediate lithofacies between B and D. (D, E) Tuff. Same lithology as sample Tcs-E-03. (F) Black mudstone with sandstone layers (Ss) above sample Tcs-E-03. (G) Siliceous mudstone with tuff beds (Oka-03). Bedding planes are indicated by arrows labeled as "bed". See Fig. 10 for location of A–F. The hammer is 33 cm long.

(→ p. 65)

Fig. 14 Thin section micrographs of analyzed tuffs. Figures C, E, G and K were taken with cross-polarized light and all others with transmitted plane-polarized light. (A–C) Tuff sample Udg-06, same field of view for B and C. (D, E) Tuffaceous mudstone sample Mna-01, same field of view. (F, G) Tuff sample Iwk-03, same field of view. (H–K) Tuff sample Szm-01, same field of view for G and H. Ap: apatite; LiTf: lithic tuff; Md: mudstone part; Pl: plagioclase; QV: quartz vein; Qz: quartz; Rad: radiolarian tests; Tf: tuff part; Zrn: zircon. Scale bars are 0.5 mm.

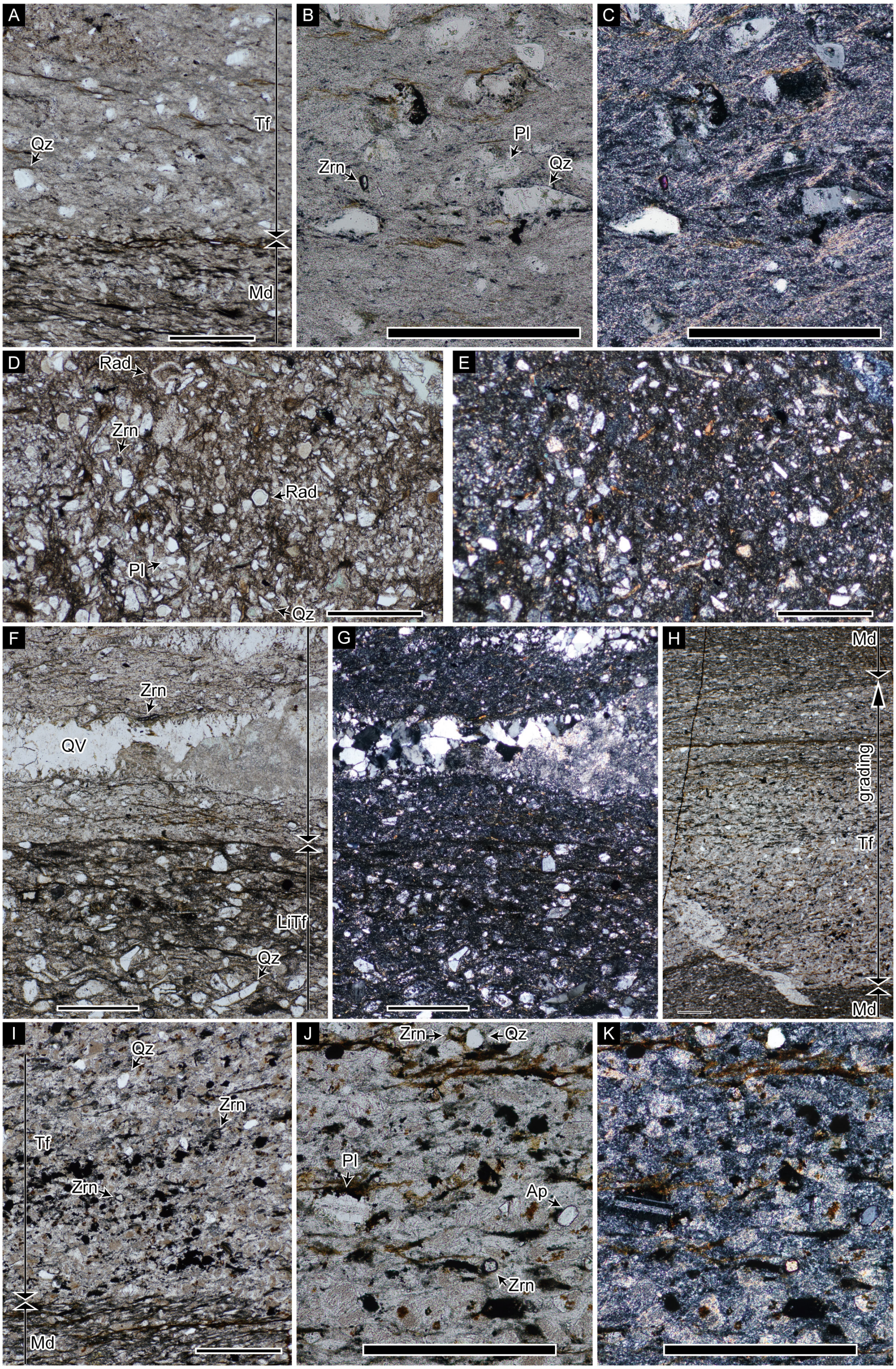
A
Tf
Qz
Md
B
Pl
Zrn
Qz
C
D
Rad
Zrn
Rad
Pl
Qz
E
F
Zrn
QV
LiTf
Qz
G
H
Md
grading
Tf
Md
I
Qz
Zrn
Tf
Zrn
Md
J
Zrn
Qz
Pl
Ap
Zrn
K

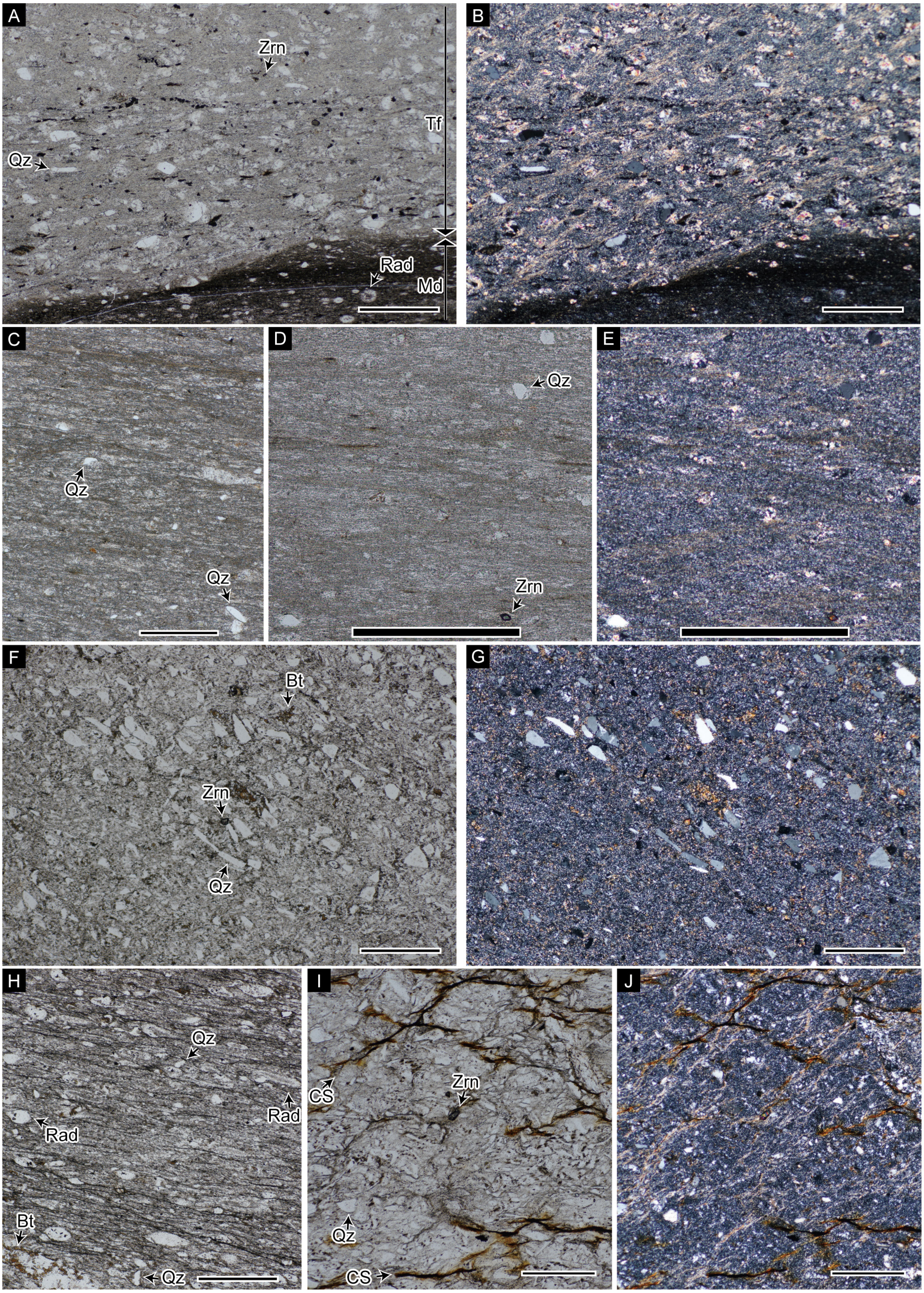
A
Zrn
Qz
Tf
Rad
Md
B
C
Qz
Qz
D
Qz
Zrn
E
F
Bt
Zrn
Qz
G
H
Qz
Rad
Rad
Bt
Qz
I
CS
Zrn
Qz
CS
J

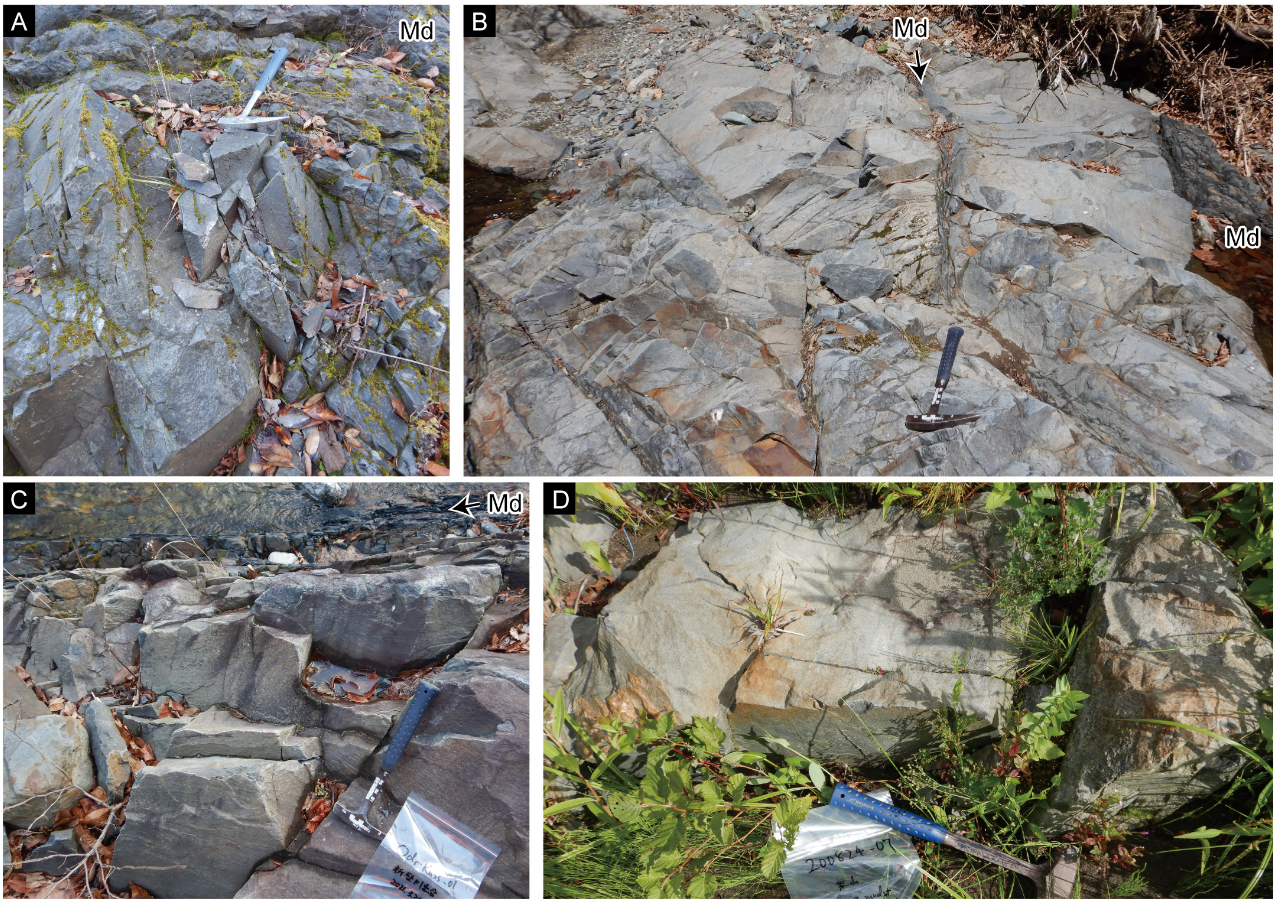

Fig. 16 Outcrop photographs of analyzed sandstones. (A) Sample Mtg-09.5. (B) Sample Mtg-12. Md: mudstone beds. (C) Sample Odr-Kass-01. (D) Sample 200824-07. The pick hammer in A–C is 33 cm long and the crack hammer in D is 40 cm long.

interbeds (Figs. 6, 16B). This sample consists mainly of grains of quartz, plagioclase and lithic fragments and also contains accessory components such as zircons (Fig. 17B). A large part of the grains is of medium size, but the sample is somewhat poorly sorted. Sixty zircon grains were analyzed for U–Pb dating, all of which yielded concordant U–Pb ages (Fig. 19L; Table A8). The majority of grains fall within the Permian to Jurassic, accompanied by grains of older Paleozoic and pre-Cambrian age (Fig. 19J, K). The late Cenozoic grains seem to consist of several populations, with peaks around 170–180, 190, 220 and 260 Ma (Fig. 19K). The YC1σ age is calculated from only two grains that belong to the youngest of these peaks and has a weighted average of 172 ± 27 Ma (Fig. 20).

(← p. 66)

Fig. 15 Thin section micrographs of analyzed tuffs. Figures B, E, G and J were taken with cross-polarized light and all others with transmitted plane-polarized light. (A, B) Tuff sample Okz-14, same field of view. (C, D, E) Tuff sample Hrp-05, same field of view for D and E. (F, G) Tuff sample Tcs-E-03, same field of view. (H) Siliceous mudstone below sample Tcs-E-03 (Fig. 13B). (I, J) Tuff sample Oka-03, same field of view. Bt: biotite; CS: clay seams; Md: mudstone part; Qz: quartz; Rad: radiolarian tests; Tf: tuff part; Zrn: zircon. Scale bars are 0.5 mm.

4. 3. Seki Unit

4. 3. 1 Tuff (Hrp-05)

This sample was obtained from the Horiappe Stream, a tributary of the Orikabe River in northeast Iwaizumi Town (Fig. 8A). The sample comes from a chert–clastic sequence composed mainly of bedded chert, grey siliceous mudstone and bedded sandstone in ascending order, which characterizes the Seki Unit (Fig. 8A). Grey siliceous mudstone is associated with grey mudstone which contains only minor amounts of radiolarian tests. However, the two rock types are usually not easily distinguished in the field, so both are included in one lithofacies as grey siliceous mudstone. Black to dark grey mudstone is partly present at the top of the grey siliceous mudstone. The analyzed sample is a grey tuff obtained from the lower part of the grey siliceous mudstone (Figs. 8A, 12E. It is composed of fine-grained white micas and microcrystalline to cryptocrystalline quartz matrix and contains minor amounts of quartz grains and

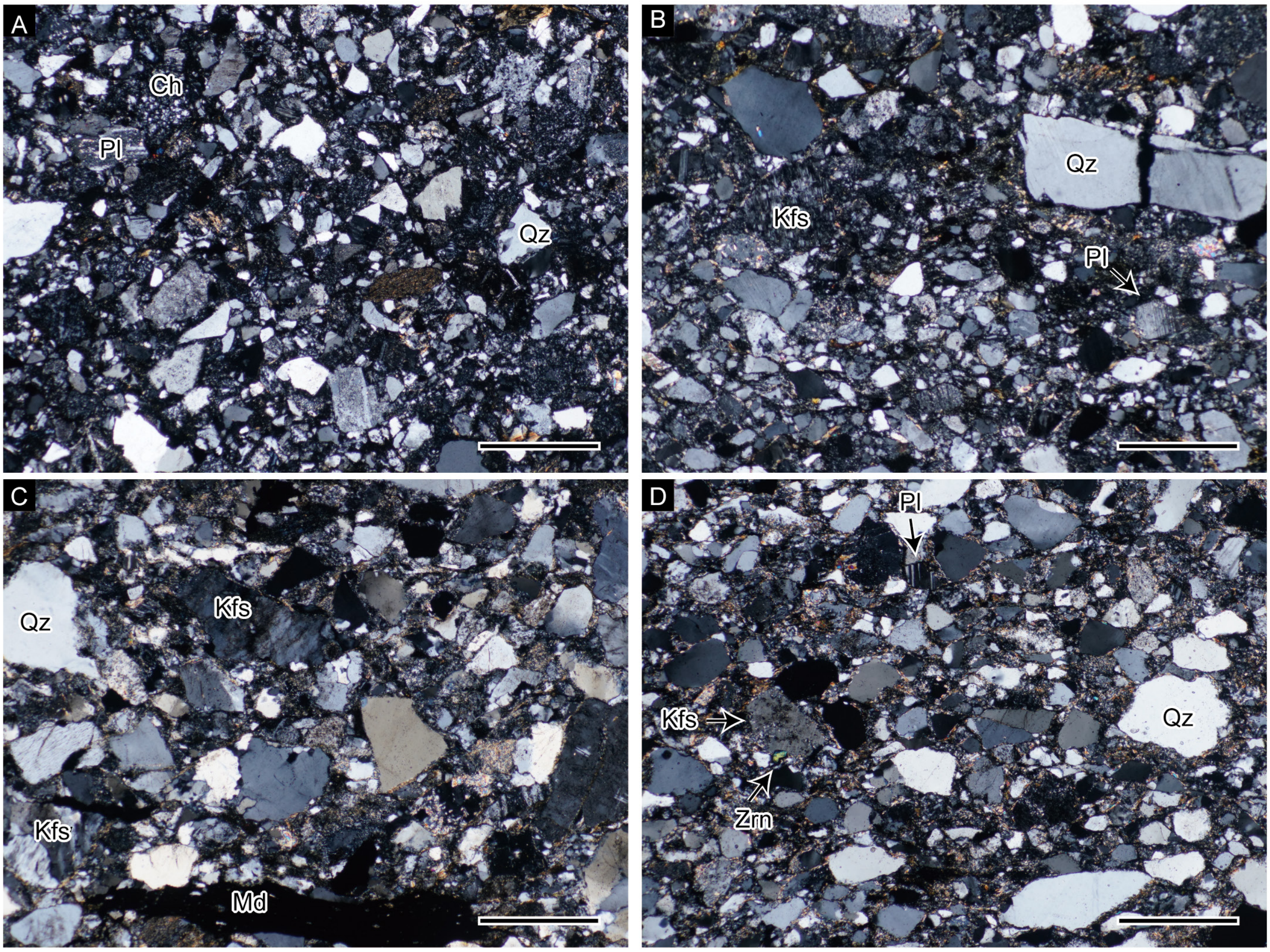

Fig. 17 Thin section micrographs of analyzed sandstones. All photographs were taken with cross-polarized light. (A) Sample Mtg-01. (B) Sample Mtg-12. (C) Sample Odr-Kass-01. (D) Sample 200824-07. Ch: chert fragment; Kfs: K-feldspar; Md: mudstone fragment; Pl: plagioclase; Qz: quartz; Zrn: zircon. Scale bars are 0.5 mm.

small zircons (Fig. 15C–E). Thirty zircon grains were analyzed for U–Pb dating, all of which yielded concordant U–Pb ages (Fig. 18F; Table A9). Most ages are gathered around 165 Ma, while six grains are distinctly younger (Fig. 18F). The young ages were obtained from zircons that were cracked during laser ablation. Twenty-two of the cluster are accepted as grains indicating the age of eruption, resulting in a weighted average of 167.4 ± 1.1 Ma (Fig. 20).

4. 3. 2 Sandstone (Odr-Kass-01)

This sample was collected at the junction of the Orikabe and Akka rivers in northeast Iwaizumi Town (Fig. 8B). The chert–clastic sequence of the Seki Unit, much like that in Horiappe Stream mentioned above but lacking the grey siliceous mudstone, is exposed around this locality. The sample was taken from an outcrop of bedded, normal-grading sandstone with intercalated black mudstone, (Figs. 8B, 16C). This sample consists mainly of medium grains of quartz, K-feldspars, plagioclase and lithic fragments and also contains accessory components such as zircons (Fig. 17C). Lithic fragments include mudstone clasts, which are easily observed also at the outcrop. Sixty-four zircon grains were analyzed for U–Pb dating, of which sixty-two yielded concordant U–Pb ages (Fig. 19O; Table A10). The zircon age spectra show that the majority of grains have Triassic to Jurassic ages, while a small number of Permian, Devonian and pre-Cambrian zircons are present (Fig. 19M, N). The Triassic to Jurassic grains seems to consist of several clusters, with peaks around 180, 190 and 220 Ma (Fig. 19N). The YC1σ age is calculated from only three grains that sit outside these main peaks and has

(→ p. 69)

Fig. 18 Concordia diagrams of zircon ages from tuffs. (A) Udg-06, Kadoma Unit. Red ellipses are concordant ages and black dashed ellipses are discordant ages. (B) Okz-14, Otori Unit. (C) Mna-01, Otori Unit. (D) Iwk-03, Otori Unit. (E) Szm-01, Otori Unit. (F) Hrp-05, Seki Unit. (G) Tcs-E-03, Takayashiki Unit. (H) Oka-03, Ekari Unit. Figures were produced by Isoplot/Ex 4.15 (Ludwig, 2012).

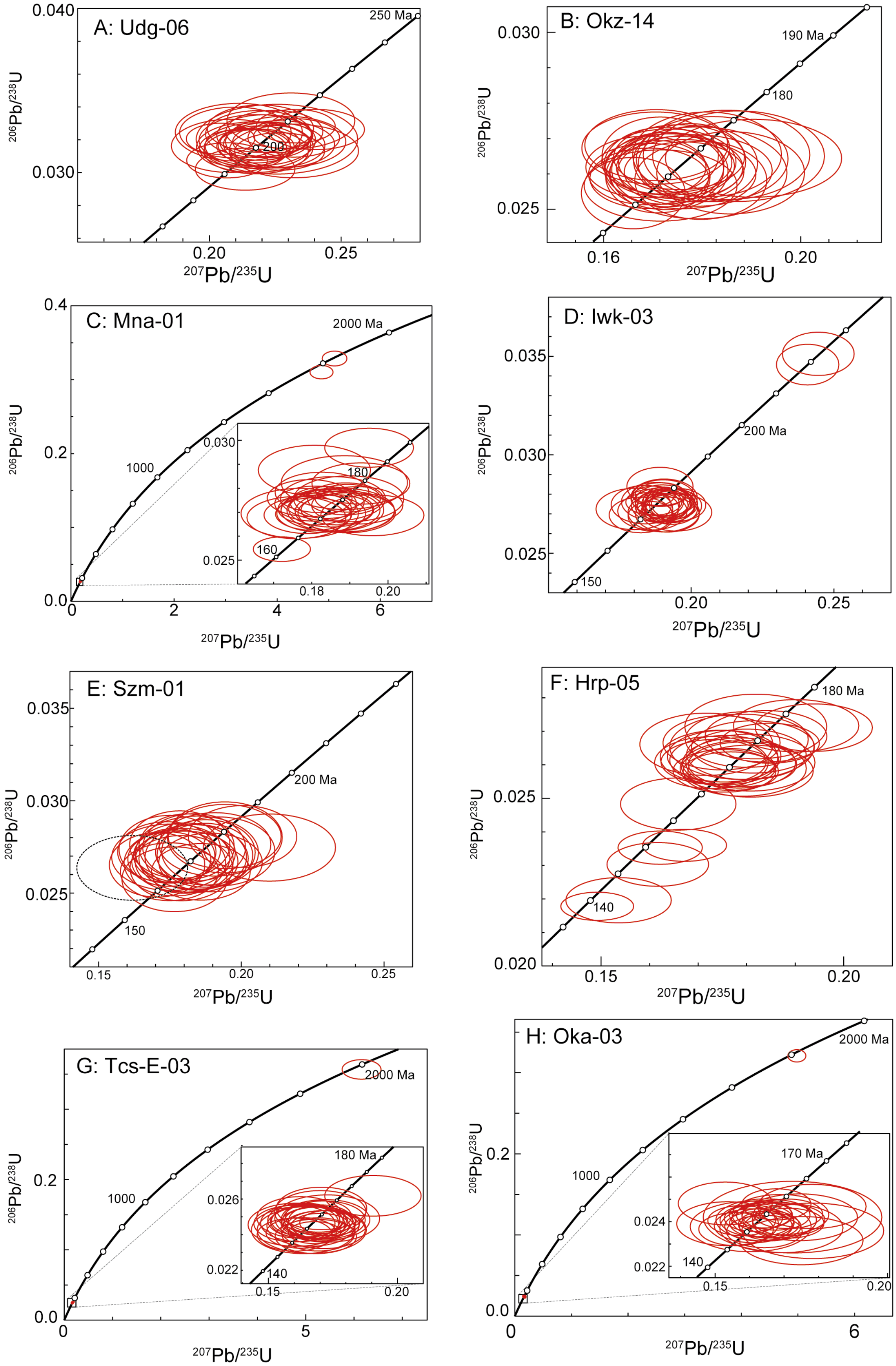
A: Udg-06
250 Ma
200
0.040
0.030
0.20
0.25
206Pb/238U
207Pb/235U
B: Okz-14
190 Ma
180
0.030
0.025
0.16
0.20
206Pb/238U
207Pb/235U
C: Mna-01
2000 Ma
1000
0.4
0.2
0.0
0
2
4
6
0.030
0.025
180
160
0.18
0.20
206Pb/238U
207Pb/235U
D: Iwk-03
200 Ma
150
0.035
0.030
0.025
0.20
0.25
206Pb/238U
207Pb/235U
E: Szm-01
200 Ma
150
0.035
0.030
0.025
0.15
0.20
0.25
206Pb/238U
207Pb/235U
F: Hrp-05
180 Ma
140
0.025
0.020
0.15
0.20
206Pb/238U
207Pb/235U
G: Tcs-E-03
2000 Ma
1000
180 Ma
140
0.026
0.022
0.15
0.20
0.2
0.0
0
5
206Pb/238U
207Pb/235U
H: Oka-03
2000 Ma
1000
170 Ma
140
0.024
0.022
0.15
0.20
0.2
0.0
0
6
206Pb/238U
207Pb/235U

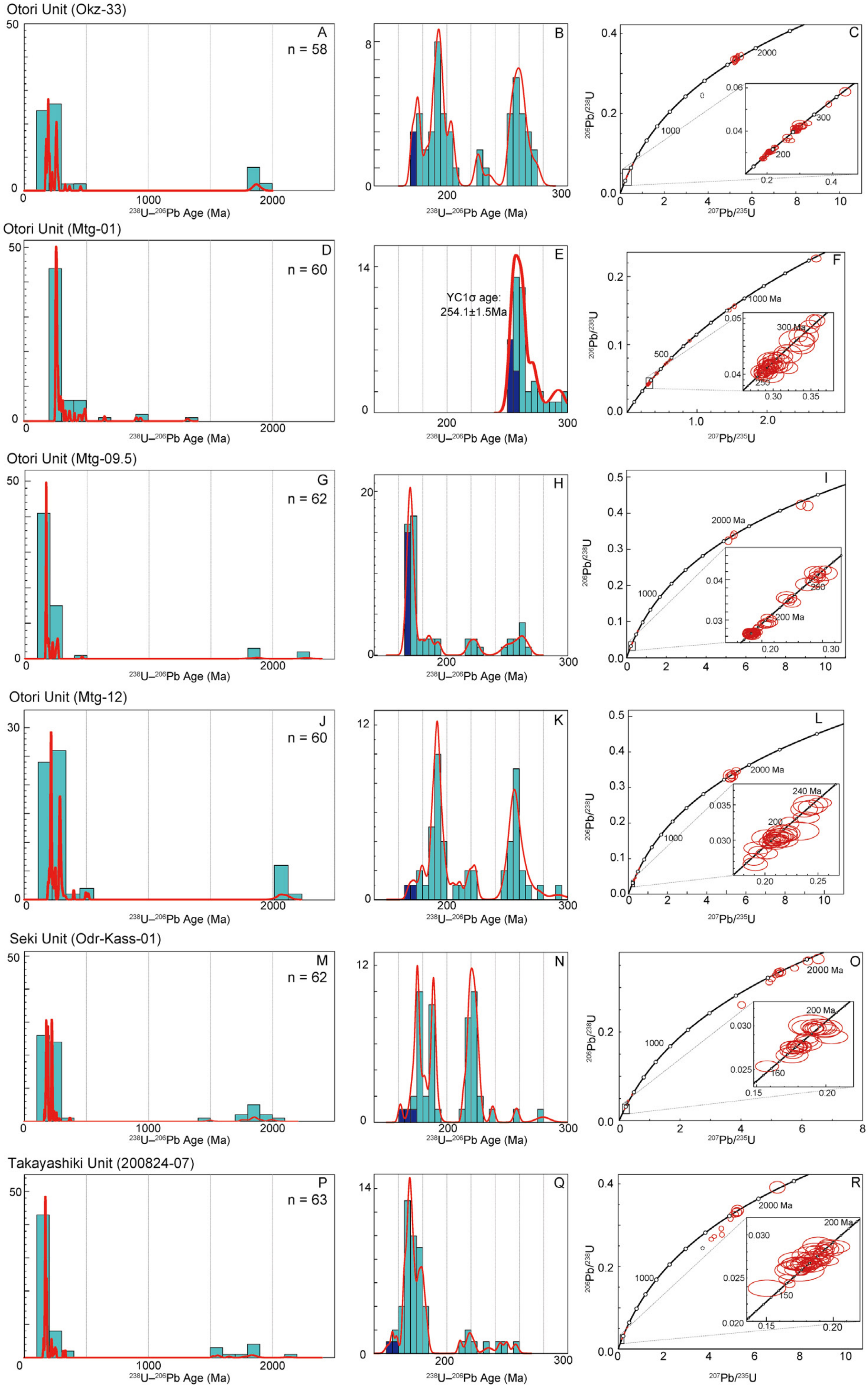
Otori Unit (Okz-33)
A
n = 58
B
C
Otori Unit (Mtg-01)
D
n = 60
E
YC1σ age:
254.1±1.5Ma
F
Otori Unit (Mtg-09.5)
G
n = 62
H
I
Otori Unit (Mtg-12)
J
n = 60
K
L
Seki Unit (Odr-Kass-01)
M
n = 62
N
O
Takayashiki Unit (200824-07)
P
n = 63
Q
R
238U–206Pb Age (Ma)
206Pb/238U
207Pb/235U
2000 Ma
1000
200 Ma

a weighted average of 171.4 ± 2.2 Ma (Fig. 20).

4. 4. Takayashiki Unit

Samples from the Takayashiki Unit was obtained from outcrops along the Akka River near Kuriyama Settlement, Iwaizumi Town, Iwate Prefecture (Fig. 9). This route is the type locality of the Takayashiki Unit. Chert, siliceous mudstone, bedded tuff, mudstone, sandstone, conglomerate and muddy mixed rocks are the main lithofacies distributed in the area and forms a tight syncline (Fig. 9). The lithofacies is generally a broken facies on scales of kilometres, and therefore strata on the two limbs of folds may not be exact equivalents, also suggested by some differences in lithofacies. On scales of hundreds of metres or less, characters such as chert–clastic sequences and sedimentary structures indicate coherent facies.

4. 4. 1 Tuff (Tcs-E-03)

This sample is a dark brownish grey tuff from a chert–clastic sequence (Fig. 9). The chert–clastic sequence is composed in ascending order of bedded chert, siliceous mudstone, tuff, mudstone and sandstone (Figs. 10, 13A–F). The general coarsening upward and layers with graded bedding (Fig. 13F), flame structures or burrows mainly in mudstone indicate a coherent facies, although folds of metre-scale or smaller are present. Siliceous mudstone and tuff in this sequence is not easily distinguished from each other in the field. They are both bedded, either dark grey to pale grey depending on the condition of the outcrop surface, hard and have conchoidal fractures similar to chert (Fig. 13B–E). End members can be clearly distinguished in thin section: siliceous mudstone contains abundant radiolarian tests (Fig. 15H), while tuff contains abundant angular mineral fragments in microcrystalline quartz matrix (Fig. 15F, G). On the other hand, there are intermediate varieties making it even harder to draw a line between siliceous mudstone and tuff in the field. Contact metamorphism probably by subsurface plutons, represented by the formation of biotite (Fig. 15F–H) may also be contributing to the difficulty. Due to the above, siliceous mudstone, tuff and intermediate lithofacies (tuffaceous mudstone) are here not distinguished in classification of lithofacies in the field.

The investigated sample was obtained from the top of the siliceous mudstone–tuff sequence and is overlain by mudstone with sandstone and tuff layers (Fig. 10). In thin section, it is composed of angular, poorly sorted quartz grains supported in a matrix of microcrystalline quartz, white mica and biotite (Fig. 15F, G). The form of many quartz grains are thin and sharp shards. Part of the quartzose and micaceous matrix appears to be pseudomorphs of felsic grains. Thirty zircon grains were analyzed for U–Pb dating, all of which yielded concordant U–Pb ages (Fig. 18G; Table A11). One grain has an age of ~2000 Ma and the age of all other grains cluster around 156 Ma (Fig. 18G). Twenty-eight of the cluster are accepted as grains indicating the age of eruption, resulting in a weighted average of 156.39 ± 0.92 Ma (Fig. 20).

4. 4. 2 Sandstone (200824-07)

This sample was collected from an outcrop of bedded sandstone within mudstone, broken alternation of sandstone and mudstone, and conglomerate (Figs. 9, 16D). This lithofacies composed of mudstone and coarse clastic rocks is situated above a sequence of chert, siliceous mudstone and mudstone to the north. Thus, the sample comes from the clastic part of a chert–clastic sequence. This sample consists mainly of medium grains of quartz, K-feldspars, plagioclase and lithic fragments and also contains accessory components such as zircons (Fig. 17D). Sixty-four zircon grains were analyzed for U–Pb dating, of which sixty-three yielded concordant U–Pb ages (Fig. 19R; Table A12). The majority of the grains fall within the Jurassic, accompanied by grains of Triassic, Permian, Carboniferous and pre-Cambrian age (Fig. 19P, Q). The Jurassic grains seems to consist of at least three populations, centred around 150, 170 and 180 Ma (Fig. 19Q). The YC1σ age is calculated from only two grains and has a weighted average of 154 ± 17 Ma (Fig. 20).

4. 5. Ekari Unit

One tuff sample from the Ekari Unit was investigated in this study. No sandstone samples were investigated.

The analyzed sample (Oka-03) was obtained in Okanai Stream, a tributaty of the Mabechi River in Ekari, southeast Kuzumaki Town, Iwate Prefecture (Fig. 11). The lithofacies around the locality is composed of mudstone, siliceous and tuffaceous mudstone, chert and broken facies of mudstone and sandstone, although exposures are limited. Sample Oka-03 was collected from a white tuff bed intercalated in bedded grey siliceous mudstone (Fig. 13G). The sample is composed of silt-sized quartz including shards with low roundness and sphericity supported in a matrix of microcrystalline to cryptocrystalline quartz and white mica (Fig. 15I, J). Part of the quartzose and micaceous matrix appear to be

(← p. 70)

Fig. 19 (A, B, D, E, G, H, J, K, M, N, P, Q) Probability density plot of concordant zircon ages from sandstone. (A, D, G, J, M, P) All grains. (B, E, H, K, N, Q) Late Phanerozoic grains. (C, F, I, L, O, R) Concordia diagrams of zircon ages from sandstone. Red ellipses are concordant ages and black dashed ellipses are discordant ages. (A–C) Okz-33, Otori Unit. (D–F) Mtg-01, Otori Unit. (G–I) Mtg-09.5, Otori Unit. (J–L) Mtg-12, Otori Unit. (M–O) Odr-Kass-01, Seki Unit. (P–R) 200824-07, Takayashiki Unit. The youngest cluster determined by overlaps of 1σ error (YC1σ) is shown with deep blue in the histograms of young grains. Red lines indicate relative probability. Figures were produced by Isoplot/Ex 4.15 (Ludwig, 2012). Data for sample Okz-33 are reillustrated from Muto *et al.* (2023).

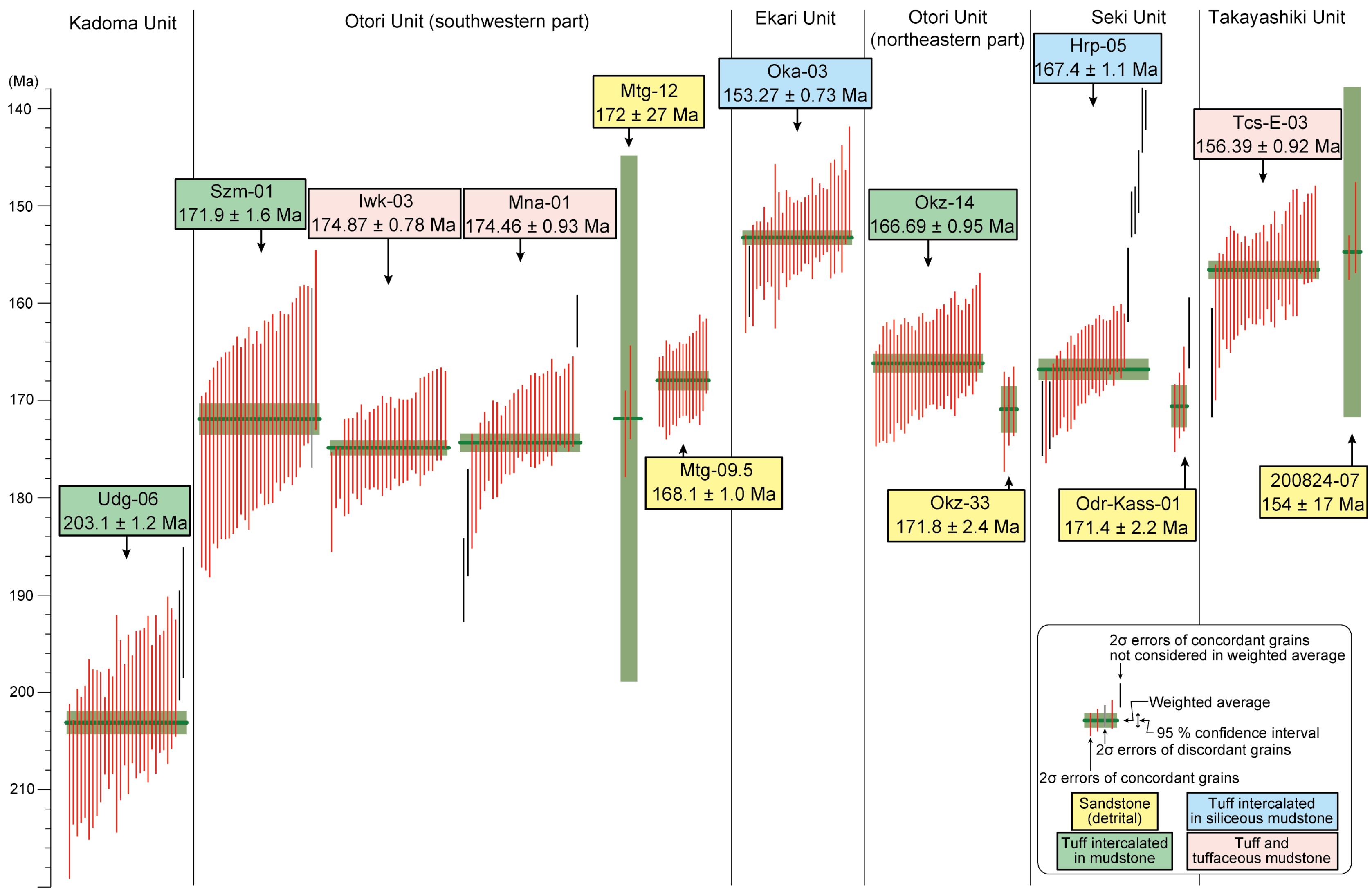

Fig. 20 Weighted average of zircons from tuffs and youngest clusters in sandstones. Samples are arranged in general order of geographic distribution. Figures were produced by Isoplot/Ex 4.15 (Ludwig, 2012). MSWD (mean square weighted deviation) for each sample is Oka-03: 1.08; Tcs-E-03: 0.86; 200824-07: 1.4; Hrp-05: 2.0; Odr-Kass-01: 0.59; Okz-14: 0.50; Mna-01: 1.2; Iwk-03: 1.00; Szm-01: 0.63; Okz-33: 0.24; Mtg-09.5: 0.27; Mtg-12: 1.7; Udg-06: 0.79. Data for sample Okz-33 are reillustrated from Muto *et al.* (2023).

pseudomorphs of felsic grains. Biotite of metamorphic origin are present, especially around clayey seams. Thirty zircon grains were analyzed for U–Pb dating, all of which yielded concordant U–Pb ages (Fig. 18H; Table A13). One has an age of ~1800 Ma and the age of all other grains cluster around 155 Ma (Fig. 18H). Twenty-eight of the cluster are accepted as grains indicating the age of eruption, resulting in a weighted average of 153.27 ± 0.73 Ma (Fig. 20).

5. Trench-arrival age of the Jurassic accretionary complex in the North Kitakami Belt

The geochronological data in this study and radiolarians from Mn-nodules reported in this issue (Muto *et al.*, 2025) provide new information on the tectonostratigraphic division of the Jurassic accretionary complex of the North Kitakami Belt. Here, I compile data that can constrain the trench-arrival age (TAA) from the main part of the northern Kitakami Mountains (Fig. 21). The compilation covers nine tectonostratigraphic units. More information is available for the seven units distributed around the Kado District, owing to the larger number of studies that conform to the concept of plate tectonics. These are the Kayamori, Takayashiki, Seki, Otori, Misugo and Kadoma units that structurally overlie one another in this order, and the Ekari Unit. Two other units in the eastern part, the Magisawa and Akashika units, are based on coherent formations defined by Sugimoto (1974) and Minoura and Tsushima (1984). They were adopted as accretionary tectonostratigraphic units in more recent works, but studies of their characters as accretionary complexes are very few. In this chapter, I will first discuss units with new data in this study and compare them with previous age data. Following this, I will give an overview on the trend of TAA across the North Kitakami Belt in the main part of the northern Kitakami Mountains.

5. 1. Tectonostratigraphic units with new data in this study

The TAA of the Kadoma Unit has been estimated in the Sotoyama and Hayachine San districts to the southwest of the Kado District (Matsuoka, 1988; Kawamura *et al.*, 2013; Uchino, 2017; Uchino, 2019; Osaka *et al.*, 2023). These studies showed that the Kadoma Unit has a TAA from the Early Jurassic or possibly late Late Triassic to the late Middle Jurassic with a younging trend towards the northeast (oceanward) direction (Fig. 21). On the other hand, the present study identified a tuff bed in mudstone that has a Rhaetian (end-Triassic) age from the northeast margin of the Kadoma Unit (Figs. 20, 21). While the confirmation of a latest Triassic TAA is in accordance with previous data, the occurrence of the oldest accretionary units in the northeast margin is unexpected. This implies that the internal structure of the Kadoma Unit is not a simple one in which younger accretionary complexes are progressively stacked towards the present oceanward direction.

The TAA of the northeast part of the Otori Unit was constrained from radiolarians from Mn-nodules in siliceous mudstone that indicate the Bajocian to Bathonian (Suzuki *et al.*, 2007b; Ehiro *et al.*, 2008; Muto *et al.*, 2023). The tuff sample Okz-14 from mudstone has a Bathonian age compatible with the radiolarian age (Fig. 21B). In contrast, the detrital zircons analyzed by Muto *et al.* (2023) has a YC1σ age ~5 Myr older (Fig. 20). Muto *et al.* (2023) suggested that the YC1σ age may be close to the depositional age. However, since sandstone is expected to be younger than siliceous mudstone in the concept of oceanic plate stratigraphy, the YC1σ age of sandstone probably does not record its depositional age. In the case of this particular sample, even the youngest single zircon is probably older than the depositional age (Fig. 20).

The TAA of the southwest part of the Otori Unit is constrained by three tuff samples of late Toarcian to Aalenian age and the sandstone sample Mtg-09.5 with a Bathonian YC1σ age (Fig. 21B). The YC1σ age of sample Mtg-09.5 is consistent with data from tuffs, and hence is likely close to its depositional age. In addition, this sample has a youngest cluster consisting of fifteen grains (~25 % of total grains), much more than in other sandstone samples. The YC1σ age of the sandstone sample Mtg-12 is not in direct contradiction with these data, but will not be considered further for TAA because of its large uncertainty. The sandstone sample Mtg-01 yielded a latest Permian YC1σ age, which is calculated from the young portion of a prominent Permian population (Fig. 19D). This age is unlikely to represent TAA considering other data from the Otori Unit. Notably, this sample is unique in containing Mesoproterozoic and Neoproterozoic grains (Fig. 19). Perhaps sample Mtg-01 has a very small portion of grains from Mesozoic provenances, so that Mesozoic grains were undetected, while in other samples, Mesoproterozoic and Neoproterozoic grains were undetected due to dilution from Mesozoic provenances.

The position of the tuffs from the southwest part of the Otori Unit in the oceanic plate stratigraphy is the upper part of the hemipelagic siliceous mudstone interval for Iwk-03, siliceous mudstone to mudstone interval for Mna-01 and the mudstone interval for sample Szm-01. The U–Pb age of these samples, that of the sandstone sample Mtg-09.5, and the age of mudstone indicated by radiolarians from Mn-nodules (Muto *et al.*, 2025) is completely consistent with the stratigraphic order assumed from the lithology of the samples (Fig. 21B). Two Mn-nodules from grey bedded mudstone that contains mostly clay-sized detrital grains and only rare silt-sized ones (Fig. 7E of Muto *et al.*, 2025) yielded Aalenian to Bajocian radiolarians (Muto *et al.*, 2025). This lithology is likely to represent the lower portion of trench-fill clastic rocks. This interval corresponds to or is close to where tuff samples Iwk-03 and Mna-01 are derived from, which is in accordance with the late Toarcian to early Aalenian U–Pb age of the tuffs (Fig. 21B). The mudstone hosting sample Szm-01 and sandstone represented by sample Mtg-09.5 are from successively higher horizons, in good agreement with the respective Aalenian and Bajocian

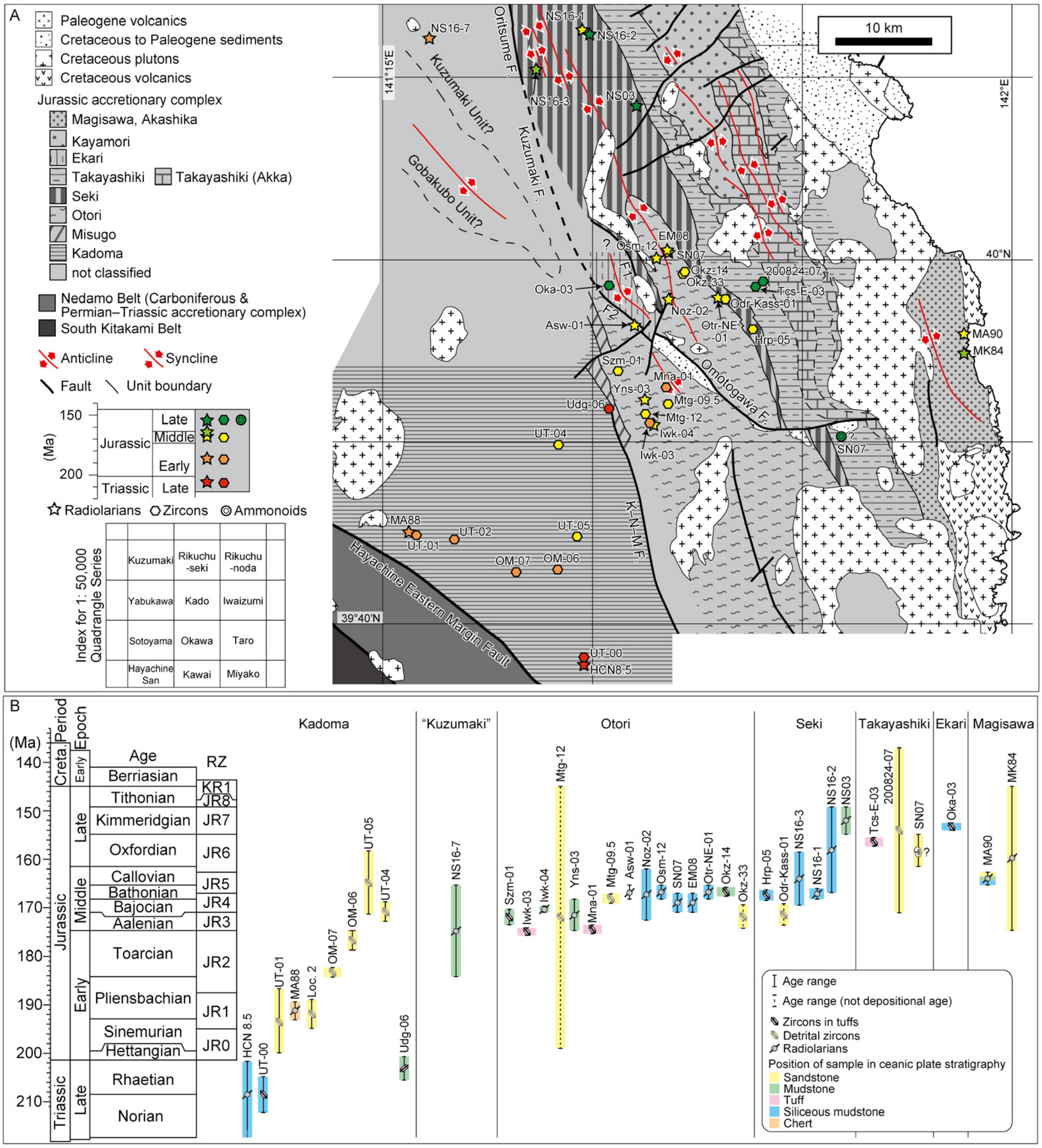

Fig. 21 (A) Constraints on the accretionary age of the North Kitakami Belt plotted on a simplified geological map of the main part of the North Kitakami Belt. Vertical and horizontal lines show the border grid of the 1: 50,000 quadrangle maps. As a useful key horizon, the palaeo-seamount comprising the Akka Limestone and its basement mafic rocks is differentiated from the rest of the Takayashiki Unit and shown as "Takayashiki (Akka)". The Kuzumaki and Gobakubo units (based respectively on Nakae *et al.*, 2021 and Ehiro *et al.*, 2008) are not well studied and hence not officially classified here. The Misugo Unit is only recognized in the Kado District, but may extend further. K–N–M F.: Kamatsuta–Natsuya–Michimata Fault. (B) Data in figure A shown with uncertainties and position of sample in the oceanic plate stratigraphy against the international chronostratigraphy (2023 version; Cohen *et al.*, 2013; updated). HCN8.5: Fig. 8.5 of Kawamura *et al.* (2013); UT-00: Uchino *et al.* (2017) (Loc. 0 of Osaka *et al.*, 2023); UT-01, 02, 04: Uchino (2019) (Locs. 1, 2 and 4 respectively therein); UT-05: Uchino (2021) (Loc. 5 therein, Loc. 3 in Osaka *et al.*, 2023, close to but not the same as Loc. 3 of Uchino, 2019); MA88: Matsuoka (1988); MA90; Matsuoka and Oji (1990); EM08: Ehiro *et al.* (2008); MK84; Minoura and Tsushima (1984); NS16: Nakae (2016), following number indicates locality number therein; NS03: Nakae and Kamada (2003); OM-06, OM-07: Osaka *et al.* (2023); SN07: Suzuki *et al.* (2007b); Okz-33: Muto *et al.* (2023); Iwk-04, Yns-03, Asw-01: Muto *et al.* (2025). RZ: radiolarian biozone.

or Bathonian ages (Fig. 21B). A Mn-nodule sample from mudstone that has possibly experienced tectonic mixing (Asw-01) yielded late Bajocian radiolarians, and is regarded to indicate the age of either mudstone or siliceous mudstone (Muto *et al.*, 2025). The former case seems more favourable considering that the structural position of this locality is apparently close to samples Mna-01 and Mtg-09.5 that indicate trench-fill clastic deposition during the Bajocian. However, a decisive conclusion is suspended, partly because geological structures around the locality of sample Asw-01 is somewhat complex. Regardless, it is safe to conclude that the southwest part of the Otori Unit consists of an oceanic plate that moved into the hemipelagic zone in the late Toarcian to Aalenian and passed into the trench during the Aalenian to Bathonian.

Based on the above, the entire Otori Unit, despite its wide distribution, has a TAA within a short window between the Aalenian to Bathonian. There appears to be a slight younging trend of TAA within the Otori unit towards the structurally lower part (Fig. 21), implying that imbricate structures during accretion is preserved in the unit. Further data constraining the entire span of depositional age of hemipelagic to trench-fill sedimentary rocks in different parts of the Otori Unit are desired in order to confirm this trend.

The TAA of the Seki Unit was constrained from siliceous mudstone that has a range from the Bathonian to Kimmeridgian and mudstone of Kimmeridgian age (Nakae and Kamada, 2003; Nakae, 2016). The tuff sample Hrp-05 from siliceous mudstone is Bathonian, consistent with the above (Fig. 21). On the other hand, the YC1σ age of detrital zircons from sandstone is ~4 Myr older (Fig. 20). As in the case of sample Okz-33 of the Otori Unit, the YC1σ age of sandstone probably does not record its depositional age. In contrast, the youngest single zircon in the sandstone sample (161.5 ± 3.3 Ma) is younger than the age of the tuff sample and may be close to the depositional age of the sandstone (Fig. 20). In sum, the TAA of this unit has a range from the Bathonian to Kimmeridgian.

The Takayashiki Unit was estimated to have an Oxfordian TAA based on an ammonoid bearing float (Suzuki *et al.*, 2007a). New data in this study indicate that the tuff between the hemipelagic and trench-fill strata was deposited in the late Oxfordian and the sandstone around the early Kimmeridgian or younger, although uncertainties are large (Figs. 20, 21). While the new data do not contradict with the previous age by the ammonoid bearing float, the ammonoid occurrence needs to be treated with great caution. Firstly, the origin of the float is quite obscure. Not only is the sample a float, but the description of the collected site is not consistent between authors. Onuki (1956) wrote that the specimen was collected in a stream southeast of the Iwaizumi Electric Powerplant, which is to the west of the junction of the Soiri and Omoto rivers (p.139 therein), but Suzuki *et al.* (2007), incorporating personal communications, stated that the float was collected to the east of the said junction (p.166 therein). Secondly, detailed surveys of the Takayashiki Unit have never reported the occurrence of macrofossil-bearing sandstones (Sugimoto, 1974, 1980; Takahashi *et al.*, 2016; Nakae *et al.*, 2021). Due to the above, I consider that the present zircon data are the only robust age constraints for the TAA.

The TAA of the Ekari Unit is constrained by the tuff from siliceous mudstone that has a Kimmeridgian age. This unit must have arrived at the trench shortly following this time, around the end of the Jurassic. This age is much younger than the accretionary age of the Otori Unit that is distributed next to the Ekari Unit with fault contacts. In fact, it is even younger than known hemipelagic or clastic rocks of the Takayashiki Unit, which is the youngest accretionary complex in the study area. Because younger accretionary complexes are accreted tectonically below older ones, the present juxtaposition of Ekari Unit to the Otori Unit can be attributed to vertical displacement by the bounding faults (F1 and F2 in Fig. 21A), although deformation structures showing the sense of displacement have not been found. This is the first time that an accretionary complex correlative to the Takayashiki Unit or younger units has been identified west of the boundary between the Takayashiki and Seki units. The lithofacies of the Ekari Unit has shared characteristics with the Takayashiki Unit such as the wide distribution of mudstone with broken beds of sandstone. However, there are also distinct differences, such as the abundance of conglomerate and basaltic rocks that is only widely distributed in the Takayashiki Unit. Therefore, the two are treated as separate units in the present study.

5. 2. Trends of trench-arrival age in the North Kitakami Belt

From compilation of available data, it is confirmed that a large part of the North Kitakami Belt in the northern Kitakami Mountains is composed of accretionary units that generally become older towards the southwest in terms of TAA (Fig. 21A). The TAA of adjacent units appears to be separated by very short gaps or even overlapping. For example, the age of mudstone in the Seki and Takayashiki units overlaps around the Kimmeridgian and the age of siliceous mudstone in the Seki and Otori units overlap in the Bathonian (Fig. 21). In addition, the TAA of the Otori and Kadoma units probably overlaps around the Aalenian to Bathonian, even though the Misugo Unit lies between them. Accordingly, the boundary of tectonostratigraphic units cannot simply be explained as temporal gaps in the formation of accretionary prisms. Rather, the boundaries are related to sudden changes in the lithology of accretionary complexes and/or post-accretion juxtaposition of accretionary complexes with different lithologies.

The general structure of tectonostratigraphic units being stacked in the NE–SW direction is interrupted by structures of smaller scales, mostly due to kilometre-scale folds and faults (Fig. 21A). These include sets of synclines and anticlines in the Kado District and to its north, many of which have been previously recognized (e.g., Sugimoto, 1974). In addition, this study identified faults with vertical displacements that caused the Ekari Unit to be uplifted from its original structurally lower position ("F1" and "F2" in Fig. 21A). The F1 fault was regarded as an extension of the Kuzumaki Tectonic Line/Fault (Sugimoto, 1974; Onuki, 1981), but this is not followed here because the nature of these faults are quite different. The F2 fault was shown by Onuki (1969) as the Kunizakaitoge Fault. Of the F1 and F2 faults, the latter with the larger displacement is tentatively regarded as an extension of the Oritsume Fault, which is an active fault, and the Kuzumaki Fault sensu Nakae (2018) and Nakae *et al.* (2021) (Fig. 21A). The Oritsume and Kuzumaki faults cut between the Seki Unit and the "Kuzumaki Unit" (see next paragraph for notes on this unit) and the Oritsume Fault is the segment that was reactivated in the late Neogene. If the assumption that the F2, Kuzumaki and Oritsume faults are connected is correct, this fault is a major geological structure cutting more than 30 km through the North Kitakami Belt. Faults with vertical displacements like the F1 and F2 faults have not received much attention in the past, but they may be important in understanding the geological structure of the North Kitakami Belt. New data of the eastern margin of the Kadoma Unit revealed a significant reversal in the trend of TAA in the unit (Fig. 21). This may be due to folds or faults similar to those explained above. In fact, the sampled locality is very close to the Kamatsuta–Natsuya–Michimata Fault, which cuts the eastern margin of the Kadoma Unit in the area (Fig. 21A). However, currently available information on geological structure is not sufficient to clarify why the TAA of the northeastern margin of the Kadoma Unit is so old.

The area to the east and northwest of the Kado District is poorly studied in terms of the tectonic history of accretionary complexes. Below is a brief summary of the current status. In the eastern area near the Pacific coast, the Magisawa and Akashika units can be recognized from lithostratigraphic formations established originally by Sugimoto (1974). Sugimoto originally defined another formation, the Koshimeguri Formation, above the Magisawa Formation, but the two were combined by Minoura and Tsushima (1984), which was followed by Ehiro *et al.* (2008). The Magisawa and Akashika units cannot yet confidently be correlated to accretionary units further inland and are maintained as distinct units herein. The Magisawa Unit yielded Middle Jurassic radiolarians from siliceous mudstone and alternating mudstone and sandstone (Matsuoka and Oji, 1990) and Middle or Late Jurassic radiolarians from mudstone intercalated in bedded sandstone (Minoura and Tsushima, 1984). This, along with the lithofacies of the Magisawa Unit which is characterized by coherent sequences of chert, siliceous mudstone, mudstone and sandstone, suggest that the unit may correspond to the Seki Unit. On the other hand, the structurally lower Akashika Unit contains limestone and greenstone, and therefore may correspond to the Takayashiki Unit. However, proof of this correlation awaits additional data from the Magisawa and Akashika units. In the area northwest of the Kado District, the Kuzumaki and Gobakubo formations were recognized before the acceptance of plate tectonics by researchers (Iwai *et al.*, 1964). These formations have been translated to tectonostratigraphic units of accretionary complexes (Ehiro *et al.*, 2008; Nakae *et al.*, 2021), but the poor description of the original definition makes it very difficult to correlate these units with more well-established accretionary units. The "Kuzumaki Unit" may be equivalent to the Otori Unit, based on TAA and structural position (Fig. 21). In the absence of clear definitions, these two units are not formally distinguished in the present compilation.

Data on TAA have been obtained in the southeastern part of the North Kitakami Belt outside the area of compilation in the present study (Yoshihara *et al.*, 2002; Suzuki and Ogane, 2004; Suzuki *et al.*, 2007a). Correlation of this area with the compilation in the present study is difficult, due to apparent discontinuity in the geological structure and lack of data in the area that lies between. Hence, the southwest part of the North Kitakami Belt will not be dealt with in this study.

6. Detrital zircon age as an indicator for trench-arrival age

Detrital zircon analysis of sandstone is often used as a means to constrain the age of fossil-barren strata, in concrete, coarse clastic rocks and metamorphosed rocks (e.g., Shimura *et al.* 2017; Uchino, 2019). In the Jurassic, Cretaceous and early Paleogene accretionary complexes of Southwest Japan in the Kii Peninsula and Shikoku, youngest clusters of detrital zircons of sandstone are generally in accordance with ages based on radiolarians and tuffs (Shimura *et al.*, 2019; Tokiwa *et al.*, 2019, 2021; Hara *et al.*, 2017, 2020). In these cases, the age of the youngest cluster of detrital zircons are likely to be close to the depositional age of the sandstone. In the case of the accretionary units around the Kado District, most sandstone samples did not yield depositional ages or had large uncertainties due to the small number of grains in the youngest cluster. In particular, parts of the Seki and Otori units formed in the Bajocian to Bathonian yielded YC1σ ages of ~170 Ma, in three out of four cases (Fig. 21B). This suggests the dominance of ~170 Ma detrital zircons and the scarcity of younger zircons in the subduction zone of the North Kitakami Belt during the Bajocian to Bathonian. In the present study, the only detrital zircon age regarded to be close to the depositional age is that of sample Mtg-09.5 of the Otori unit. This sample is outstanding in that the youngest cluster consists of ~25 % of all grains, whereas the percentage is generally less than 10 % in the North Kitakami Belt (Uchino, 2019, 2021; Muto *et al.*, 2023, Osaka *et al.*, 2023; this study).

It is noteworthy that the number of grains measured for each sample in this study (~60) is smaller than that in previous studies which at least partly obtained detrital zircon ages compatible with radiolarian-based depositional ages (Shimura *et al.*, 2019; Tokiwa *et al.*, 2019, 2021; Hara *et al.*, 2020). In theory, 60 grains would suffice to detect a population that constitutes 5 % of the entire population by 95 % (Dodson *et al.*, 1988). Based on the same theoretical calculation (e.g., Johnstone *et al.*, 2019; updated), in order to obtain at least three grains by a probability of 95 %, which would generally give a YC1σ age with small enough errors for meaningful discussion, the youngest population needs to be more than 10 % of the entire population. The necessary number of grains to detect one or any given number of the youngest population depends on the relative abundance of the youngest population. Therefore, there can be no universal criteria for the number of grains to analyze to obtain depositional ages (Sharman and Malkowski, 2020). In reality, even in active trenches, where zircons with ages close to the sedimentary age are relatively abundant, the proportion of zircons within 10 Myr of the depositional age can be less than 1 % (Clift *et al.*, 2013). This will require analysis of 630 grains in order to capture 3 grains from the youngest population (Johnstone *et al.* 2019; updated). On the other hand, analysis of 60 grains have yielded YC1σ ages compatible with microfossil age in some ancient sediments (e.g., Hara *et al.*, 2017). In the case of the Middle Jurassic units of the North Kitakami Belt, the situation is closer to the former case.

7. Summary

Tuffs and sandstones from the Kado District of the 1: 50,000 Quadrangle Series were analyzed for U–Pb dating in order to better understand the division and accretionary history of the North Kitakami Belt. The new data provide constraints for the trench-arrival age (TAA) of the Jurassic accretionary complex in the Kado District. Based on compilation of new data and previous data, the following points were clarified.

(1) The main tectonostratigraphic units and their TAA in the northern Kitakami Mountains are in structurally ascending order, the Kayamori Unit of undetermined age, the Oxfordian to Kimmeridgian Takayashiki Unit, the Bathonian to Kimmeridgean Seki Unit, the Aalenian to Bathonian Otori Unit, the Misugo Unit of undetermined age and the Rhaetian to Middle or early Late Jurassic Kadoma Unit.

(2) In addition to the above, the Kimmeridgian Ekari Unit, equivalent to the Takayashiki Unit or a structurally lower unit, was recognized.

(3) These units are distributed with a general younging polarity to the northeast, but the polarity is interrupted by folds and faults with vertical displacements. Some folds and faults that contribute to these interruptions are probably not yet recognized.

(4) Accretionary complexes in the east, northwest and southeast part of the northern Kitakami Mountains remain poorly correlated.

(5) Zircons in tuffs in hemipelagic and trench-fill sediments are useful material in constraining TAA, while detrital zircons in sandstone are generally less reliable, particularly in the Middle Jurassic of the North Kitakami Belt.

Acknowledgements: The authors thank Hideki Iwano and Tohru Danhara of Kyoto Fission-Track Co. Ltd. for extraction and analysis of detrital zircons. The author is grateful to the members of the Geological Sample Preparation Group of the Geoinformation Service Center, GSJ for preparing thin sections for this study. Sincere gratitude is offered to Yusuke Shimura and Tadashi Maruyama who provided fruitful comments that benefited the manuscript.

References

Clift, P. D., Carter, A., Nicholson, U. and Masago, H. (2013) Zircon and apatite thermochronology of the Nankai Trough accretionary prism and trench, Japan: Sediment transport in an active and collisional margin setting. *Tectonics*, **32**, 377–395. doi: 10.1002/tect.20033.

Cohen, K.M., Finney, S.C., Gibbard, P.L. and Fan, J.-X. (2013; updated) The ICS International Chronostratigraphic Chart. *Episodes*, **36**, 199–204.

Dickinson, W. R. and Gehrels, G. E. (2009) Use of U–Pb ages of detrital zircons to infer maximum depositional ages of strata: A test against a Colorado Plateau Mesozoic database. *Earth and Planetary Science Letters*, **288**, 115–125. doi: 10.1016/j.epsl.2009.09.013.

Dodson, M. H., Compston, W., Williams, I. S. and Wilson, J. F. (1988) A search for ancient detrital zircons in Zimbabwean sediments. *Journal of the Geological Society, London*, **145**, 977–983. doi: 10.1144/gsjgs.145.6.0977.

Ehiro, M., Kawamura, M. and Kawamura, T. (2005) 1.1 Summary and Tectonostratigraphic divisions. *In* The Publishing Committee of the Geology of Japan, ed., *The Geology of Japan*. *The Supplement*. Kyoritsu Pub. Co. Ltd., Tokyo. 49–50. (in Japanese)

Ehiro, M., Yamakita, S., Takahashi, S. and Suzuki, N. (2008) Jurassic accretionary complexes of the North Kitakami Belt in the Akka-Kuji area. *The Journal of the Geological Society of Japan*, **114**, 121–139. (in Japanese)

Hara, H., Nakamura, Y., Hara, K., Kurihara, T., Mori, H., Iwano, H., Danhara, T., Sakata, S. and Hirata, T. (2017) Detrital zircon multi-chronology, provenance, and low-grade metamorphism of the Cretaceous Shimanto accretionary complex, eastern Shikoku, Southwest Japan: Tectonic evolution in response to igneous activity within a subduction zone. *Island Arc*, **26**, 1–24. doi: 10.1111/iar.12218.

Hara, H., Ueki, T. and Hara, K. (2020) *Geology of the Umaji District*. Quadrangle Series, 1:50,000, Geological Survey of Japan, AIST. (in Japanese with Engish abstract)

Hirata, T., Iizuka, T. and Orihashi, Y. (2005) Reduction of mercury background on ICP-mass spectrometry for in situ U–Pb age determinations of zircon samples. *Journal of Analytical Atomic Spectrometry*, **20**, 696–701. doi: 10.1039/b504153h.

Iizuka, T. and Hirata, T. (2004) Simultaneous determinations of U-Pb age and REE abundances for zircons using ArF excimer laser ablation-ICPMS. *Geochemical Journal,* **38**, 229–241. doi: 10.2343/geochemj.38.229.

Isozaki, Y., Maruyama, S., Aoki, K., Nakama, T., Miyashita, A. and Otoh, S. (2010) Geotectonic subdivision of the Japanese Islands revisited: categorization and definition of elements and boundaries of Pacific-type (Miyashiro-type) orogen. *Chigaku Zasshi (Jounal of Geography)*, **119**, 999–1053. doi: 10.5026/jgeography.119.235. (in Japanese with English abstract)

Iwai, J., Murata, M., Hase, H. and Omura, K. (1964) Paleozoic strata of the northern Kitakami Mountains around Kuzumaki. *Journal of the Geological Society of Japan*, **70**, 382–383. (in Japanese, title translated)

Iwano, H., Orihashi, Y., Hirata, T., Ogasawara, M., Danhara, T., Horie, K., Hasebe, N., Sueoka, S., Tamura, A., Hayasaka, Y., Katsube, A., Ito, H., Tani, K., Kimura, J. I., Chang, Q., Kouchi, Y., Haruta, Y. and Yamamoto, K. (2013) An inter-laboratory evaluation of OD-3 zircon for use as a secondary U-Pb dating standard. *Island Arc*, **22**, 382–394. doi: 10.1111/iar.12038.

Johnstone, S. A., Schwartz, T. M. and Holm-Denoma, C. S. (2019; updated) A stratigraphic approach to inferring depositional ages from detrital geochronology data. *Frontiers in Earth Science*, **7**, 1–19. doi: 10.3389/feart.2019.00057.

Kawamura, T., Uchino, T., Kawamura, M., Yoshida, K., Nakagawa, M. and Nagata, H. (2013) *Geology of the Hayachinesan District.* Quadrangle Series, 1:50,000, Geological Survey of Japan, AIST. (in Japanese with English abstract)

Kojima, S., Hayasaka, Y., Hiroi, Y., Matsuoka, A., Sano, H., Sugamori, Y., Suzuki, N., Takemura, S., Tsujimori, T. and Uchino, T. (2016) 2b Pre-Cretaceous accretionary complexes. *In* Moreno, T., Wallis, S., Kojima, T. and Gibbons, W. eds., *The Geology of Japan*. Geological Society of London, London, 61–100.

Matsuoka, A. (1988) Discovery of Early Jurassic radiolarians from the North Kitakami Belt (s. s.), northeast Japan. *Earth Science (Chikyu Kagaku)*, **42**, 104–106. (in Japanese)

Matsuoka, A. and Oji, T. (1990) Middle Jurassic radiolarian fossils from the Magisawa Formation in the Taro Belt, North Kitakami Mountains. *The Journal of the Geological Society of Japan*, **96**, 239–241. (in Japanese)

Matsuoka, A., Yamakita, S., Sakakibara, M. and Hisada, K. (1998) Unit division for the Chichibu Composite Belt from a view point of accretionary tectonics and geology of western Shikoku, Japan. *The Journal of the Geological Society of Japan*, **104**, 634–653. (in Japanese with English abstract)

Minoura, K. and Tsushima, M. (1984) Geology of the Omoto district in the eastern margin of the North Kitakami Massif. *Science reports of the Hirosaki University*, **31**, 93–107. (in Japanese with English abstract)

Murai, T., Okami, K. and Oishi, M. (1985) *Geology of the Pre-Cretaceous in Iwaizumi Town. Part 1*. The Education Board of the Iwaizumi Town, Iwaizumi. (*in Japanese, reference information translated by Suzuki et al., 2007*)

Murai, T., Okami, K., Ehiro, M. and Oishi, M. (1986) *Geology of the Pre-Cretaceous in Iwaizumi Town. Part 2*. The Education Board of the Iwaizumi Town, Iwaizumi. (*in Japanese, reference information translated by Suzuki et al., 2007*)

Muto, S., Ito, T. and Murayama, M. (2023) Geology and accretionary age of the Otori Unit, North Kitakami Belt. *Bulletin of the Geological Survey of Japan*, **74**, 1–40.

Muto, S., Ito, T. and Ozeki, M. (2025) Middle Jurassic radiolarians from manganese nodules from the western part of the Kado District, northern Kitakami Mountains. *Bulletin of the Geological Survey of Japan*, **76**, 29–48.

Nakae, S. (2000) Regional correlation of the Jurassic accretionary complex in the Inner Zone of Southwest Japan. *The Memoirs of the Geological Society of Japan*, **55**, 73–98. (in Japanese with English abstract)

Nakae, S. (2016) Jurassic radiolarians from the Ichinohe–Kunohe area (Iwate Prefecture) in the North Kitakami Belt, Japan. *Bulletin of the Geological Survey of Japan*, **67**, 81–100. doi: 10.9795/bullgsj.67.81.

Nakae, S. (2018) *Geology of the Ichinohe Disrict*, 3, Jurassic of the North Kitakami Belt. Quadrangle Series, 1:50,000, Geological Survey of Japan, AIST, 102–119. (in Japanese)

Nakae, S. and Kamada, K. (2003) Late Jurassic radiolarians from the Rikuchu-Seki district in the North Kitakami Belt, Northeast Japan. *The Journal of the Geological Society of Japan*, **109**, 722–725. (in Japanese with English abstract)

Nakae, S., Kamada, K., Kubo, K. and Kudo, T. (2021) *Geology of the Rikuchu Seki District*. Quadrangle Series, 1:50,000, Geological Survey of Japan, AIST. (in Japanese with English abstract)

Onuki, Y. (1956) Geology of the Kitakami Mountains. *In* IwatePrefecture ed., *Explanatory Notes on the Geology of Iwate Prefecture. Part 2*. Iwate Prefecture, Morioka, 1–189. (in Japanese)

Onuki, Y. (1969) Geology of the Kitakami Massif, Northeast Japan. *Contributions from the Institute of Geology and Paleontology, Tohoku University*, **69**, 1–239. (in Japanese with English abstract)

Onuki, Y. (1981) Part 1. The Kitakami Mountains (in Japanese). *In* Hase Chishitsu Chosa Jimusho ed., *Explanation of the Geological Map of the Kitakami River Area, Kitakami Mountains, at the Scale of 1: 20,000*. Hase Chishitsu Chosa Jimusho, Sendai, 3–223.

Osaka, M., Aoki, S., Uchino, T. and Fukuyama, M. (2023) Constraint on the spatial distribution of the Early and Middle Jurassic units within the Nakatsugawa Complex of the North Kitakami Belt by detrital zircon U – Pb dating. *Bulletin of the Geological Survey of Japan*, **74**, 155–166.

Sharman, G. R. and Malkowski, M. A. (2020) Needles in a haystack: Detrital zircon U–Pb ages and the maximum depositional age of modern global sediment. *Earth-Science Reviews*, **203**, 103109. doi: 10.1016/j.earscirev.2020.103109.

Shimura, Y., Tokiwa, T., Takeuchi, M. and Yamamoto, K. (2017) Geology and detrital zircon U-Pb age of the Cretaceous Mugitani Formation in the Shimanto Belt, central Kii Peninsula, Southwest Japan. *The Journal of the Geological Society of Japan*, **123**, 925–937. doi: 10.5575/geosoc.2017.0032.

Shimura, Y., Tokiwa, T., Takeuchi, M., Mori, H. and Yamamoto, K. (2019) Lithological, structural, and chronological relationships between the Sanbagawa Metamorphic Complex and the Cretaceous Shimanto Accretionary Complex on the central Kii Peninsula, SW Japan. *Island Arc*, **28**, 1–19. doi: 10.1111/iar.12325.

Sláma, J., Košler, J., Condon, D. J., Crowley, J. L., Gerdes, A., Hanchar, J. M., Horstwood, M. S. A., Morris, G. A., Nasdala, L., Norberg, N., Schaltegger, U., Schoene, B., Tubrett, M. N. and Whitehouse, M. J. (2008) Plešovice zircon - A new natural reference material for U-Pb and Hf isotopic microanalysis. *Chemical Geology*, **249**, 1–35. doi: 10.1016/j.chemgeo.2007.11.005.

Sugimoto, M. (1980) Geological structure of the Akka-Iwaizumi District, Northern Kitakami Massif, Northeast Japan (Preliminary report). *In Report on the Multidiscipline Research Project A with 1979 Foundation of Grant-in-Aid for Scientific Research by the Education Ministry of Japan*. Tokyo Print Insatsu, Ltd., Tokyo, 37–44. (in Japanese)

Sugimoto, M. (1974) Stratigraphical study in the outer belt of the Kitakami Miassif, Northeast Japan. *Contributions from the Institute of Geology and Paleontology, Tohoku University*, **74**, 1–48. (in Japanese with English abstract)

Suzuki, N. and Ogane, K. (2004) Paleoceanographic affinities of radiolarian faunas in late Aalenian time (Middle Jurassic) recorded in the Jurassic accretionary complex of Japan. J*ournal of Asian Earth Sciences*, **23**, 343–357. doi: 10.1016/S1367-9120(03)00113-5.

Suzuki, N., Ehiro, M., Yoshihara, K., Kimura, Y., Kawashima, G., Yoshimoto, H. and Nogi, T. (2007a) Geology of the Kuzumaki-Kamaishi Subbelt of the North Kitakami Belt (a Jurassic accretionary complex), Northeast Japan: Case study of the Kawai-Yamada area, eastern Iwate Prefecture. *Bulletin of the Tohoku University Museum*, **6**, 103–174.

Suzuki, N., Yamakita, S., Takahashi, S. and Ehiro, M. (2007b) Middle Jurassic radiolarians from carbonate manganese nodules in the Otori Formation in the eastern part of the Kuzumaki-Kamaishi Subbelt, the North Kitakami Belt, Northeast Japan. *The Journal of the Geological Society of Japan*, **113**, 274–277. doi: 10.5575/geosoc.113.274. (in Japanese with English abstract)

Takahashi, S., Ehiro, M., Suzuki, N. and Yamakita, S. (2016) Subdivisional scheme of the North Kitakami Belt, Northeast Japan and its tectonostratigraphic correlation to the Oshima and South Chichibu belts: an examination of the Jurassic accretionary complex in the west Akka area. *Journal of the Geological Society of Japan*, **122**, 1–22. doi: 10.5575/geosoc.2015.0034. (in Japanese with English abstract)

Tokiwa, T., Shimura, Y., Takeuchi, M., Shimosato, S., Yamamoto, K. and Mori, H. (2019) Provenance of trench-fill deposits of the Jurassic Chichibu accretionary complex, Southwest Japan. *Journal of Asian Earth Sciences*, **184**, 103970. doi: 10.1016/j.jseaes.2019.103970.

Tokiwa, T., Shimura, Y., Takeuchi, M. and Mori, H. (2021) Use of detrital zircon U–Pb ages to assess the timing of deposition of Cretaceous trench-fill deposits in the active continental arc along the East Asian margin. *Journal of Asian Earth Sciences*, **207**. doi: 10.1016/j.jseaes.2020.104657.

Uchino, T. (2017) Late Triassic U-Pb-zircon age from tuffaceous mudstone in the Kadoma Complex, North Kitakami Belt, Northeast Japan. *The Journal of the Geological Society of Japan*, **123**, 977–982. doi: 10.5575/geosoc.2017.0024. (in Japanese with English abstract)

Uchino, T. (2019) Detrital zircon U–Pb ages of sandstone within the Jurassic accretionary complex in the North Kitakami Belt of the Sotoyama District, Iwate Prefecture. *Bulletin of the Geological Survey of Japan*, **70**, 357–372. (in Japanese with English abstract)

Uchino, T. (2021) Middle Jurassic zircon age from sandstone within the accretionary complex in the North Kitakami Belt, Kamatsuda area in Iwaizumi Town, Iwate Prefecture, Northeast Japan: Verifying the age of the accretionary complex containing the Okawa Sample. *Bulletin of the Geological Survey of Japan*, **72**, 99–107. (in Japanese with English abstract)

Uchino, T. and Suzuki, N. (2020) Late Jurassic radiolarians from mudstone near the U–Pb-dated sandstone of the North Kitakami Belt in the northeastern Shimokita Peninsula, Tohoku, Japan. *Bulletin of the Geological Survey of Japan*, **71**, 313–330. doi: 10.9795/bullgsj.71.313.

Ueda, H., Kimura, S., Saito, T., Takano, Y., Iizuka, N. and

Orihashi, Y. (2018) Material recycling in a sediment-starved trench recorded in the Early Cretaceous Shiriya accretionary complex, Northeast Japan. *Island Arc*, **27**, 1–20. doi: 10.1111/iar.12272.
Wiedenbeck, M., Alle, P., Corfu, F. y, Griffin, W. L., Meier, M., Oberli, F. v, Quadt, A. von, Roddick, J. C. and Spiegel, W. (1995) Three natural zircon standards for U-Th-Pb, Lu-Hf, trace element and REE analyses. *Geostandards newsletter*, **19**, 1–23.
Yamaguchi, Y. (1981) Geological structure of the eastern part of the North Kitakami Mountains, Japan—with special reference to structural subdivision. *Contributions from the Institute of Geology and Paleontology, Tohoku University*, **83**, 1–19. (in Japanese with English abstract)
Yoshihara, K., Suzuki, N. and Ehiro, M. (2002) Middle Jurassic radiolarian-bearing manganese nodules from the Kuzumaki-Kamaishi Belt in the Northern Kitakami Massif and its significance (in Japanese with English abstract). *Journal of the Geological Society of Japan*, **108**, 536–539.

Recieved February 13, 2024
Accepted November 29, 2024

北部北上帯ジュラ紀付加体の付加年代：「門」地域からの新たなジルコン地質年代学データ

武藤　俊

要　旨

東北日本北部北上帯ジュラ紀付加体では，白亜紀深成岩類の変成作用に起因して放散虫の報告が少なく，付加体の形成時期の検討にはジルコン年代学が用いられてきている．本研究では，5 万分の 1 地質図幅「門」地域のジュラ紀付加体中の砂岩中の砕屑性ジルコンと凝灰岩中の火成ジルコンの U–Pb 年代を報告する．先行研究と合わせて，北上山地北部に分布する主なジュラ紀付加体の構造層序ユニットとその砕屑岩の年代は下記の通りである：レーティアン期から中期ジュラ紀または後期ジュラ紀前期の門馬ユニット，付加年代未詳の三巣子ユニット，アーレニアン期からバトニアン期の大鳥ユニット，バトニアン期からキンメリッジアン期の関ユニット，オックスフォーディアン期からキンメリッジアン期の高屋敷ユニット，付加年代未詳の茅森ユニット，キンメリッジアン期直後の江刈ユニット．これらのうち前者の 6 ユニットはこの順に構造的に累重している．江刈ユニットの厳密な構造的位置は確かではないが，年代からは高屋敷ユニットまたはより下位に対比され，垂直変位を持つ断層によってより古いユニットの間に再配置したと判断される．このような断層やキロメートルオーダーの褶曲構造によって，北部北上帯の付加体に見られる大局的な海洋側への若化極性は乱されている．

難読･重要地名

Akka：安家，Chinzawa Stream：沈沢，Ekari：江刈，Kayamori：茅森，Misugo：三巣子，Kadoma：門馬，Minai River：見内川，Mitakai：三田貝，Okanai Stream：岡内沢，Omotogawa：小本川，Orikabe Stream：オリカベ沢，Otori：大鳥

Appendix

Table A1 Zircon U–Pb isotopic data for sample Udg-06 obtained by quadrupole inductively coupled plasma mass spectrometry.

No.	Isotopic ratios						U-Pb age (Ma)						U (ppm)	Th (ppm)
	$^{207}Pb/^{206}Pb$	Error 2σ	$^{206}Pb/^{238}U$	Error 2σ	$^{207}Pb/^{235}U$	Error 2σ	$^{206}Pb/^{238}U$		Error 2σ	$^{207}Pb/^{235}U$		Error 2σ		
1	0.0472	0.0040	0.0325	0.0014	0.2112	0.0197	205.9	±	9.3	194.6	±	19.8	136	80
2	0.0511	0.0052	0.0320	0.0017	0.2257	0.0250	203.3	±	11.2	206.6	±	25.1	89	15
3	0.0534	0.0029	0.0326	0.0010	0.2406	0.0150	207.0	±	6.4	218.9	±	15.1	316	202
4	0.0517	0.0036	0.0317	0.0012	0.2265	0.0172	201.3	±	7.6	207.3	±	17.3	205	95
5	0.0462	0.0021	0.0321	0.0008	0.2043	0.0106	203.4	±	5.0	188.7	±	10.7	586	429
6	0.0524	0.0028	0.0321	0.0010	0.2320	0.0142	203.8	±	6.2	211.9	±	14.3	339	208
7	0.0501	0.0030	0.0325	0.0011	0.2247	0.0150	206.2	±	6.8	205.8	±	15.2	278	167
8	0.0508	0.0023	0.0319	0.0008	0.2233	0.0118	202.4	±	5.2	204.7	±	11.9	517	353
9	0.0493	0.0027	0.0315	0.0009	0.2144	0.0134	200.2	±	6.0	197.3	±	13.5	344	228
10	0.0512	0.0034	0.0317	0.0011	0.2236	0.0166	201.0	±	7.3	204.9	±	16.7	220	131
11	0.0500	0.0025	0.0318	0.0009	0.2192	0.0124	201.8	±	5.5	201.3	±	12.5	440	275
12	0.0537	0.0042	0.0313	0.0013	0.2321	0.0201	198.8	±	8.6	211.9	±	20.2	150	57
13	0.0499	0.0038	0.0316	0.0013	0.2173	0.0181	200.3	±	8.1	199.6	±	18.2	172	65
14	0.0487	0.0026	0.0308	0.0009	0.2067	0.0125	195.3	±	5.6	190.8	±	12.6	384	258
15	0.0490	0.0028	0.0315	0.0010	0.2128	0.0135	199.9	±	6.1	195.9	±	13.7	330	149
16	0.0490	0.0033	0.0324	0.0012	0.2187	0.0164	205.3	±	7.5	200.8	±	16.5	217	119
17	0.0495	0.0037	0.0320	0.0013	0.2182	0.0181	202.9	±	8.2	200.4	±	18.2	174	69
18	0.0504	0.0034	0.0313	0.0011	0.2178	0.0162	198.7	±	7.2	200.0	±	16.3	222	111
19	0.0500	0.0034	0.0316	0.0011	0.2184	0.0164	200.8	±	7.3	200.6	±	16.5	218	124
20	0.0505	0.0039	0.0331	0.0014	0.2310	0.0198	210.2	±	9.0	211.0	±	19.9	153	80
21	0.0499	0.0024	0.0316	0.0008	0.2175	0.0120	200.6	±	5.3	199.8	±	12.1	471	307
22	0.0477	0.0039	0.0316	0.0013	0.2082	0.0184	200.7	±	8.5	192.0	±	18.5	155	63
23	0.0469	0.0035	0.0324	0.0013	0.2099	0.0173	205.8	±	8.1	193.5	±	17.4	181	90
24	0.0521	0.0038	0.0319	0.0013	0.2290	0.0186	202.3	±	8.2	209.4	±	18.7	174	86
25	0.0512	0.0034	0.0302	0.0010	0.2136	0.0154	191.9	±	6.7	196.6	±	15.6	242	110
26	0.0496	0.0030	0.0323	0.0010	0.2209	0.0147	204.7	±	6.7	202.6	±	14.9	285	161
27	0.0514	0.0023	0.0328	0.0008	0.2328	0.0122	208.2	±	5.4	212.5	±	12.3	511	364
28	0.0525	0.0029	0.0313	0.0009	0.2267	0.0139	198.6	±	6.0	207.5	±	14.0	343	131
29	0.0487	0.0033	0.0327	0.0012	0.2194	0.0165	207.3	±	7.6	201.4	±	16.6	216	134
30	0.0513	0.0017	0.0322	0.0006	0.2281	0.0092	204.5	±	4.0	208.6	±	9.3	1234	972

Standards are the same as in Table A8

Table A2 Zircon U–Pb isotopic data for sample Okz-14 obtained by quadrupole inductively coupled plasma mass spectrometry.

No.	Isotopic ratios						U-Pb age (Ma)						U (ppm)	Th (ppm)
	$^{207}Pb/^{206}Pb$	Error 2σ	$^{207}Pb/^{235}U$	Error 2σ	$^{206}Pb/^{238}U$	Error 2σ	$^{206}Pb/^{238}U$		Error 2σ	$^{207}Pb/^{235}U$		Error 2σ		
1	0.0499	0.0025	0.1790	0.0107	0.0260	0.0008	165.4	±	5.1	167.2	±	10.8	504	207
2	0.0488	0.0021	0.1784	0.0095	0.0265	0.0007	168.5	±	4.8	166.7	±	9.6	735	314
3	0.0488	0.0021	0.1768	0.0094	0.0262	0.0007	166.9	±	4.8	165.3	±	9.5	749	635
4	0.0486	0.0022	0.1766	0.0097	0.0263	0.0008	167.6	±	4.9	165.1	±	9.8	652	276
5	0.0494	0.0020	0.1785	0.0092	0.0262	0.0007	166.6	±	4.7	166.8	±	9.3	839	692
6	0.0473	0.0024	0.1743	0.0107	0.0267	0.0008	170.1	±	5.4	163.1	±	10.8	467	388
7	0.0525	0.0030	0.1916	0.0128	0.0264	0.0009	168.3	±	5.8	178.0	±	12.9	341	346
8	0.0471	0.0023	0.1744	0.0104	0.0268	0.0008	170.6	±	5.3	163.2	±	10.5	516	293
9	0.0499	0.0018	0.1793	0.0087	0.0261	0.0007	165.8	±	4.5	167.5	±	8.8	1059	306
10	0.0477	0.0019	0.1725	0.0087	0.0262	0.0007	166.7	±	4.6	161.6	±	8.8	917	603
11	0.0489	0.0017	0.1777	0.0082	0.0263	0.0007	167.5	±	4.4	166.1	±	8.3	1317	729
12	0.0503	0.0026	0.1812	0.0112	0.0261	0.0008	166.1	±	5.3	169.1	±	11.3	446	213
13	0.0494	0.0027	0.1751	0.0111	0.0257	0.0008	163.4	±	5.3	163.9	±	11.2	427	336
14	0.0485	0.0019	0.1731	0.0086	0.0259	0.0007	164.7	±	4.5	162.1	±	8.7	976	576
15	0.0483	0.0019	0.1731	0.0088	0.0260	0.0007	165.4	±	4.6	162.1	±	8.9	903	476
16	0.0478	0.0016	0.1751	0.0084	0.0265	0.0009	168.7	±	5.7	163.8	±	8.5	962	447
17	0.0489	0.0018	0.1762	0.0089	0.0261	0.0009	166.0	±	5.7	164.8	±	9.0	789	660
18	0.0506	0.0024	0.1843	0.0110	0.0264	0.0010	168.1	±	6.3	171.7	±	11.1	447	397
19	0.0506	0.0030	0.1819	0.0128	0.0260	0.0011	165.7	±	6.8	169.7	±	12.9	285	240
20	0.0496	0.0015	0.1803	0.0081	0.0264	0.0009	167.8	±	5.6	168.3	±	8.2	1241	730
21	0.0489	0.0015	0.1764	0.0081	0.0261	0.0009	166.2	±	5.5	165.0	±	8.2	1155	910
22	0.0488	0.0014	0.1746	0.0076	0.0259	0.0008	165.0	±	5.4	163.4	±	7.7	1547	1300
23	0.0510	0.0027	0.1868	0.0121	0.0265	0.0010	168.9	±	6.6	173.9	±	12.2	351	347
24	0.0485	0.0018	0.1757	0.0087	0.0262	0.0009	166.9	±	5.7	164.4	±	8.8	862	267
25	0.0501	0.0017	0.1817	0.0086	0.0263	0.0009	167.3	±	5.7	169.6	±	8.7	981	394
26	0.0517	0.0028	0.1890	0.0124	0.0265	0.0010	168.6	±	6.7	175.7	±	12.6	330	161
27	0.0501	0.0024	0.1834	0.0108	0.0266	0.0010	168.9	±	6.3	171.0	±	10.9	468	371
28	0.0522	0.0024	0.1876	0.0107	0.0260	0.0009	165.7	±	6.1	174.5	±	10.8	502	238
29	0.0512	0.0020	0.1823	0.0096	0.0258	0.0009	164.3	±	5.8	170.0	±	9.7	676	560
30	0.0485	0.0014	0.1703	0.0075	0.0255	0.0008	162.1	±	5.3	159.7	±	7.6	1441	827
Standards														
91500epo 4-1	0.0762	0.0032	1.9001	0.1263	0.1808	0.0091	1071.3	±	58.3	1081.1	±	120.8	78	26
91500epo 4-2	0.0754	0.0031	1.9344	0.1258	0.1860	0.0091	1099.6	±	58.6	1093.1	±	120.3	82	31
91500epo 4-3	0.0748	0.0031	1.9631	0.1297	0.1901	0.0095	1121.9	±	61.1	1102.9	±	123.8	78	38
91500epo 4-4	0.0734	0.0030	1.8238	0.1175	0.1802	0.0087	1068.1	±	55.7	1054.0	±	112.8	86	31
91500epo 4-5	0.0708	0.0029	1.7801	0.1152	0.1823	0.0088	1079.5	±	56.3	1038.2	±	110.7	86	33
GJ1 4-1	0.0596	0.0020	0.7859	0.0367	0.0956	0.0027	588.6	±	17.6	588.8	±	36.6	391	24
GJ1 4-2	0.0601	0.0019	0.8070	0.0371	0.0973	0.0028	598.6	±	17.7	600.8	±	37.0	411	28
GJ1 4-3	0.0608	0.0019	0.8188	0.0375	0.0976	0.0028	600.3	±	17.7	607.4	±	37.4	415	25
GJ1 4-4	0.0600	0.0019	0.7888	0.0364	0.0953	0.0027	587.0	±	17.3	590.5	±	36.3	413	21
GJ1 4-5	0.0593	0.0019	0.7988	0.0371	0.0976	0.0028	600.4	±	17.9	596.2	±	37.0	396	27
OD-3 4-1	0.0487	0.0041	0.0346	0.0030	0.0052	0.0002	33.1	±	1.0	34.6	±	3.1	799	1123
OD-3 4-2	0.0447	0.0037	0.0315	0.0027	0.0051	0.0002	32.9	±	1.0	31.5	±	2.7	920	1294
OD-3 4-3	0.0487	0.0038	0.0346	0.0028	0.0051	0.0002	33.1	±	1.0	34.5	±	2.9	947	1349
OD-3 4-4	0.0454	0.0041	0.0324	0.0030	0.0052	0.0002	33.2	±	1.1	32.4	±	3.0	749	804
OD-3 4-5	0.0430	0.0037	0.0308	0.0027	0.0052	0.0002	33.3	±	1.0	30.8	±	2.8	872	1093

Table A3 Zircon U–Pb isotopic data for sample Mna-01 obtained by quadrupole inductively coupled plasma mass spectrometry.

No.	Isotopic ratios						U-Pb age (Ma)				U (ppm)	Th (ppm)
	$^{207}Pb/^{206}Pb$	Error 2σ	$^{207}Pb/^{235}U$	Error 2σ	$^{206}Pb/^{238}U$	Error 2σ	$^{206}Pb/^{238}U$	Error 2σ	$^{207}Pb/^{235}U$	Error 2σ		
1	0.0456	0.0028	0.1807	0.0120	0.0288	0.0009	182.7	± 5.5	168.7	± 12.1	186	66
2	0.0496	0.0025	0.1929	0.0105	0.0282	0.0007	179.3	± 4.5	179.1	± 10.6	305	204
3	0.0476	0.0021	0.1950	0.0095	0.0297	0.0007	188.6	± 4.3	180.9	± 9.6	427	263
4	0.0487	0.0019	0.1840	0.0079	0.0274	0.0005	174.3	± 3.5	171.5	± 8.0	712	213
5	0.0491	0.0023	0.1825	0.0095	0.0269	0.0006	171.4	± 4.1	170.2	± 9.6	365	191
6	0.0476	0.0024	0.1827	0.0100	0.0278	0.0007	176.9	± 4.5	170.4	± 10.1	310	234
7	0.0490	0.0015	0.1722	0.0061	0.0255	0.0004	162.1	± 2.7	161.3	± 6.2	2202	1220
8	0.0496	0.0027	0.1854	0.0110	0.0271	0.0007	172.3	± 4.7	172.7	± 11.1	245	184
9	0.0484	0.0032	0.1886	0.0135	0.0282	0.0009	179.5	± 5.9	175.4	± 13.6	148	87
10	0.0488	0.0027	0.1856	0.0112	0.0276	0.0008	175.3	± 4.9	172.8	± 11.3	233	144
11	0.0497	0.0019	0.1888	0.0081	0.0276	0.0005	175.2	± 3.5	175.6	± 8.2	704	224
12	0.0483	0.0019	0.1808	0.0079	0.0271	0.0005	172.6	± 3.5	168.7	± 8.0	687	347
13	0.0508	0.0026	0.1892	0.0104	0.0270	0.0007	171.6	± 4.4	175.9	± 10.5	297	131
14	0.0499	0.0029	0.1897	0.0118	0.0276	0.0008	175.3	± 5.0	176.4	± 11.9	212	137
15	0.0486	0.0020	0.1805	0.0082	0.0269	0.0006	171.2	± 3.6	168.5	± 8.3	594	342
16	0.0495	0.0021	0.1851	0.0091	0.0271	0.0006	172.5	± 3.9	172.5	± 9.2	454	240
17	0.1136	0.0029	4.8587	0.1820	0.3101	0.0074	1741.4	± 47.6	1795.1	± 169.8	280	73
18	0.0510	0.0023	0.1919	0.0098	0.0273	0.0006	173.5	± 4.1	178.3	± 9.9	395	233
19	0.1127	0.0029	5.1118	0.1953	0.3286	0.0082	1831.7	± 52.6	1838.1	± 181.1	245	202
20	0.0528	0.0027	0.1959	0.0110	0.0269	0.0007	170.9	± 4.5	181.7	± 11.2	285	138
21	0.0480	0.0020	0.1810	0.0088	0.0274	0.0006	174.0	± 3.9	168.9	± 8.9	493	222
22	0.0482	0.0022	0.1789	0.0093	0.0269	0.0006	171.0	± 4.1	167.1	± 9.4	392	239
23	0.0476	0.0031	0.1768	0.0126	0.0270	0.0009	171.4	± 5.5	165.3	± 12.7	168	91
24	0.0502	0.0028	0.1876	0.0115	0.0271	0.0008	172.2	± 4.9	174.6	± 11.6	233	154
25	0.0499	0.0017	0.1866	0.0077	0.0271	0.0005	172.4	± 3.3	173.7	± 7.8	924	588
26	0.0471	0.0021	0.1795	0.0091	0.0276	0.0006	175.4	± 4.1	167.6	± 9.2	426	188
27	0.0476	0.0026	0.1760	0.0106	0.0268	0.0007	170.3	± 4.6	164.6	± 10.7	259	103
28	0.0495	0.0025	0.1849	0.0106	0.0271	0.0007	172.2	± 4.5	172.3	± 10.7	286	140
29	0.0498	0.0015	0.1895	0.0070	0.0276	0.0005	175.4	± 3.0	176.2	± 7.1	1656	665
30	0.0506	0.0026	0.1887	0.0107	0.0270	0.0007	172.0	± 4.5	175.5	± 10.8	293	200
Standards												
91500 tef 1-1	0.0758	0.0032	1.9032	0.0853	0.1819	0.0073	1077.3	± 47.2	1082.2	± 83.2	102	30
91500 tef 1-2	0.0728	0.0030	1.7870	0.0792	0.1780	0.0071	1055.9	± 45.4	1040.7	± 77.4	108	36
91500 tef 1-3	0.0766	0.0031	1.9128	0.0825	0.1811	0.0071	1072.9	± 45.5	1085.6	± 80.5	114	38
91500 tef 1-4	0.0751	0.0031	1.8754	0.0821	0.1809	0.0072	1072.0	± 45.9	1072.4	± 80.1	110	37
91500 tef 1-5	0.0766	0.0031	1.9165	0.0820	0.1814	0.0071	1074.7	± 45.3	1086.8	± 80.0	116	34
91500 tef 1-6	0.0759	0.0025	1.8875	0.0921	0.1802	0.0061	1067.8	± 39.3	1076.7	± 89.4	109	34
91500 tef 1-7	0.0738	0.0025	1.8124	0.0887	0.1780	0.0060	1056.3	± 38.8	1049.9	± 86.3	109	35
GJ1 1-1	0.0604	0.0024	0.8149	0.0278	0.0978	0.0030	601.6	± 19.4	605.2	± 27.9	374	20
GJ1 1-2	0.0607	0.0023	0.8258	0.0276	0.0986	0.0030	606.3	± 19.3	611.3	± 27.7	406	24
GJ1 1-3	0.0602	0.0023	0.8130	0.0270	0.0979	0.0030	602.0	± 19.1	604.1	± 27.1	420	23
GJ1 1-4	0.0613	0.0024	0.8303	0.0275	0.0982	0.0030	603.9	± 19.1	613.8	± 27.5	422	24
GJ1 1-5	0.0610	0.0024	0.8083	0.0270	0.0960	0.0029	591.1	± 18.8	601.5	± 27.1	410	22
GJ1 1-6	0.0593	0.0018	0.7893	0.0310	0.0965	0.0021	594.1	± 13.5	590.8	± 31.0	410	23
GJ1 1-7	0.0596	0.0018	0.7950	0.0314	0.0967	0.0021	595.2	± 13.7	594.0	± 31.4	393	24
OD3 1-1	0.0488	0.0044	0.0346	0.0030	0.0051	0.0002	33.1	± 1.2	34.6	± 3.0	431	506

Table A3 Continued.

No.	Isotopic ratios						U-Pb age (Ma)						U (ppm)	Th (ppm)
	$^{207}Pb/^{206}Pb$	Error 2σ	$^{207}Pb/^{235}U$	Error 2σ	$^{206}Pb/^{238}U$	Error 2σ	$^{206}Pb/^{238}U$		Error 2σ	$^{207}Pb/^{235}U$		Error 2σ		
OD3 1-2	0.0466	0.0037	0.0336	0.0025	0.0052	0.0002	33.6	±	1.1	33.5	±	2.5	610	819
OD3 1-3	0.0442	0.0035	0.0320	0.0024	0.0052	0.0002	33.8	±	1.1	32.0	±	2.4	621	762
OD3 1-4	0.0440	0.0035	0.0318	0.0024	0.0052	0.0002	33.7	±	1.1	31.8	±	2.4	650	719
OD3 1-5	0.0515	0.0039	0.0370	0.0026	0.0052	0.0002	33.5	±	1.1	36.9	±	2.6	631	825

Table A4 Zircon U–Pb isotopic data for sample Iwk-03 obtained by quadrupole inductively coupled plasma mass spectrometry.

No.	Isotopic ratios						U-Pb age (Ma)						U	Th
	$^{207}Pb/^{206}Pb$	Error 2σ	$^{207}Pb/^{235}U$	Error 2σ	$^{206}Pb/^{238}U$	Error 2σ	$^{206}Pb/^{238}U$		Error 2σ	$^{207}Pb/^{235}U$		Error 2σ	(ppm)	(ppm)
1	0.0490	0.0017	0.1893	0.0072	0.0280	0.0005	177.9	±	3.2	176.0	±	7.3	481	160
2	0.0491	0.0019	0.1869	0.0080	0.0276	0.0005	175.5	±	3.5	174.0	±	8.1	353	199
3	0.0485	0.0014	0.1869	0.0059	0.0279	0.0004	177.5	±	2.6	173.9	±	6.0	888	304
4	0.0521	0.0023	0.1948	0.0101	0.0271	0.0008	172.3	±	5.0	180.7	±	10.2	273	208
5	0.0514	0.0015	0.1932	0.0074	0.0273	0.0006	173.4	±	4.2	179.4	±	7.5	763	379
6	0.0496	0.0021	0.1905	0.0095	0.0278	0.0008	176.9	±	5.0	177.0	±	9.6	313	268
7	0.0505	0.0017	0.2445	0.0103	0.0351	0.0009	222.5	±	5.8	222.1	±	10.4	438	369
8	0.0490	0.0021	0.1823	0.0090	0.0269	0.0007	171.4	±	4.8	170.1	±	9.1	331	284
9	0.0479	0.0026	0.1801	0.0110	0.0272	0.0009	173.3	±	5.5	168.1	±	11.1	193	125
10	0.0505	0.0012	0.1918	0.0065	0.0275	0.0006	175.2	±	4.0	178.2	±	6.6	1321	1385
11	0.0493	0.0023	0.1879	0.0101	0.0276	0.0008	175.6	±	5.2	174.8	±	10.2	259	224
12	0.0511	0.0018	0.1935	0.0083	0.0274	0.0007	174.3	±	4.5	179.6	±	8.4	490	450
13	0.0503	0.0020	0.1902	0.0091	0.0274	0.0007	174.5	±	4.8	176.8	±	9.2	351	326
14	0.0502	0.0016	0.1897	0.0076	0.0274	0.0007	174.2	±	4.3	176.3	±	7.7	646	234
15	0.0515	0.0017	0.1952	0.0081	0.0275	0.0007	174.6	±	4.4	181.1	±	8.2	558	382
16	0.0506	0.0016	0.1920	0.0076	0.0275	0.0007	174.9	±	4.3	178.3	±	7.7	650	572
17	0.0498	0.0023	0.1864	0.0099	0.0271	0.0008	172.6	±	5.0	173.6	±	10.0	268	183
18	0.0515	0.0020	0.1917	0.0091	0.0270	0.0007	171.5	±	4.7	178.1	±	9.2	361	377
19	0.0498	0.0019	0.1899	0.0078	0.0276	0.0007	175.7	±	4.4	176.5	±	7.9	344	266
20	0.0511	0.0016	0.1942	0.0066	0.0275	0.0006	175.0	±	4.0	180.2	±	6.7	526	563
21	0.0505	0.0017	0.2408	0.0089	0.0346	0.0008	219.1	±	5.4	219.1	±	9.0	357	183
22	0.0509	0.0017	0.1924	0.0070	0.0274	0.0006	174.1	±	4.1	178.6	±	7.1	450	258
23	0.0501	0.0016	0.1859	0.0065	0.0269	0.0006	171.0	±	4.0	173.1	±	6.6	512	427
24	0.0485	0.0024	0.1839	0.0098	0.0275	0.0008	174.7	±	5.1	171.4	±	9.9	199	139
25	0.0503	0.0012	0.1893	0.0052	0.0273	0.0006	173.5	±	3.7	176.0	±	5.3	932	293
26	0.0483	0.0023	0.1891	0.0095	0.0284	0.0008	180.5	±	5.1	175.8	±	9.6	221	206
27	0.0496	0.0022	0.1902	0.0091	0.0278	0.0008	176.8	±	4.9	176.8	±	9.2	243	139
28	0.0510	0.0026	0.1904	0.0102	0.0271	0.0008	172.1	±	5.1	177.0	±	10.3	188	126
29	0.0499	0.0014	0.1903	0.0058	0.0276	0.0006	175.7	±	3.8	176.8	±	5.9	710	287
30	0.0494	0.0011	0.1871	0.0049	0.0274	0.0006	174.4	±	3.6	174.1	±	4.9	1112	622
Standards														
91500 1-1	0.0760	0.0021	1.9221	0.0777	0.1832	0.0056	1084.6	±	35.78	1088.8	±	76.01	96	38
91500 1-2	0.0759	0.0021	1.8588	0.0749	0.1774	0.0053	1052.8	±	34.36	1066.6	±	73.38	98	40
91500 1-3	0.0748	0.0021	1.8806	0.0771	0.1823	0.0056	1079.5	±	36.08	1074.3	±	75.44	94	38
91500 1-4	0.0749	0.0021	1.8907	0.0786	0.1829	0.0057	1083.0	±	36.80	1077.8	±	76.79	90	36
91500 1-5	0.0750	0.0021	1.8259	0.0760	0.1765	0.0055	1048.0	±	35.43	1054.8	±	74.39	91	36
91500 2-1	0.0759	0.0021	1.8773	0.0817	0.1794	0.0068	1063.6	±	43.94	1073.1	±	79.78	72	28
GJ 1-1	0.0632	0.0014	0.8602	0.0249	0.0987	0.0017	606.9	±	11.13	630.2	±	25.01	405	25
GJ 1-2	0.0627	0.0015	0.8524	0.0255	0.0985	0.0018	605.5	±	11.53	626.0	±	25.53	362	23
GJ 1-3	0.0622	0.0014	0.8325	0.0243	0.0970	0.0017	596.8	±	10.97	615.0	±	24.38	401	25
GJ 1-4	0.0628	0.0015	0.8461	0.0248	0.0976	0.0017	600.3	±	11.14	622.5	±	24.88	391	24
GJ 1-5	0.0618	0.0014	0.8375	0.0248	0.0983	0.0018	604.2	±	11.34	617.8	±	24.88	378	24
GJ 2-1	0.0616	0.0012	0.8347	0.0216	0.0982	0.0023	603.9	±	14.73	616.2	±	21.73	382	24
GJ 2-2	0.0615	0.0012	0.8259	0.0215	0.0973	0.0023	598.6	±	14.63	611.3	±	21.64	377	24

Table A5 Zircon U–Pb isotopic data for sample Szm-01 obtained by quadrupole inductively coupled plasma mass spectrometry. Shadowed data indicate discordant age data.

No.	Isotopic ratios						U-Pb age (Ma)						U (ppm)	Th (ppm)
	$^{207}Pb/^{206}Pb$	Error 2σ	$^{206}Pb/^{238}U$	Error 2σ	$^{207}Pb/^{235}U$	Error 2σ	$^{206}Pb/^{238}U$		Error 2σ	$^{207}Pb/^{235}U$		Error 2σ		
1	0.0484	0.0036	0.0275	0.0015	0.1835	0.0147	174.7	±	9.6	171.1	±	14.8	255	247
2	0.0499	0.0035	0.0272	0.0014	0.1874	0.0143	173.0	±	9.3	174.4	±	14.4	291	664
3	0.0497	0.0039	0.0257	0.0014	0.1766	0.0150	163.9	±	9.2	165.1	±	15.1	224	182
4	0.0476	0.0033	0.0275	0.0014	0.1809	0.0136	175.0	±	9.3	168.8	±	13.7	308	363
5	0.0503	0.0039	0.0280	0.0016	0.1943	0.0164	178.1	±	10.1	180.3	±	16.6	210	155
6	0.0481	0.0037	0.0266	0.0015	0.1768	0.0145	169.4	±	9.4	165.3	±	14.7	244	250
7	0.0492	0.0044	0.0272	0.0016	0.1845	0.0176	172.9	±	10.4	171.9	±	17.7	161	119
8	0.0494	0.0039	0.0269	0.0015	0.1833	0.0156	170.9	±	9.7	170.9	±	15.7	215	215
9	0.0466	0.0035	0.0265	0.0014	0.1705	0.0137	168.8	±	9.2	159.9	±	13.8	272	251
10	0.0492	0.0038	0.0263	0.0014	0.1790	0.0147	167.7	±	9.3	167.2	±	14.8	244	209
11	0.0488	0.0035	0.0267	0.0014	0.1800	0.0141	170.1	±	9.2	168.1	±	14.2	279	211
12	0.0502	0.0034	0.0270	0.0014	0.1873	0.0137	172.0	±	9.1	174.3	±	13.8	329	385
13	0.0495	0.0036	0.0269	0.0015	0.1841	0.0145	171.3	±	9.3	171.6	±	14.6	266	229
14	0.0510	0.0040	0.0273	0.0015	0.1919	0.0162	173.3	±	9.8	178.3	±	16.3	213	182
15	0.0468	0.0035	0.0276	0.0015	0.1785	0.0144	175.6	±	9.6	166.7	±	14.5	259	163
16	0.0463	0.0036	0.0274	0.0015	0.1750	0.0145	174.1	±	9.7	163.7	±	14.6	241	155
17	0.0515	0.0036	0.0267	0.0013	0.1892	0.0148	169.6	±	8.4	176.0	±	14.9	308	130
18	0.0463	0.0033	0.0272	0.0013	0.1739	0.0141	173.2	±	8.6	162.8	±	14.2	296	338
19	0.0472	0.0028	0.0268	0.0012	0.1748	0.0119	170.7	±	7.7	163.6	±	12.0	555	681
20	0.0481	0.0034	0.0272	0.0013	0.1804	0.0144	172.8	±	8.5	168.4	±	14.5	303	320
21	0.0518	0.0035	0.0281	0.0014	0.2005	0.0155	178.4	±	8.8	185.5	±	15.6	304	297
22	0.0502	0.0037	0.0281	0.0014	0.1942	0.0162	178.4	±	9.1	180.2	±	16.3	248	154
23	0.0445	0.0040	0.0264	0.0014	0.1618	0.0158	167.7	±	9.2	152.3	±	16.0	181	128
24	0.0515	0.0034	0.0261	0.0013	0.1859	0.0141	166.4	±	8.1	173.1	±	14.2	344	274
25	0.0554	0.0045	0.0275	0.0015	0.2099	0.0189	174.6	±	9.6	193.4	±	19.0	183	102
26	0.0500	0.0037	0.0276	0.0014	0.1908	0.0160	175.7	±	9.0	177.3	±	16.1	245	517
27	0.0473	0.0027	0.0270	0.0012	0.1765	0.0116	171.9	±	7.7	165.1	±	11.7	629	581
28	0.0489	0.0037	0.0267	0.0013	0.1803	0.0152	169.9	±	8.7	168.3	±	15.3	253	172
29	0.0484	0.0035	0.0262	0.0013	0.1749	0.0140	166.5	±	8.2	163.6	±	14.2	301	294
30	0.0472	0.0041	0.0269	0.0015	0.1753	0.0169	171.4	±	9.5	164.0	±	17.0	176	146
Standards														
91500 1-1	0.0748	0.0043	0.1776	0.0099	1.8315	0.1734	1053.8	±	63.4	1056.8	±	162.3	98	41
91500 1-2	0.0763	0.0044	0.1817	0.0105	1.9107	0.1836	1076.0	±	67.1	1084.8	±	171.1	89	40
91500 1-3	0.0746	0.0042	0.1789	0.0098	1.8412	0.1726	1061.2	±	62.7	1060.3	±	161.7	104	43
91500 1-4	0.0748	0.0043	0.1794	0.0100	1.8507	0.1752	1063.6	±	64.1	1063.7	±	163.9	98	43
91500 1-5	0.0721	0.0041	0.1866	0.0104	1.8549	0.1756	1102.7	±	66.7	1065.2	±	164.3	97	46
91500 3-1	0.0745	0.0039	0.1719	0.0107	1.7669	0.1349	1022.4	±	68.5	1033.4	±	128.5	85	32
91500 3-2	0.0758	0.0040	0.1755	0.0109	1.8345	0.1389	1042.2	±	69.6	1057.9	±	132.0	86	31
91500 5-1	0.0773	0.0044	0.1847	0.0108	1.9708	0.1574	1092.4	±	69.3	1105.6	±	148.4	79	32
91500 5-2	0.0773	0.0043	0.1756	0.0098	1.8734	0.1450	1042.7	±	63.0	1071.7	±	137.5	90	31
91500 5-3	0.0736	0.0042	0.1779	0.0102	1.8057	0.1429	1055.5	±	65.4	1047.5	±	135.7	84	34
91500 5-4	0.0724	0.0041	0.1853	0.0107	1.8520	0.1471	1095.9	±	68.5	1064.1	±	139.3	82	31
91500 5-5	0.0766	0.0043	0.1849	0.0107	1.9538	0.1547	1093.5	±	68.5	1099.8	±	146.1	82	31
GJ1 1-1	0.0594	0.0031	0.0928	0.0036	0.7607	0.0636	572.2	±	23.2	574.4	±	62.6	401	29
GJ1 1-2	0.0609	0.0032	0.0952	0.0037	0.7996	0.0667	586.2	±	23.8	596.6	±	65.5	405	22
GJ1 1-3	0.0581	0.0031	0.0974	0.0038	0.7799	0.0653	598.9	±	24.4	585.4	±	64.2	393	25

Table A5 Continued.

No.	Isotopic ratios						U-Pb age (Ma)						U (ppm)	Th (ppm)
	$^{207}Pb/^{206}Pb$	Error 2σ	$^{206}Pb/^{238}U$	Error 2σ	$^{207}Pb/^{235}U$	Error 2σ	$^{206}Pb/^{238}U$		Error 2σ	$^{207}Pb/^{235}U$		Error 2σ		
GJ1 1-4	0.0606	0.0032	0.0981	0.0038	0.8199	0.0685	603.0	±	24.6	608.0	±	67.2	394	28
GJ1 1-5	0.0594	0.0031	0.0986	0.0038	0.8081	0.0674	606.4	±	24.6	601.4	±	66.2	404	28
Gj1 3-1	0.0586	0.0027	0.0950	0.0044	0.7679	0.0463	585.3	±	28.3	578.5	±	45.9	351	20
Gj1 3-2	0.0615	0.0029	0.0965	0.0045	0.8195	0.0491	594.1	±	28.7	607.8	±	48.7	352	17
GJ1 5-1	0.0613	0.0031	0.0954	0.0037	0.8073	0.0512	587.6	±	24.0	601.0	±	50.7	345	13
GJ1 5-2	0.0595	0.0030	0.0999	0.0039	0.8196	0.0520	613.8	±	25.2	607.8	±	51.5	339	11
GJ1 5-3	0.0604	0.0031	0.0976	0.0038	0.8133	0.0515	600.6	±	24.5	604.3	±	50.9	349	20
GJ1 5-4	0.0618	0.0031	0.0976	0.0038	0.8317	0.0521	600.2	±	24.3	614.6	±	51.6	369	20
GJ1 5-5	0.0608	0.0031	0.0957	0.0037	0.8029	0.0506	588.9	±	23.9	598.5	±	50.2	359	13
OD-3 1-1	0.0437	0.0050	0.0052	0.0002	0.0315	0.0041	33.6	±	1.5	31.5	±	4.1	574	745
OD-3 1-2	0.0472	0.0052	0.0052	0.0002	0.0339	0.0043	33.5	±	1.5	33.8	±	4.3	588	751
OD-3 1-3	0.0483	0.0060	0.0050	0.0002	0.0331	0.0045	31.9	±	1.5	33.0	±	4.6	460	572
OD-3 1-4	0.0406	0.0041	0.0051	0.0002	0.0287	0.0034	33.0	±	1.3	28.7	±	3.4	853	1138
OD-3 1-5	0.0442	0.0045	0.0050	0.0002	0.0304	0.0036	32.1	±	1.3	30.4	±	3.6	800	1096
OD-3 3-1	0.0440	0.0044	0.0050	0.0002	0.0305	0.0032	32.3	±	1.6	30.5	±	3.2	723	904
OD-3 3-2	0.0466	0.0044	0.0051	0.0002	0.0330	0.0033	33.0	±	1.6	32.9	±	3.3	771	943
OD-3 5-1	0.0491	0.0047	0.0051	0.0002	0.0343	0.0034	32.6	±	1.3	34.3	±	3.4	813	993
OD-3 5-2	0.0484	0.0047	0.0051	0.0002	0.0342	0.0034	32.9	±	1.3	34.1	±	3.5	786	995
OD-3 5-3	0.0511	0.0047	0.0052	0.0002	0.0366	0.0035	33.4	±	1.3	36.5	±	3.6	821	995
OD-3 5-4	0.0466	0.0045	0.0051	0.0002	0.0328	0.0033	32.8	±	1.3	32.8	±	3.3	829	1021
OD-3 5-5	0.0489	0.0046	0.0052	0.0002	0.0351	0.0034	33.5	±	1.3	35.1	±	3.5	839	1027

Table A6 Zircon U–Pb isotopic data for sample Mtg-01 obtained by quadrupole inductively coupled plasma mass spectrometry.

No.	Isotopic ratios						U-Pb age (Ma)						U (ppm)	Th (ppm)
	$^{207}Pb/^{206}Pb$	Error 2σ	$^{207}Pb/^{235}U$	Error 2σ	$^{206}Pb/^{238}U$	Error 2σ	$^{206}Pb/^{238}U$		Error 2σ	$^{207}Pb/^{235}U$		Error 2σ		
1	0.0520	0.0013	0.2959	0.0086	0.0412	0.0009	260.4	±	5.9	263.2	±	8.7	167	139
2	0.0542	0.0019	0.3379	0.0137	0.0452	0.0013	285.0	±	8.2	295.6	±	13.8	73	85
3	0.0513	0.0010	0.2876	0.0064	0.0406	0.0008	256.6	±	5.1	256.6	±	6.5	332	173
4	0.0539	0.0011	0.4351	0.0110	0.0585	0.0013	366.7	±	8.2	366.8	±	11.1	180	86
5	0.0520	0.0009	0.3365	0.0070	0.0469	0.0009	295.7	±	5.9	294.6	±	7.1	349	316
6	0.0511	0.0016	0.2945	0.0108	0.0418	0.0011	263.7	±	6.9	262.1	±	10.9	100	87
7	0.0518	0.0010	0.3535	0.0081	0.0494	0.0010	310.9	±	6.4	307.3	±	8.2	266	339
8	0.0514	0.0008	0.3052	0.0053	0.0430	0.0008	271.6	±	5.0	270.4	±	5.3	668	517
9	0.0554	0.0009	0.5420	0.0111	0.0709	0.0014	441.4	±	9.1	439.7	±	11.2	274	195
10	0.0517	0.0013	0.2943	0.0082	0.0413	0.0009	260.7	±	5.8	261.9	±	8.3	187	350
11	0.0517	0.0011	0.2898	0.0070	0.0407	0.0008	256.9	±	5.3	258.4	±	7.0	271	201
12	0.0512	0.0007	0.2864	0.0045	0.0406	0.0007	256.3	±	4.6	255.7	±	4.6	998	270
13	0.0526	0.0012	0.2982	0.0076	0.0411	0.0009	259.6	±	5.5	265.0	±	7.7	230	155
14	0.0531	0.0022	0.3193	0.0151	0.0436	0.0014	275.2	±	8.8	281.3	±	15.3	54	16
15	0.0516	0.0011	0.2877	0.0073	0.0404	0.0008	255.2	±	5.4	256.7	±	7.4	238	200
16	0.0712	0.0007	1.5346	0.0217	0.1563	0.0028	936.2	±	18.1	944.4	±	21.8	636	261
17	0.0571	0.0008	0.6211	0.0103	0.0788	0.0015	489.0	±	9.4	490.6	±	10.4	483	135
18	0.0534	0.0021	0.4250	0.0204	0.0577	0.0019	361.4	±	12.4	359.6	±	20.5	43	36
19	0.0528	0.0013	0.3029	0.0086	0.0416	0.0009	262.5	±	5.9	268.6	±	8.7	173	240
20	0.0542	0.0013	0.3087	0.0086	0.0413	0.0009	260.9	±	5.9	273.2	±	8.7	179	97
21	0.0542	0.0011	0.3450	0.0084	0.0461	0.0010	290.6	±	6.2	301.0	±	8.5	233	223
22	0.0534	0.0012	0.2964	0.0074	0.0402	0.0008	254.3	±	5.4	263.6	±	7.5	243	162
23	0.0572	0.0007	0.6063	0.0091	0.0768	0.0014	477.2	±	8.8	481.2	±	9.2	734	159
24	0.0526	0.0021	0.3402	0.0160	0.0469	0.0015	295.3	±	9.5	297.4	±	16.1	53	49
25	0.0525	0.0013	0.2888	0.0080	0.0398	0.0009	251.9	±	5.6	257.7	±	8.1	191	121
26	0.0541	0.0021	0.2982	0.0131	0.0399	0.0012	252.4	±	7.5	265.0	±	13.2	66	37
27	0.0519	0.0009	0.3135	0.0063	0.0438	0.0008	276.3	±	5.4	276.9	±	6.4	406	417
28	0.0508	0.0010	0.2828	0.0067	0.0403	0.0008	254.8	±	5.2	252.9	±	6.8	287	205
29	0.0514	0.0010	0.2945	0.0063	0.0415	0.0008	262.1	±	5.2	262.1	±	6.4	364	378
30	0.0514	0.0008	0.2819	0.0050	0.0398	0.0007	251.3	±	4.6	252.1	±	5.0	670	460
31	0.0534	0.0006	0.3887	0.0080	0.0528	0.0008	331.6	±	5.3	333.4	±	8.1	661	402
32	0.0518	0.0010	0.2872	0.0074	0.0402	0.0007	254.2	±	4.6	256.4	±	7.5	308	258
33	0.0865	0.0008	2.7042	0.0573	0.2265	0.0041	1316.3	±	26.3	1329.6	±	56.6	238	109
34	0.0515	0.0025	0.3001	0.0173	0.0422	0.0014	266.7	±	9.2	266.5	±	17.5	39	27
35	0.0580	0.0008	0.6320	0.0147	0.0789	0.0014	489.8	±	9.0	497.3	±	14.8	278	148
36	0.0518	0.0013	0.2921	0.0096	0.0409	0.0009	258.4	±	5.5	260.2	±	9.7	151	129
37	0.0513	0.0011	0.2957	0.0082	0.0418	0.0008	263.7	±	5.0	263.0	±	8.3	239	107
38	0.0515	0.0010	0.2916	0.0079	0.0411	0.0007	259.4	±	4.8	259.9	±	8.0	263	190
39	0.0538	0.0007	0.4823	0.0106	0.0650	0.0011	405.8	±	7.0	399.6	±	10.7	407	159
40	0.0565	0.0010	0.5696	0.0148	0.0731	0.0014	454.6	±	9.0	457.7	±	14.9	195	95
41	0.0504	0.0012	0.2907	0.0090	0.0418	0.0008	263.8	±	5.4	259.1	±	9.1	177	94
42	0.0513	0.0009	0.2951	0.0075	0.0417	0.0007	263.3	±	4.7	262.6	±	7.6	326	358
43	0.0521	0.0011	0.3484	0.0102	0.0485	0.0010	305.3	±	6.2	303.5	±	10.3	183	72
44	0.0510	0.0008	0.2825	0.0066	0.0402	0.0007	253.8	±	4.2	252.7	±	6.6	470	253
45	0.0513	0.0019	0.2858	0.0127	0.0404	0.0011	255.3	±	6.9	255.3	±	12.8	72	85
46	0.0701	0.0006	1.4559	0.0273	0.1505	0.0023	903.8	±	15.0	912.3	±	27.3	665	247
47	0.0515	0.0009	0.2902	0.0074	0.0409	0.0007	258.2	±	4.6	258.7	±	7.5	327	356

Table A6 Continued.

No.	Isotopic ratios						U-Pb age (Ma)						U (ppm)	Th (ppm)
	$^{207}Pb/^{206}Pb$	Error 2σ	$^{207}Pb/^{235}U$	Error 2σ	$^{206}Pb/^{238}U$	Error 2σ	$^{206}Pb/^{238}U$		Error 2σ	$^{207}Pb/^{235}U$		Error 2σ		
48	0.0526	0.0016	0.3026	0.0112	0.0417	0.0010	263.4	±	6.2	268.4	±	11.3	107	82
49	0.0521	0.0025	0.3307	0.0188	0.0460	0.0016	289.7	±	10.2	290.1	±	19.0	37	26
50	0.0514	0.0011	0.3043	0.0085	0.0429	0.0008	270.8	±	5.2	269.8	±	8.6	231	194
51	0.0514	0.0007	0.2871	0.0064	0.0405	0.0006	255.7	±	4.2	256.3	±	6.5	555	348
52	0.0526	0.0014	0.3131	0.0106	0.0432	0.0009	272.4	±	6.0	276.6	±	10.7	133	186
53	0.0523	0.0008	0.3580	0.0085	0.0496	0.0008	311.9	±	5.5	310.7	±	8.6	356	189
54	0.0507	0.0010	0.2874	0.0080	0.0411	0.0008	259.4	±	4.9	256.5	±	8.1	244	92
55	0.0529	0.0024	0.3060	0.0165	0.0419	0.0013	264.6	±	8.7	271.0	±	16.6	44	48
56	0.0512	0.0013	0.2855	0.0090	0.0404	0.0008	255.5	±	5.3	255.0	±	9.1	172	48
57	0.0523	0.0010	0.3014	0.0081	0.0417	0.0008	263.6	±	4.9	267.5	±	8.2	265	125
58	0.0503	0.0011	0.2966	0.0085	0.0427	0.0008	269.9	±	5.2	263.7	±	8.6	221	169
59	0.0565	0.0013	0.3206	0.0099	0.0411	0.0008	259.8	±	5.4	282.3	±	10.0	167	100
60	0.0613	0.0007	0.8939	0.0193	0.1057	0.0018	647.8	±	11.7	648.5	±	19.4	317	258
Standards														
91500epo 4-4	0.0745	0.0013	1.8405	0.0502	0.1790	0.00480	1061	±	31	1060	±	50	75	30
91500epo 4-5	0.0749	0.0013	1.8677	0.0509	0.1807	0.00485	1071	±	31	1070	±	50	75	31
91500epo 4-6	0.0746	0.0012	1.8807	0.0564	0.1827	0.00462	1082	±	30	1074	±	56	73	27
91500epo 4-7	0.0754	0.0011	1.8872	0.0559	0.1814	0.00453	1074	±	29	1077	±	55	76	26
OD3 4-4	0.0454	0.0016	0.0320	0.0012	0.0051	0.00010	32.8	±	0.6	32.0	±	1.2	722	984
OD3 4-5	0.0481	0.0017	0.0338	0.0012	0.0051	0.00010	32.8	±	0.6	33.8	±	1.2	705	963
OD3 4-6	0.0471	0.0016	0.0332	0.0013	0.0051	0.00009	32.9	±	0.6	33.2	±	1.3	709	945

Table A7 Zircon U–Pb isotopic data for sample Mtg-09.5 obtained by quadrupole inductively coupled plasma mass spectrometry.

No.	Isotopic ratios						U-Pb age (Ma)				U (ppm)	Th (ppm)
	$^{207}Pb/^{206}Pb$	Error 2σ	$^{207}Pb/^{235}U$	Error 2σ	$^{206}Pb/^{238}U$	Error 2σ	$^{206}Pb/^{238}U$	Error 2σ	$^{207}Pb/^{235}U$	Error 2σ		
1	0.0507	0.0019	0.1875	0.0075	0.0268	0.0006	170.6	± 4.1	174.5	± 7.6	276	199
2	0.0519	0.0011	0.2965	0.0073	0.0414	0.0008	261.6	± 5.3	263.7	± 7.4	618	349
3	0.0530	0.0026	0.2905	0.0157	0.0397	0.0013	251.0	± 8.1	258.9	± 15.8	99	92
4	0.1150	0.0016	5.4020	0.1368	0.3403	0.0088	1888.2	± 56.5	1885.2	± 130.2	151	128
5	0.0497	0.0018	0.1843	0.0071	0.0268	0.0006	170.8	± 4.0	171.7	± 7.2	300	243
6	0.0491	0.0028	0.1817	0.0109	0.0268	0.0008	170.7	± 5.3	169.5	± 11.0	118	87
7	0.0491	0.0019	0.2389	0.0099	0.0352	0.0009	223.3	± 5.7	217.5	± 10.0	208	115
8	0.0500	0.0016	0.1855	0.0063	0.0269	0.0006	170.9	± 3.8	172.8	± 6.4	402	375
9	0.0525	0.0030	0.3011	0.0189	0.0416	0.0015	262.7	± 9.7	267.3	± 19.1	70	48
10	0.0496	0.0018	0.2087	0.0083	0.0305	0.0007	193.8	± 4.7	192.5	± 8.4	252	222
11	0.0500	0.0016	0.1949	0.0066	0.0283	0.0006	179.7	± 4.0	180.8	± 6.7	388	162
12	0.0521	0.0012	0.3045	0.0083	0.0424	0.0009	267.6	± 5.6	269.9	± 8.3	472	244
13	0.0506	0.0021	0.1868	0.0085	0.0268	0.0007	170.3	± 4.4	173.9	± 8.6	208	103
14	0.0515	0.0015	0.2153	0.0070	0.0303	0.0007	192.3	± 4.2	198.0	± 7.1	396	165
15	0.0513	0.0027	0.2750	0.0160	0.0389	0.0013	245.9	± 8.3	246.7	± 16.1	88	40
16	0.0559	0.0017	0.5699	0.0209	0.0738	0.0020	459.3	± 12.9	457.9	± 21.0	143	63
17	0.0522	0.0024	0.2101	0.0104	0.0292	0.0008	185.3	± 5.2	193.6	± 10.5	157	219
18	0.0513	0.0012	0.2955	0.0079	0.0417	0.0009	263.5	± 5.5	262.9	± 8.0	494	369
19	0.0526	0.0023	0.2494	0.0120	0.0344	0.0010	217.9	± 6.2	226.1	± 12.1	143	93
20	0.0495	0.0014	0.1817	0.0057	0.0266	0.0006	169.2	± 3.6	169.6	± 5.8	499	421
21	0.0521	0.0012	0.2922	0.0070	0.0407	0.0009	257.0	± 5.8	260.3	± 7.1	924	283
22	0.0511	0.0015	0.1870	0.0057	0.0265	0.0006	168.8	± 4.0	174.0	± 5.8	588	411
23	0.0512	0.0021	0.2051	0.0088	0.0290	0.0008	184.5	± 5.1	189.4	± 8.9	230	122
24	0.0513	0.0026	0.2058	0.0108	0.0291	0.0009	184.7	± 5.7	190.0	± 10.9	145	50
25	0.0488	0.0019	0.1775	0.0072	0.0263	0.0007	167.6	± 4.4	165.9	± 7.3	294	167
26	0.0522	0.0027	0.2124	0.0114	0.0295	0.0009	187.4	± 6.0	195.6	± 11.5	134	57
27	0.0489	0.0022	0.1823	0.0083	0.0270	0.0007	171.9	± 4.8	170.0	± 8.4	218	110
28	0.1149	0.0020	5.3386	0.1033	0.3368	0.0074	1871.2	± 47.6	1875.1	± 99.8	769	53
29	0.0518	0.0019	0.2908	0.0114	0.0407	0.0011	257.0	± 7.1	259.2	± 11.5	217	104
30	0.0508	0.0014	0.1851	0.0053	0.0264	0.0006	168.0	± 3.9	172.4	± 5.4	721	135
31	0.0494	0.0017	0.1822	0.0065	0.0267	0.0007	170.2	± 4.2	170.0	± 6.6	403	190
32	0.0518	0.0011	0.2473	0.0053	0.0346	0.0007	219.1	± 4.7	224.4	± 5.3	1811	618
33	0.0508	0.0030	0.1838	0.0114	0.0262	0.0009	167.0	± 5.7	171.3	± 11.5	110	63
34	0.0486	0.0023	0.1795	0.0088	0.0268	0.0008	170.4	± 5.0	167.6	± 8.9	190	104
35	0.1500	0.0027	8.7685	0.1973	0.4238	0.0105	2277.5	± 67.1	2314.2	± 182.8	292	35
36	0.0505	0.0023	0.1871	0.0090	0.0268	0.0008	170.8	± 5.0	174.2	± 9.1	190	194
37	0.0492	0.0018	0.1824	0.0070	0.0269	0.0007	170.9	± 4.4	170.1	± 7.1	327	224
38	0.0509	0.0024	0.1895	0.0094	0.0270	0.0008	171.6	± 5.1	176.2	± 9.5	177	83
39	0.1574	0.0029	9.1239	0.2134	0.4202	0.0107	2261.3	± 68.6	2350.5	± 196.4	246	66
40	0.0496	0.0017	0.1836	0.0066	0.0268	0.0007	170.6	± 4.3	171.2	± 6.7	393	294
41	0.0497	0.0020	0.1842	0.0050	0.0268	0.0006	170.8	± 4.1	171.7	± 5.1	746	222
42	0.0483	0.0024	0.1771	0.0072	0.0266	0.0007	169.0	± 4.6	165.6	± 7.3	290	178
43	0.0519	0.0021	0.2837	0.0084	0.0396	0.0010	250.3	± 6.4	253.6	± 8.5	428	134
44	0.0491	0.0030	0.2408	0.0138	0.0356	0.0012	225.3	± 7.9	219.1	± 14.0	105	83
45	0.0498	0.0026	0.2865	0.0136	0.0417	0.0013	263.3	± 8.4	255.8	± 13.7	138	114
46	0.0510	0.0019	0.1911	0.0044	0.0272	0.0006	172.8	± 4.0	177.5	± 4.4	1241	407
47	0.0479	0.0025	0.1789	0.0079	0.0270	0.0008	172.0	± 4.9	167.1	± 8.0	239	170

Table A7 Continued.

No.	Isotopic ratios						U-Pb age (Ma)				U (ppm)	Th (ppm)
	$^{207}Pb/^{206}Pb$	Error 2σ	$^{207}Pb/^{235}U$	Error 2σ	$^{206}Pb/^{238}U$	Error 2σ	$^{206}Pb/^{238}U$	Error 2σ	$^{207}Pb/^{235}U$	Error 2σ		
48	0.0515	0.0023	0.1869	0.0066	0.0263	0.0007	167.3	± 4.3	174.0	± 6.6	391	379
49	0.0499	0.0022	0.1876	0.0066	0.0273	0.0007	173.4	± 4.5	174.6	± 6.7	387	149
50	0.0513	0.0022	0.1887	0.0063	0.0267	0.0007	169.7	± 4.3	175.5	± 6.4	440	322
51	0.0512	0.0020	0.2498	0.0063	0.0354	0.0008	224.0	± 5.3	226.4	± 6.3	745	371
52	0.0487	0.0027	0.1786	0.0087	0.0266	0.0008	169.1	± 5.1	166.8	± 8.8	193	204
53	0.0501	0.0024	0.1811	0.0091	0.0262	0.0007	166.6	± 4.6	169.0	± 9.2	181	112
54	0.0500	0.0016	0.1822	0.0063	0.0264	0.0006	168.0	± 3.7	170.0	± 6.4	460	413
55	0.1145	0.0022	5.1158	0.1505	0.3238	0.0089	1808.3	± 56.9	1838.7	± 142.3	135	201
56	0.0497	0.0022	0.1812	0.0086	0.0264	0.0007	168.0	± 4.4	169.1	± 8.7	211	124
57	0.0500	0.0015	0.1932	0.0064	0.0280	0.0006	178.1	± 3.9	179.4	± 6.4	506	201
58	0.0490	0.0017	0.1793	0.0065	0.0265	0.0006	168.8	± 3.8	167.4	± 6.6	411	143
59	0.0511	0.0018	0.1835	0.0070	0.0260	0.0006	165.6	± 3.8	171.1	± 7.0	360	298
60	0.0505	0.0023	0.1866	0.0090	0.0268	0.0007	170.3	± 4.6	173.7	± 9.1	197	184
61	0.0510	0.0016	0.1873	0.0062	0.0266	0.0006	169.2	± 3.7	174.3	± 6.3	515	311
62	0.0485	0.0016	0.1766	0.0061	0.0264	0.0006	168.0	± 3.7	165.2	± 6.1	484	442
Standards												
91500epo 1-6	0.0746	0.0031	1.8124	0.0736	0.1760	0.0066	1044.8	± 42.5	1049.9	± 72.1	66	23
91500epo 1-7	0.0749	0.0030	1.8774	0.0741	0.1816	0.0067	1075.5	± 43.0	1073.1	± 72.6	70	27
91500epo 2-1	0.0762	0.0022	1.8779	0.0792	0.1787	0.0064	1059.8	± 41.0	1073.3	± 77.3	64	24
91500epo 2-2	0.0751	0.0022	1.8137	0.0752	0.1751	0.0061	1040.3	± 39.3	1050.4	± 73.6	67	24
OD3 1-6	0.0485	0.0023	0.0342	0.0012	0.0051	0.0001	32.8	± 0.8	34.1	± 1.3	1732	2059
OD3 1-7	0.0473	0.0022	0.0331	0.0011	0.0051	0.0001	32.5	± 0.8	33.0	± 1.1	2057	2502
OD3 1-8	0.0460	0.0034	0.0332	0.0022	0.0052	0.0001	33.6	± 1.0	33.1	± 2.2	472	500
OD3 2-1	0.0480	0.0018	0.0331	0.0013	0.0050	0.0001	32.1	± 0.6	33.0	± 1.3	1638	1936

Table A8 Zircon U–Pb isotopic data for sample Mtg-12 obtained by quadrupole inductively coupled plasma mass spectrometry.

No.	Isotopic ratios						U-Pb age (Ma)						U (ppm)	Th (ppm)
	$^{207}Pb/^{206}Pb$	Error 2σ	$^{207}Pb/^{235}U$	Error 2σ	$^{206}Pb/^{238}U$	Error 2σ	$^{206}Pb/^{238}U$		Error 2σ	$^{207}Pb/^{235}U$		Error 2σ		
1	0.0513	0.0022	0.2174	0.0109	0.0307	0.0008	195.2	±	5.2	199.8	±	11.0	283	125
2	0.0546	0.0024	0.3292	0.0176	0.0437	0.0013	275.5	±	8.4	289.0	±	17.7	164	76
3	0.0519	0.0020	0.2881	0.0138	0.0403	0.0011	254.4	±	6.8	257.0	±	13.9	263	91
4	0.0509	0.0017	0.2110	0.0087	0.0300	0.0007	190.8	±	4.4	194.4	±	8.8	616	297
5	0.0503	0.0022	0.2111	0.0110	0.0304	0.0008	193.3	±	5.3	194.5	±	11.1	257	207
6	0.1155	0.0029	5.3023	0.2300	0.3327	0.0111	1851.5	±	71.0	1869.2	±	210.2	98	100
7	0.0531	0.0017	0.3110	0.0129	0.0425	0.0010	268.1	±	6.4	275.0	±	13.0	445	293
8	0.0539	0.0031	0.2326	0.0151	0.0313	0.0010	198.6	±	6.7	212.3	±	15.2	127	84
9	0.0498	0.0016	0.2046	0.0084	0.0298	0.0007	189.2	±	4.3	189.0	±	8.5	659	329
10	0.0509	0.0024	0.2085	0.0114	0.0297	0.0008	188.8	±	5.4	192.3	±	11.6	220	147
11	0.0516	0.0013	0.2970	0.0105	0.0417	0.0009	263.6	±	5.5	264.0	±	10.6	1379	26
12	0.0505	0.0024	0.2130	0.0117	0.0306	0.0009	194.1	±	5.5	196.0	±	11.8	215	60
13	0.0497	0.0032	0.2814	0.0208	0.0410	0.0016	259.2	±	10.2	251.8	±	20.9	78	51
14	0.0530	0.0029	0.2972	0.0188	0.0407	0.0014	256.9	±	8.9	264.2	±	18.9	110	65
15	0.0520	0.0017	0.2017	0.0084	0.0281	0.0006	178.8	±	4.1	186.6	±	8.5	636	233
16	0.1145	0.0027	5.2554	0.1492	0.3328	0.0056	1851.8	±	36.3	1861.6	±	141.2	385	201
17	0.0538	0.0017	0.4210	0.0149	0.0567	0.0010	355.5	±	6.5	356.8	±	15.0	380	151
18	0.0518	0.0031	0.2146	0.0136	0.0300	0.0009	190.8	±	5.6	197.4	±	13.7	125	75
19	0.1157	0.0027	5.4523	0.1553	0.3417	0.0058	1894.8	±	37.6	1893.1	±	146.6	374	78
20	0.1152	0.0029	5.5085	0.1836	0.3465	0.0081	1917.8	±	52.2	1901.9	±	171.2	160	50
21	0.0509	0.0022	0.2139	0.0100	0.0305	0.0006	193.4	±	4.2	196.8	±	10.1	267	178
22	0.0508	0.0020	0.2097	0.0087	0.0299	0.0006	189.9	±	3.6	193.3	±	8.8	381	246
23	0.0521	0.0021	0.2389	0.0101	0.0332	0.0006	210.7	±	4.2	217.5	±	10.2	324	136
24	0.0559	0.0017	0.5494	0.0189	0.0713	0.0013	443.9	±	8.3	444.6	±	19.0	349	406
25	0.0511	0.0017	0.2132	0.0076	0.0302	0.0005	192.0	±	3.1	196.2	±	7.7	626	307
26	0.0509	0.0022	0.2844	0.0131	0.0405	0.0009	255.7	±	5.8	254.1	±	13.2	222	220
27	0.0517	0.0017	0.2520	0.0088	0.0353	0.0006	223.7	±	3.6	228.2	±	8.9	600	466
28	0.0515	0.0022	0.2116	0.0096	0.0297	0.0006	188.9	±	3.9	194.9	±	9.7	294	251
29	0.0499	0.0016	0.2085	0.0071	0.0303	0.0005	192.4	±	2.9	192.3	±	7.2	760	438
30	0.0485	0.0026	0.1933	0.0109	0.0289	0.0007	183.6	±	4.6	179.5	±	11.0	181	112
31	0.0508	0.0016	0.2063	0.0070	0.0295	0.0004	187.1	±	2.8	190.5	±	7.1	760	411
32	0.0561	0.0019	0.5729	0.0220	0.0740	0.0016	460.3	±	10.1	459.9	±	22.1	230	158
33	0.0551	0.0037	0.3000	0.0218	0.0395	0.0015	249.6	±	9.4	266.4	±	21.9	69	43
34	0.0514	0.0026	0.2889	0.0166	0.0408	0.0014	257.5	±	8.7	257.7	±	16.8	136	102
35	0.0527	0.0030	0.3038	0.0195	0.0418	0.0015	263.8	±	9.9	269.4	±	19.6	98	83
36	0.0509	0.0027	0.2172	0.0130	0.0309	0.0010	196.5	±	6.5	199.6	±	13.1	154	83
37	0.0503	0.0018	0.1895	0.0080	0.0273	0.0007	173.6	±	4.5	176.2	±	8.0	548	217
38	0.0509	0.0017	0.2431	0.0096	0.0346	0.0009	219.3	±	5.6	220.9	±	9.7	580	671
39	0.0499	0.0019	0.2369	0.0103	0.0344	0.0009	218.1	±	5.8	215.9	±	10.4	398	262
40	0.0524	0.0018	0.2973	0.0122	0.0411	0.0011	259.7	±	6.9	264.3	±	12.4	411	215
41	0.0520	0.0023	0.1909	0.0095	0.0266	0.0007	169.3	±	4.8	177.4	±	9.6	299	137
42	0.0513	0.0014	0.2883	0.0098	0.0408	0.0009	257.6	±	6.1	257.2	±	10.0	1330	614
43	0.0570	0.0043	0.3644	0.0309	0.0463	0.0023	292.0	±	14.6	315.5	±	30.9	44	31
44	0.0516	0.0019	0.2813	0.0124	0.0395	0.0011	249.9	±	6.9	251.7	±	12.5	330	243
45	0.0504	0.0018	0.2118	0.0087	0.0305	0.0008	193.5	±	5.0	195.1	±	8.8	543	184
46	0.0518	0.0021	0.2887	0.0134	0.0404	0.0011	255.4	±	7.3	257.5	±	13.5	265	117
47	0.0529	0.0026	0.2908	0.0162	0.0399	0.0013	252.0	±	8.3	259.2	±	16.3	148	110

Table A8 Continued.

No.	Isotopic ratios						U-Pb age (Ma)						U (ppm)	Th (ppm)
	$^{207}Pb/^{206}Pb$	Error 2σ	$^{207}Pb/^{235}U$	Error 2σ	$^{206}Pb/^{238}U$	Error 2σ	$^{206}Pb/^{238}U$		Error 2σ	$^{207}Pb/^{235}U$		Error 2σ		
48	0.1141	0.0028	5.2773	0.1847	0.3352	0.0091	1863.3	±	58.2	1865.2	±	172.1	274	236
49	0.0518	0.0020	0.2903	0.0133	0.0406	0.0011	256.8	±	7.3	258.8	±	13.5	273	88
50	0.1123	0.0033	5.1578	0.2538	0.3328	0.0139	1851.8	±	89.1	1845.7	±	229.6	56	92
51	0.0501	0.0016	0.2087	0.0081	0.0302	0.0007	191.6	±	4.8	192.5	±	8.2	728	289
52	0.1148	0.0031	5.2148	0.2194	0.3292	0.0114	1834.4	±	73.0	1855.0	±	201.4	98	179
53	0.0496	0.0016	0.1935	0.0073	0.0283	0.0007	179.9	±	4.4	179.6	±	7.4	910	374
54	0.0509	0.0021	0.2177	0.0103	0.0310	0.0009	196.9	±	5.5	200.0	±	10.4	309	163
55	0.0481	0.0024	0.2013	0.0113	0.0303	0.0009	192.7	±	6.0	186.2	±	11.4	198	55
56	0.0519	0.0018	0.2923	0.0118	0.0408	0.0010	257.9	±	6.7	260.4	±	11.9	461	331
57	0.0524	0.0021	0.2893	0.0136	0.0400	0.0011	253.1	±	7.4	258.0	±	13.8	250	140
58	0.0513	0.0016	0.2846	0.0106	0.0403	0.0010	254.4	±	6.3	254.3	±	10.7	712	452
59	0.0502	0.0024	0.2429	0.0134	0.0350	0.0011	222.1	±	7.0	220.8	±	13.5	178	143
60	0.0499	0.0013	0.2229	0.0075	0.0324	0.0007	205.4	±	4.7	204.3	±	7.6	1977	553
Standards														
91500epo 2-1	0.0728	0.0026	1.7618	0.0953	0.1754	0.0070	1042	±	45	1031	±	92	60	23
91500epo 2-2	0.0775	0.0027	1.9074	0.1026	0.1785	0.0072	1059	±	46	1084	±	99	59	20
91500epo 2-3	0.0757	0.0027	1.8690	0.0934	0.1789	0.0066	1061	±	43	1070	±	91	58	20
91500epo 2-4	0.0772	0.0028	1.9245	0.1017	0.1807	0.0075	1071	±	48	1090	±	98	58	22
OD-3 2-1	0.0496	0.0059	0.0350	0.0042	0.0051	0.0002	32.9	±	1.31	35.0	±	4.25	171	181
OD-3 2-2	0.0475	0.0054	0.0339	0.0039	0.0052	0.0002	33.3	±	1.26	33.8	±	3.94	194	162
OD-3 2-3	0.0462	0.0052	0.0314	0.0035	0.0049	0.0002	31.7	±	1.06	31.4	±	3.57	210	219
OD-3 2-4	0.0447	0.0042	0.0303	0.0029	0.0049	0.0002	31.6	±	1.07	30.3	±	2.90	315	350

Table A9 Zircon U–Pb isotopic data for sample Hrp-05 obtained by quadrupole inductively coupled plasma mass spectrometry.

No.	Isotopic ratios						U-Pb age (Ma)						U (ppm)	Th (ppm)
	$^{207}Pb/^{206}Pb$	Error 2σ	$^{207}Pb/^{235}U$	Error 2σ	$^{206}Pb/^{238}U$	Error 2σ	$^{206}Pb/^{238}U$		Error 2σ	$^{207}Pb/^{235}U$		Error 2σ		
1	0.0492	0.0022	0.1754	0.0087	0.0258	0.0005	164.3	±	3.3	164.1	±	8.7	885	391
2	0.0497	0.0019	0.1492	0.0061	0.0218	0.0003	138.9	±	2.2	141.2	±	6.2	2325	1493
3	0.0496	0.0021	0.1767	0.0080	0.0258	0.0005	164.3	±	3.0	165.2	±	8.1	1226	1001
4	0.0496	0.0026	0.1799	0.0101	0.0263	0.0006	167.4	±	4.0	168.0	±	10.2	568	288
5	0.0497	0.0026	0.1840	0.0102	0.0269	0.0006	170.8	±	4.0	171.5	±	10.3	565	183
6	0.0508	0.0028	0.1808	0.0105	0.0258	0.0006	164.3	±	4.1	168.8	±	10.6	498	176
7	0.0500	0.0020	0.1622	0.0071	0.0235	0.0004	149.9	±	2.6	152.6	±	7.2	1557	1329
8	0.0481	0.0023	0.1732	0.0088	0.0261	0.0005	166.0	±	3.5	162.2	±	8.9	790	322
9	0.0514	0.0020	0.1672	0.0071	0.0236	0.0004	150.4	±	2.5	157.0	±	7.1	1800	1380
10	0.0503	0.0021	0.1847	0.0083	0.0266	0.0005	169.5	±	3.1	172.1	±	8.4	1199	871
11	0.0518	0.0024	0.1938	0.0099	0.0271	0.0006	172.4	±	3.7	179.9	±	10.0	729	358
12	0.0493	0.0020	0.1763	0.0079	0.0259	0.0005	165.0	±	3.0	164.9	±	8.0	1283	993
13	0.0499	0.0023	0.1791	0.0091	0.0260	0.0005	165.6	±	3.5	167.3	±	9.2	782	570
14	0.0495	0.0026	0.1813	0.0104	0.0265	0.0006	168.8	±	4.1	169.2	±	10.5	529	329
15	0.0507	0.0026	0.1902	0.0105	0.0272	0.0006	172.8	±	4.1	176.8	±	10.7	556	401
16	0.0509	0.0022	0.1617	0.0085	0.0230	0.0005	146.8	±	3.4	152.2	±	8.6	1675	2668
17	0.0468	0.0026	0.1717	0.0112	0.0266	0.0008	169.3	±	4.9	160.9	±	11.3	546	514
18	0.0507	0.0024	0.1536	0.0089	0.0220	0.0006	140.0	±	3.6	145.1	±	9.0	1022	1320
19	0.0486	0.0027	0.1819	0.0119	0.0271	0.0008	172.6	±	5.1	169.7	±	12.0	505	253
20	0.0480	0.0022	0.1727	0.0096	0.0261	0.0006	165.9	±	4.1	161.8	±	9.7	1167	781
21	0.0484	0.0024	0.1659	0.0097	0.0248	0.0006	158.1	±	4.1	155.9	±	9.8	889	455
22	0.0503	0.0025	0.1808	0.0109	0.0261	0.0007	165.9	±	4.5	168.7	±	11.0	731	345
23	0.0488	0.0023	0.1800	0.0103	0.0268	0.0007	170.2	±	4.4	168.1	±	10.4	913	562
24	0.0496	0.0021	0.1784	0.0095	0.0261	0.0006	165.8	±	3.9	166.7	±	9.6	1454	856
25	0.0502	0.0025	0.1793	0.0106	0.0259	0.0007	164.8	±	4.4	167.5	±	10.7	791	507
26	0.0489	0.0029	0.1790	0.0121	0.0265	0.0008	168.8	±	5.1	167.2	±	12.3	453	475
27	0.0482	0.0022	0.1743	0.0099	0.0262	0.0007	166.9	±	4.2	163.2	±	10.0	999	658
28	0.0484	0.0021	0.1754	0.0096	0.0263	0.0006	167.1	±	4.1	164.1	±	9.7	1266	726
29	0.0475	0.0022	0.1748	0.0099	0.0267	0.0007	169.6	±	4.3	163.6	±	10.0	1039	665
30	0.0486	0.0020	0.1754	0.0092	0.0261	0.0006	166.3	±	3.9	164.1	±	9.3	1714	838

Standards are the same as in Table A1

Table A10 Zircon U–Pb isotopic data for sample Odr-Kass-01 obtained by quadrupole inductively coupled plasma mass spectrometry. Shadowed data indicate discordant age data.

No.	Isotopic ratios						U-Pb age (Ma)				U (ppm)	Th (ppm)
	^{207}Pb/^{206}Pb	Error 2σ	^{207}Pb/^{235}U	Error 2σ	^{206}Pb/^{238}U	Error 2σ	^{206}Pb/^{238}U	Error 2σ	^{207}Pb/^{235}U	Error 2σ		
1	0.0506	0.0017	0.2495	0.0087	0.0357	0.0006	226.4	± 4.2	226.2	± 8.7	374	182
2	0.1143	0.0018	5.2501	0.1058	0.3328	0.0055	1852.1	± 35.7	1860.8	± 102.1	385	207
3	0.0524	0.0015	0.2946	0.0087	0.0408	0.0007	257.7	± 4.3	262.2	± 8.8	490	172
4	0.0502	0.0011	0.2335	0.0051	0.0337	0.0004	213.8	± 2.7	213.1	± 5.1	1404	490
5	0.0513	0.0022	0.2084	0.0093	0.0294	0.0006	187.0	± 4.1	192.2	± 9.4	246	110
6	0.1145	0.0018	5.2831	0.0970	0.3345	0.0050	1860.0	± 31.9	1866.1	± 94.0	560	171
7	0.0530	0.0018	0.2524	0.0090	0.0345	0.0006	218.7	± 4.2	228.6	± 9.1	344	166
8	0.0455	0.0044	0.2544	0.0263	0.0405	0.0020	255.8	± 13.1	230.1	± 26.3	36	35
9	0.0540	0.0024	0.2140	0.0098	0.0287	0.0006	182.7	± 4.2	196.9	± 9.9	228	156
10	0.1136	0.0018	5.1435	0.0942	0.3282	0.0048	1829.5	± 31.2	1843.3	± 91.4	568	108
11	0.0492	0.0013	0.1878	0.0052	0.0277	0.0004	176.1	± 2.6	174.8	± 5.3	819	441
12	0.0502	0.0013	0.1907	0.0052	0.0276	0.0004	175.3	± 2.5	177.3	± 5.2	876	442
13	0.1146	0.0021	5.2972	0.1435	0.3349	0.0079	1862.0	± 50.8	1868.4	± 136.2	154	43
14	0.0515	0.0014	0.2670	0.0074	0.0376	0.0006	238.0	± 3.7	240.3	± 7.5	623	229
15	0.0492	0.0014	0.2019	0.0057	0.0297	0.0004	188.9	± 2.8	186.7	± 5.7	751	385
16	0.1135	0.0018	5.0057	0.1009	0.3197	0.0053	1788.4	± 34.2	1820.3	± 97.6	387	120
17	0.0508	0.0018	0.2083	0.0079	0.0297	0.0006	188.8	± 3.9	192.2	± 8.0	369	137
18	0.0479	0.0023	0.2285	0.0120	0.0346	0.0009	219.0	± 5.9	209.0	± 12.1	166	107
19	0.0531	0.0020	0.4286	0.0187	0.0586	0.0015	366.8	± 10.0	362.2	± 18.8	153	79
20	0.0490	0.0013	0.2008	0.0060	0.0297	0.0005	188.6	± 3.2	185.8	± 6.1	691	500
21	0.0497	0.0014	0.1898	0.0061	0.0277	0.0005	176.0	± 3.1	176.4	± 6.2	600	334
22	0.0478	0.0021	0.1969	0.0093	0.0298	0.0007	189.5	± 4.5	182.5	± 9.4	236	183
23	0.0508	0.0014	0.2494	0.0077	0.0356	0.0006	225.2	± 4.1	226.1	± 7.8	537	740
24	0.0490	0.0016	0.2372	0.0084	0.0351	0.0007	222.2	± 4.4	216.1	± 8.5	389	323
25	0.0495	0.0023	0.2044	0.0102	0.0299	0.0007	189.9	± 4.8	188.8	± 10.3	203	138
26	0.0500	0.0012	0.2382	0.0063	0.0345	0.0006	218.6	± 3.6	216.9	± 6.4	821	643
27	0.0498	0.0015	0.1966	0.0065	0.0286	0.0005	181.9	± 3.3	182.2	± 6.6	541	325
28	0.0611	0.0036	0.2889	0.0188	0.0342	0.0012	217.1	± 7.7	257.7	± 18.9	87	105
29	0.0491	0.0019	0.1865	0.0078	0.0275	0.0006	175.1	± 3.7	173.6	± 7.9	327	189
30	0.0501	0.0015	0.2408	0.0082	0.0349	0.0007	220.9	± 4.2	219.1	± 8.3	433	280
31	0.0485	0.0010	0.1992	0.0046	0.0298	0.0004	189.1	± 2.8	184.5	± 4.7	1437	631
32	0.1214	0.0014	5.7653	0.1084	0.3441	0.0056	1906.2	± 35.9	1941.2	± 104.5	614	44
33	0.1144	0.0013	4.9316	0.0936	0.3123	0.0051	1752.2	± 32.8	1807.7	± 90.9	601	223
34	0.0479	0.0018	0.1675	0.0069	0.0254	0.0005	161.5	± 3.3	157.3	± 6.9	376	98
35	0.0496	0.0013	0.2415	0.0072	0.0353	0.0006	223.4	± 3.9	219.7	± 7.3	588	422
36	0.0509	0.0019	0.2432	0.0099	0.0346	0.0008	219.4	± 4.9	221.0	± 10.0	280	202
37	0.0510	0.0023	0.2093	0.0103	0.0298	0.0008	189.0	± 5.2	193.0	± 10.4	211	109
38	0.0485	0.0032	0.2964	0.0219	0.0443	0.0018	279.6	± 11.5	263.6	± 22.0	66	36
39	0.0504	0.0013	0.1918	0.0060	0.0276	0.0006	175.5	± 3.6	178.2	± 6.1	717	320
40	0.0525	0.0018	0.2500	0.0101	0.0345	0.0008	218.5	± 5.4	226.5	± 10.2	291	154
41	0.0521	0.0018	0.2548	0.0103	0.0355	0.0009	224.7	± 5.6	230.5	± 10.4	290	36
42	0.0517	0.0015	0.2509	0.0089	0.0351	0.0008	222.7	± 5.1	227.3	± 9.0	405	301
43	0.0479	0.0029	0.1988	0.0129	0.0301	0.0010	190.9	± 6.4	184.1	± 13.0	120	53
44	0.0505	0.0024	0.1856	0.0095	0.0266	0.0007	169.5	± 4.7	172.9	± 9.6	215	195
45	0.0506	0.0011	0.2433	0.0069	0.0348	0.0007	220.8	± 4.5	221.1	± 7.0	789	558
46	0.0498	0.0012	0.1896	0.0056	0.0276	0.0005	175.6	± 3.5	176.3	± 5.7	856	438
47	0.0489	0.0016	0.1857	0.0069	0.0275	0.0006	175.0	± 3.9	173.0	± 7.0	452	276

Table A10 Continued.

No.	Isotopic ratios						U-Pb age (Ma)				U (ppm)	Th (ppm)
	^{207}Pb/^{206}Pb	Error 2σ	^{207}Pb/^{235}U	Error 2σ	^{206}Pb/^{238}U	Error 2σ	^{206}Pb/^{238}U	Error 2σ	^{207}Pb/^{235}U	Error 2σ		
48	0.0515	0.0020	0.2489	0.0109	0.0350	0.0009	222.1	± 5.8	225.6	± 11.0	243	162
49	0.0501	0.0014	0.1861	0.0062	0.0269	0.0006	171.3	± 3.6	173.3	± 6.2	620	362
50	0.1117	0.0014	4.0239	0.1045	0.2611	0.0063	1495.6	± 40.7	1639.0	± 100.9	241	67
51	0.0502	0.0016	0.1959	0.0070	0.0283	0.0006	179.9	± 4.0	181.6	± 7.1	482	315
52	0.1248	0.0012	6.1996	0.1335	0.3600	0.0074	1982.1	± 47.7	2004.4	± 127.2	501	64
53	0.1138	0.0025	5.2361	0.1249	0.3336	0.0079	1855.7	± 50.5	1858.5	± 119.5	299	71
54	0.0507	0.0015	0.2419	0.0066	0.0346	0.0007	219.1	± 4.6	220.0	± 6.7	847	383
55	0.0501	0.0020	0.1906	0.0076	0.0276	0.0007	175.4	± 4.3	177.2	± 7.7	367	209
56	0.0503	0.0013	0.2379	0.0058	0.0343	0.0007	217.2	± 4.3	216.7	± 5.8	1305	747
57	0.0510	0.0021	0.1974	0.0080	0.0280	0.0007	178.2	± 4.4	182.9	± 8.1	343	228
58	0.0496	0.0023	0.2408	0.0115	0.0352	0.0010	223.0	± 6.3	219.1	± 11.6	198	178
59	0.1301	0.0029	6.5462	0.1568	0.3648	0.0087	2004.7	± 55.8	2052.1	± 147.9	284	73
60	0.0504	0.0017	0.2459	0.0081	0.0354	0.0008	224.1	± 5.1	223.3	± 8.2	477	118
61	0.0519	0.0023	0.2479	0.0111	0.0346	0.0009	219.5	± 6.0	224.9	± 11.2	224	123
62	0.0491	0.0016	0.1840	0.0058	0.0272	0.0006	172.7	± 3.7	171.5	± 5.9	684	330
63	0.0493	0.0017	0.2018	0.0069	0.0297	0.0007	188.6	± 4.3	186.7	± 7.0	514	195
64	0.0484	0.0026	0.2359	0.0132	0.0353	0.0011	223.9	± 7.1	215.1	± 13.4	140	98
Standards												
91500epo 3-1	0.0754	0.0020	1.8638	0.0708	0.1792	0.0054	1063	± 35	1068	± 69	89	36
91500epo 3-2	0.0733	0.0020	1.7753	0.0671	0.1755	0.0053	1042	± 34	1036	± 66	91	38
91500epo 3-3	0.0748	0.0018	1.8439	0.0742	0.1788	0.0061	1060	± 39	1061	± 73	87	33
91500epo 3-4	0.0737	0.0018	1.8351	0.0734	0.1804	0.0061	1069	± 39	1058	± 72	88	34
91500epo 3-5	0.0732	0.0023	1.8379	0.0743	0.1820	0.0063	1078	± 41	1059	± 73	84	31
OD-3 3-1	0.0502	0.0030	0.0362	0.0022	0.0052	0.0001	33.6	± 0.67	36.1	± 2.18	659	927
OD-3 3-2	0.0490	0.0043	0.0343	0.0030	0.0051	0.0001	32.6	± 0.89	34.2	± 3.02	315	341
OD-3 3-3	0.0451	0.0029	0.0328	0.0021	0.0053	0.0001	33.9	± 0.84	32.8	± 2.16	639	709
OD-3 3-4	0.0429	0.0040	0.0313	0.0029	0.0053	0.0002	34.0	± 1.05	31.3	± 2.95	314	314
OD-3 3-5	0.0463	0.0039	0.0329	0.0027	0.0052	0.0002	33.1	± 0.98	32.9	± 2.76	374	367

Table A11 Zircon U–Pb isotopic data for sample Tcs-E-03 obtained by quadrupole inductively coupled plasma mass spectrometry.

No.	Isotopic ratios						U-Pb age (Ma)						U (ppm)	Th (ppm)
	$^{207}Pb/^{206}Pb$	Error 2σ	$^{207}Pb/^{235}U$	Error 2σ	$^{206}Pb/^{238}U$	Error 2σ	$^{206}Pb/^{238}U$		Error 2σ	$^{207}Pb/^{235}U$		Error 2σ		
1	0.1251	0.0042	6.1566	0.3293	0.3567	0.0114	1966.4	±	72.8	1998.3	±	289.1	286	183
2	0.0491	0.0024	0.1694	0.0104	0.0250	0.0007	159.4	±	4.7	158.9	±	10.5	323	127
3	0.0485	0.0035	0.1706	0.0143	0.0255	0.0010	162.1	±	6.3	159.9	±	14.4	582	247
4	0.0476	0.0031	0.1621	0.0123	0.0247	0.0009	157.0	±	5.5	152.5	±	12.5	397	291
5	0.0488	0.0044	0.1635	0.0164	0.0243	0.0011	154.5	±	7.0	153.8	±	16.5	1250	800
6	0.0488	0.0036	0.1700	0.0145	0.0253	0.0010	160.9	±	6.3	159.5	±	14.6	171	129
7	0.0502	0.0035	0.1721	0.0140	0.0248	0.0009	158.1	±	6.0	161.2	±	14.1	137	106
8	0.0471	0.0035	0.1624	0.0138	0.0250	0.0010	159.0	±	6.1	152.8	±	13.9	343	295
9	0.0503	0.0043	0.1728	0.0166	0.0249	0.0011	158.6	±	7.0	161.8	±	16.7	281	195
10	0.0479	0.0028	0.1637	0.0114	0.0248	0.0008	157.9	±	5.2	153.9	±	11.5	418	302
11	0.0511	0.0034	0.1712	0.0133	0.0243	0.0009	154.6	±	5.6	160.5	±	13.4	814	420
12	0.0497	0.0023	0.1702	0.0101	0.0248	0.0007	158.0	±	4.5	159.6	±	10.2	173	251
13	0.0493	0.0036	0.1664	0.0139	0.0245	0.0009	155.9	±	6.0	156.3	±	14.0	265	189
14	0.0511	0.0028	0.1692	0.0114	0.0240	0.0008	153.0	±	4.9	158.7	±	11.5	788	371
15	0.0501	0.0032	0.1715	0.0130	0.0248	0.0009	158.1	±	5.6	160.7	±	13.2	386	95
16	0.0498	0.0031	0.1693	0.0118	0.0247	0.0007	157.1	±	4.8	158.8	±	12.0	363	268
17	0.0527	0.0038	0.1905	0.0152	0.0262	0.0009	166.6	±	6.0	177.0	±	15.4	319	197
18	0.0471	0.0034	0.1601	0.0128	0.0246	0.0008	156.8	±	5.4	150.8	±	12.9	393	224
19	0.0486	0.0032	0.1657	0.0122	0.0247	0.0008	157.4	±	5.0	155.7	±	12.4	644	202
20	0.0475	0.0042	0.1608	0.0153	0.0246	0.0010	156.4	±	6.4	151.4	±	15.4	526	296
21	0.0507	0.0030	0.1712	0.0114	0.0245	0.0007	155.9	±	4.5	160.5	±	11.5	1079	1063
22	0.0505	0.0020	0.1679	0.0083	0.0241	0.0005	153.6	±	3.3	157.6	±	8.4	370	263
23	0.0503	0.0023	0.1701	0.0093	0.0245	0.0006	156.0	±	3.7	159.5	±	9.4	295	217
24	0.0489	0.0030	0.1627	0.0112	0.0241	0.0007	153.5	±	4.5	153.1	±	11.3	183	138
25	0.0483	0.0029	0.1650	0.0113	0.0248	0.0007	157.7	±	4.7	155.1	±	11.4	274	212
26	0.0511	0.0023	0.1738	0.0095	0.0247	0.0006	157.0	±	3.7	162.7	±	9.6	904	368
27	0.0498	0.0048	0.1668	0.0173	0.0243	0.0011	154.6	±	7.0	156.6	±	17.4	261	189
28	0.0511	0.0035	0.1684	0.0129	0.0239	0.0008	152.3	±	5.1	158.0	±	13.0	272	82
29	0.0484	0.0032	0.1602	0.0119	0.0240	0.0008	152.9	±	4.9	150.9	±	12.0	229	170
30	0.0492	0.0025	0.1682	0.0098	0.0248	0.0006	157.8	±	4.0	157.9	±	9.9	410	111

Standards are the same as in Table A1

Table A12 Zircon U–Pb isotopic data for sample 200824-07 obtained by quadrupole inductively coupled plasma mass spectrometry. Shadowed data indicate discordant age data.

No.	Isotopic ratios						U-Pb age (Ma)						U (ppm)	Th (ppm)
	^{207}Pb/^{206}Pb	Error 2σ	^{207}Pb/^{235}U	Error 2σ	^{206}Pb/^{238}U	Error 2σ	^{206}Pb/^{238}U		Error 2σ	^{207}Pb/^{235}U		Error 2σ		
1	0.0466	0.0031	0.1735	0.0120	0.0270	0.0008	171.7	±	5.4	162.5	±	12.1	120	108
2	0.0486	0.0032	0.1849	0.0128	0.0276	0.0009	175.3	±	5.6	172.2	±	12.9	113	148
3	0.1141	0.0026	5.2235	0.1702	0.3317	0.0091	1846.8	±	58.5	1856.5	±	159.6	119	79
4	0.0484	0.0021	0.1731	0.0077	0.0259	0.0005	165.0	±	3.3	162.1	±	7.8	317	122
5	0.0489	0.0041	0.1747	0.0151	0.0259	0.0010	164.7	±	6.5	163.5	±	15.2	75	139
6	0.0522	0.0030	0.2668	0.0164	0.0370	0.0012	234.5	±	7.5	240.1	±	16.5	108	100
7	0.1124	0.0023	4.2247	0.0855	0.2725	0.0037	1553.4	±	24.1	1678.8	±	83.3	641	84
8	0.0497	0.0018	0.1833	0.0064	0.0267	0.0004	170.0	±	2.8	170.9	±	6.5	529	483
9	0.1116	0.0023	4.0948	0.0875	0.2658	0.0040	1519.6	±	25.8	1653.3	±	85.2	495	68
10	0.0500	0.0019	0.1841	0.0068	0.0267	0.0005	169.6	±	2.9	171.5	±	6.9	467	362
11	0.0488	0.0024	0.1796	0.0091	0.0267	0.0006	169.6	±	4.0	167.7	±	9.2	225	190
12	0.0481	0.0025	0.1763	0.0093	0.0266	0.0006	169.0	±	4.1	164.9	±	9.4	210	207
13	0.0458	0.0034	0.1504	0.0115	0.0238	0.0008	151.7	±	5.0	142.2	±	11.6	110	147
14	0.0485	0.0021	0.1830	0.0080	0.0274	0.0005	174.0	±	3.5	170.6	±	8.1	316	272
15	0.0496	0.0023	0.1871	0.0088	0.0274	0.0006	174.0	±	3.8	174.1	±	8.9	261	146
16	0.0471	0.0025	0.1728	0.0096	0.0266	0.0006	169.4	±	3.9	161.9	±	9.7	229	87
17	0.1132	0.0031	5.0970	0.1617	0.3263	0.0060	1820.5	±	38.7	1835.6	±	152.2	278	40
18	0.0521	0.0022	0.1938	0.0083	0.0270	0.0005	171.7	±	3.0	179.9	±	8.4	429	161
19	0.1134	0.0034	5.2470	0.2177	0.3354	0.0104	1864.4	±	66.6	1860.3	±	200.0	91	127
20	0.0496	0.0029	0.1815	0.0112	0.0265	0.0007	168.7	±	4.5	169.4	±	11.3	168	173
21	0.0471	0.0024	0.1736	0.0093	0.0267	0.0006	170.0	±	3.8	162.6	±	9.4	246	94
22	0.0511	0.0018	0.2785	0.0103	0.0395	0.0006	249.5	±	3.8	249.4	±	10.4	530	12
23	0.0474	0.0027	0.1705	0.0102	0.0261	0.0006	166.1	±	4.1	159.8	±	10.3	192	117
24	0.0507	0.0025	0.2000	0.0102	0.0286	0.0006	181.9	±	4.0	185.1	±	10.3	252	116
25	0.1296	0.0037	7.0014	0.2805	0.3915	0.0117	2129.8	±	74.8	2111.6	±	251.0	98	113
26	0.0496	0.0026	0.1847	0.0098	0.0270	0.0006	171.7	±	3.9	172.1	±	9.9	239	82
27	0.0511	0.0019	0.2724	0.0107	0.0386	0.0006	244.2	±	4.1	244.6	±	10.8	422	47
28	0.1144	0.0033	5.2160	0.1916	0.3305	0.0083	1840.9	±	53.5	1855.2	±	178.0	140	68
29	0.0507	0.0020	0.1889	0.0077	0.0270	0.0004	171.7	±	2.8	175.7	±	7.8	499	312
30	0.0518	0.0020	0.2906	0.0117	0.0406	0.0007	256.8	±	4.6	259.0	±	11.8	375	214
31	0.0510	0.0013	0.2406	0.0069	0.0342	0.0007	216.8	±	4.3	218.9	±	7.0	219	222
32	0.0504	0.0008	0.2313	0.0045	0.0333	0.0005	211.0	±	3.3	211.3	±	4.6	762	944
33	0.0494	0.0009	0.1760	0.0036	0.0258	0.0004	164.4	±	2.6	164.6	±	3.7	803	351
34	0.0496	0.0009	0.1902	0.0042	0.0278	0.0005	176.8	±	2.9	176.8	±	4.3	578	262
35	0.0499	0.0015	0.1841	0.0060	0.0267	0.0005	170.0	±	3.5	171.6	±	6.0	205	119
36	0.1133	0.0013	4.9411	0.0962	0.3161	0.0059	1770.9	±	38.0	1809.3	±	93.3	170	136
37	0.0501	0.0012	0.1819	0.0050	0.0263	0.0005	167.4	±	3.1	169.7	±	5.0	319	192
38	0.0484	0.0018	0.1781	0.0068	0.0267	0.0006	169.9	±	3.9	166.4	±	6.9	141	76
39	0.0497	0.0009	0.1769	0.0037	0.0258	0.0004	164.3	±	2.6	165.4	±	3.7	773	461
40	0.0497	0.0009	0.1904	0.0039	0.0278	0.0004	176.6	±	2.8	176.9	±	3.9	755	881
41	0.1196	0.0013	4.5639	0.0858	0.2766	0.0050	1574.1	±	32.1	1742.7	±	83.6	200	96
42	0.0510	0.0009	0.2433	0.0052	0.0346	0.0006	219.1	±	3.6	221.1	±	5.2	537	154
43	0.1127	0.0012	4.5349	0.0823	0.2917	0.0051	1649.8	±	32.7	1737.4	±	80.3	236	124
44	0.0522	0.0010	0.3587	0.0082	0.0498	0.0009	313.3	±	5.6	311.2	±	8.3	313	80
45	0.0499	0.0017	0.1953	0.0073	0.0283	0.0006	180.2	±	4.1	181.1	±	7.4	139	76
46	0.0499	0.0011	0.1950	0.0048	0.0283	0.0005	179.9	±	3.1	180.9	±	4.9	396	319
47	0.0510	0.0017	0.1992	0.0072	0.0283	0.0006	179.9	±	4.0	184.4	±	7.3	147	55
48	0.0490	0.0012	0.1841	0.0049	0.0272	0.0005	173.3	±	3.1	171.6	±	4.9	344	123

Table A12 Continued.

No.	Isotopic ratios						U-Pb age (Ma)				U (ppm)	Th (ppm)
	$^{207}Pb/^{206}Pb$	Error 2σ	$^{207}Pb/^{235}U$	Error 2σ	$^{206}Pb/^{238}U$	Error 2σ	$^{206}Pb/^{238}U$	Error 2σ	$^{207}Pb/^{235}U$	Error 2σ		
49	0.1102	0.0011	3.7128	0.0570	0.2441	0.0036	1408.0	± 23.4	1574.1	± 56.3	778	14
50	0.0498	0.0009	0.1673	0.0034	0.0243	0.0004	155.1	± 2.4	157.1	± 3.4	877	674
51	0.0503	0.0012	0.1840	0.0049	0.0265	0.0004	168.6	± 2.8	171.5	± 5.0	365	240
52	0.0491	0.0012	0.1786	0.0047	0.0264	0.0004	167.8	± 2.7	166.8	± 4.7	392	196
53	0.0492	0.0015	0.1889	0.0060	0.0278	0.0005	176.9	± 3.3	175.7	± 6.1	222	180
54	0.0483	0.0027	0.1867	0.0107	0.0280	0.0008	178.0	± 5.5	173.8	± 10.8	58	51
55	0.0495	0.0010	0.1819	0.0039	0.0266	0.0004	169.3	± 2.4	169.7	± 4.0	727	554
56	0.0568	0.0011	0.4114	0.0088	0.0525	0.0008	329.7	± 5.1	349.9	± 8.9	388	154
57	0.0496	0.0012	0.1936	0.0051	0.0283	0.0005	179.7	± 2.9	179.7	± 5.1	366	495
58	0.0490	0.0008	0.1755	0.0033	0.0260	0.0003	165.4	± 2.2	164.2	± 3.3	1385	597
59	0.0480	0.0014	0.1863	0.0057	0.0281	0.0005	178.8	± 3.2	173.5	± 5.8	246	224
60	0.0496	0.0012	0.1799	0.0047	0.0263	0.0004	167.3	± 2.7	168.0	± 4.8	387	420
61	0.0481	0.0013	0.1650	0.0047	0.0249	0.0004	158.4	± 2.7	155.0	± 4.7	335	216
62	0.0475	0.0023	0.1887	0.0094	0.0288	0.0008	182.9	± 4.9	175.5	± 9.5	78	58
63	0.0492	0.0013	0.1959	0.0056	0.0288	0.0005	183.3	± 3.2	181.7	± 5.7	285	239
64	0.0502	0.0014	0.2430	0.0071	0.0351	0.0006	222.1	± 4.1	220.9	± 7.2	224	268
Standards												
91500epo 5-1	0.0817	0.0026	2.0551	0.0938	0.1823	0.00671	1079.8	± 43.1	1134.0	± 91.0	66	25
91500epo 5-2	0.0797	0.0026	2.0292	0.0943	0.1846	0.00691	1092.1	± 44.4	1125.4	± 91.5	63	42
91500epo 5-3	0.0816	0.0026	2.0735	0.0952	0.1842	0.00683	1090.0	± 43.9	1140.1	± 92.3	65	35
91500epo 5-4	0.0818	0.0030	2.0800	0.1042	0.1844	0.00678	1090.9	± 43.6	1142.2	± 100.7	65	25
91500epo 5-5	0.0837	0.0030	2.1430	0.1065	0.1855	0.00678	1097.1	± 43.6	1162.8	± 102.7	66	27
91500epo 5-6	0.0841	0.0030	2.0622	0.0964	0.1777	0.00596	1054.6	± 38.3	1136.3	± 93.5	79	25
OD3 5-1	0.0445	0.0036	0.0318	0.0025	0.0052	0.00012	33.3	± 0.8	31.8	± 2.5	442	865
OD3 5-2	0.0458	0.0034	0.0326	0.0024	0.0052	0.00011	33.2	± 0.7	32.6	± 2.4	557	804
91500epo 2-4	0.0745	0.0015	1.8132	0.0544	0.1764	0.00461	1047.2	± 29.6	1050.2	± 53.7	59	23
91500epo 2-5	0.0741	0.0015	1.8181	0.0540	0.1779	0.00461	1055.5	± 29.6	1052.0	± 53.4	60	33
91500epo 2-6	0.0738	0.0014	1.8520	0.0552	0.1819	0.00473	1077.6	± 30.4	1064.1	± 54.5	59	33
91500epo 2-7	0.0746	0.0016	1.8194	0.0546	0.1767	0.00440	1048.7	± 28.3	1052.5	± 54.0	61	26
91500epo 2-8	0.0750	0.0016	1.8391	0.0558	0.1777	0.00448	1054.6	± 28.8	1059.5	± 55.2	59	36
OD3 2-4	0.0479	0.0025	0.0334	0.0017	0.0051	0.00012	32.6	± 0.8	33.4	± 1.8	342	663
OD3 2-5	0.0475	0.0024	0.0339	0.0017	0.0052	0.00011	33.3	± 0.7	33.9	± 1.7	375	813

Table A13 Zircon U–Pb isotopic data for sample Oka-03 obtained by quadrupole inductively coupled plasma mass spectrometry.

No.	Isotopic ratios						U-Pb age (Ma)						U (ppm)	Th (ppm)
	$^{207}Pb/^{206}Pb$	Error 2σ	$^{207}Pb/^{235}U$	Error 2σ	$^{206}Pb/^{238}U$	Error 2σ	$^{206}Pb/^{238}U$		Error 2σ	$^{207}Pb/^{235}U$		Error 2σ		
1	0.0548	0.0043	0.1750	0.0146	0.0232	0.0009	147.5	±	5.7	163.7	±	14.7	333	443
2	0.0505	0.0026	0.1643	0.0090	0.0236	0.0006	150.1	±	3.8	154.4	±	9.1	36	48
3	0.0548	0.0049	0.1783	0.0168	0.0236	0.0010	150.3	±	6.5	166.6	±	16.9	76	176
4	0.0478	0.0025	0.1561	0.0088	0.0237	0.0006	150.8	±	3.9	147.3	±	8.9	259	363
5	0.0517	0.0043	0.1692	0.0146	0.0237	0.0009	151.1	±	5.9	158.7	±	14.7	101	75
6	0.0489	0.0042	0.1603	0.0143	0.0238	0.0009	151.5	±	5.9	151.0	±	14.4	307	91
7	0.0506	0.0020	0.1660	0.0073	0.0238	0.0005	151.5	±	3.2	155.9	±	7.4	114	177
8	0.0495	0.0024	0.1626	0.0080	0.0238	0.0005	151.6	±	3.5	153.0	±	8.1	272	453
9	0.0490	0.0026	0.1610	0.0092	0.0238	0.0006	151.7	±	4.0	151.6	±	9.3	281	329
10	0.0502	0.0020	0.1655	0.0072	0.0239	0.0005	152.1	±	3.2	155.5	±	7.3	91	63
11	0.0466	0.0035	0.1536	0.0120	0.0239	0.0008	152.3	±	5.2	145.1	±	12.2	74	135
12	0.0519	0.0025	0.1712	0.0084	0.0239	0.0005	152.5	±	3.5	160.5	±	8.5	260	381
13	0.0495	0.0021	0.1635	0.0076	0.0239	0.0005	152.5	±	3.4	153.8	±	7.7	128	76
14	0.0475	0.0024	0.1577	0.0080	0.0240	0.0006	153.2	±	3.5	148.7	±	8.1	390	639
15	0.0488	0.0025	0.1621	0.0087	0.0241	0.0006	153.3	±	3.8	152.6	±	8.8	106	252
16	0.0516	0.0024	0.1713	0.0086	0.0241	0.0006	153.3	±	3.7	160.6	±	8.7	339	425
17	0.0503	0.0028	0.1671	0.0101	0.0241	0.0007	153.4	±	4.3	156.9	±	10.2	196	561
18	0.0496	0.0035	0.1648	0.0119	0.0241	0.0008	153.4	±	5.0	154.9	±	12.0	116	246
19	0.0484	0.0020	0.1611	0.0069	0.0241	0.0005	153.8	±	3.1	151.7	±	7.0	187	154
20	0.0523	0.0040	0.1745	0.0137	0.0242	0.0009	154.1	±	5.5	163.3	±	13.8	237	259
21	0.0516	0.0061	0.1724	0.0211	0.0242	0.0013	154.2	±	8.4	161.5	±	21.2	330	520
22	0.0500	0.0022	0.1676	0.0081	0.0243	0.0006	154.8	±	3.6	157.3	±	8.2	59	89
23	0.0490	0.0018	0.1643	0.0066	0.0243	0.0005	154.8	±	3.1	154.4	±	6.7	407	690
24	0.0504	0.0033	0.1689	0.0114	0.0243	0.0007	154.9	±	4.7	158.5	±	11.5	290	438
25	0.0486	0.0022	0.1632	0.0074	0.0243	0.0005	154.9	±	3.3	153.5	±	7.5	211	630
26	0.0509	0.0024	0.1711	0.0082	0.0243	0.0005	155.1	±	3.5	160.4	±	8.3	161	96
27	0.0523	0.0036	0.1780	0.0128	0.0247	0.0008	157.2	±	5.2	166.4	±	13.0	256	197
28	0.0491	0.0022	0.1678	0.0082	0.0248	0.0006	157.8	±	3.7	157.5	±	8.3	204	129
29	0.0447	0.0031	0.1529	0.0111	0.0248	0.0008	158.0	±	5.0	144.5	±	11.2	77	135
30	0.1125	0.0025	4.9805	0.1299	0.3207	0.0062	1793.4	±	39.8	1816.0	±	124.0	265	263
Standards														
91500epo 4-1	0.0753	0.0026	1.8673	0.0905	0.1796	0.0068	1065	±	44	1070	±	88	58	15
91500epo 4-2	0.0731	0.0026	1.8479	0.0913	0.1832	0.0071	1084	±	45	1063	±	89	55	20
OD-3 4-1	0.0419	0.0048	0.0297	0.0033	0.0051	0.0002	33.1	±	1.09	29.7	±	3.38	222	231
OD-3 4-2	0.0440	0.0049	0.0306	0.0034	0.0050	0.0002	32.4	±	1.07	30.6	±	3.43	223	230